Atmos. Chem. Phys. Discuss.,
https://doi.org/10.5194/acp-2018-186-AC1, 2018

Atmospheric Chemistry and Physics Discussions

Interactive comment on "Cloud and aerosol radiative effects as key players for anthropogenic changes in atmospheric dynamics over southernWest Africa" *by* Konrad Deetz et al.

Konrad Deetz et al.

konrad.deetz@kit.edu

Received and published: 19 June 2018

Answer to Referee #1 Konrad Deetz 19 June 2018

Dear Referee (Atmospheric Chemistry and Physics),

thank you for your report from 13 April 2018. We have accounted for the comments and suggestions in the revised manuscript version. Please find our replies (marked with #) to the individual comments in the following. Before the detailed replies to your comments we want to stress one important overarching point: This study mainly focuses on the sensitivity of atmospheric dynamics and cloud properties to aerosols and not on a

Printer-friendly version

Discussion paper

detailed validation of the model system. Nevertheless, we have done a comprehensive evaluation of the model with the available observations of the DACCIWA measurement campaign. We show corresponding figures in our replies which appear at the end of this document. (The complete figure captions are given within the text because the figure caption space for the uploaded figures is not sufficient.)

Sincerely, Konrad Deetz on behalf of all coauthors

Referee comments:

(0) The authors analyze six simulations of the COSMO-ART regional model with an outer domain of roughly 40 x 40 degrees centered around the Bight of Benin and an inner domain of roughly 10 x 15 degrees aligned along the Gold Coast of Southern West Africa. A main strength of the study is that the authors conduct an extensive analysis of the simulations to suss out patterns of response to aerosol conditions, and to draw some conclusions about some mechanisms and hypotheses about others. A main weakness of the study is that almost no comparisons to observations are made nor are the realism of assumed meteorological or surface or aerosol properties discussed, leaving the reader necessarily uncertain as to the degree to which the simulations are basically realistic, either in the baseline state or in the dynamic range of aerosol conditions investigated. Especially in today's satellite age, it should not be considered a sufficient evaluation of a regional model simulation to compare results only to droplet number concentration observations. Based on the simulations, the authors advance a schematic diagram of how near-coastal meteorological conditions could be impacted by increasing regional pollution during the monsoonal period when no land-sea breeze period occurs. Observational work, for instance using satellite observations, would be required to confirm the robustness of the proposed mechanism and its strength for a given dynamic range of aerosol relative to other regional-scale drivers that are held fixed in the current study, such as sea surface temperature.

The high resolution realizations with COSMO-ART are computational expensive and

therefore we had to restrict to a short time period. We commonly agreed on the 3-4 July 2016 as a golden day due to the intensive stratus period observed over Save (Kalthoff et al., 2018). The data analysis of the COSMO-ART results revealed that the AI is most pronounced and coherent over Ivory Coast (Figure 5 in the manuscript). Therefore, we decided to focus on this area although we are aware of the fact, that the DACCIWA measurement campaign with its supersites and aircraft operations focus more on the eastern part of the domain. For 3-4 July, no aircraft observations are available for the coastal region of Ivory Coast. Furthermore, a detailed assessment of the MODIS AOD data revealed that the data availability over SWA (land area) is substantially reduced by the presence of clouds (see Review-Figure 6). Nevertheless, we comprehensively evaluated COSMO-ART in (a) past studies and also (b) within DACCIWA for SWA. (a) The full capacity of COSMO-ART was applied in numerous studies. Knote et al. (2011) validated the aerosol and gaseous compounds in detail against observations for the European area.Stanelle et al. (2010) analyzed the ADE of mineral dust over the Sahara that alters the near-surface temperature up to 4 K in case of elevated mineral dust layers. Furthermore, feedbacks between the mineral dust ADE and the atmospheric dynamics lead to modifications in the mineral dust emission. Athanasopoulou et al. (2014) quantified a severe wildfire event over Greece in 2007 in terms of air quality and ADE that reveals AOD values between 0.75 and 1 and a cooling of 0.5 K.Walter et al. (2016) extended COSMO-ART with a plume-rise model to describe biomass burning pollution injection heights and applied the model to Canadian forest fires in 2010. The ADE related to the biomass burning plume leads to a near-surface cooling of up to 6 K. The ADE of sea salt over the Mediterranean Sea, Northeast Atlantic, North Sea and Baltic Sea was modeled by Lundgren et al. (2013) in accordance to the observations from remote sensing. Kraut (2015) applied an ensemble approach by including random temperature pertubations to isolate the sea salt AIE on the characteristics of a cyclone over the Mediterranean Sea in 2011, revealing spatial shifts and intensity differences in the precipitation patterns. By considering the AIE on post-frontal convective clouds over Germany in 2008, the cloud properties were changed significantly, leading to a

reduction in precipitation with increasing aerosol amounts (Rieger et al., 2014). (b) In the preparation of the high resolution process study simulations with COSMO-ART for SWA, we conducted operational forecasts for the area over the time period 8 March to 31 July with a grid mesh size of 28 km. This allows us to comprehensively analyze the model performance with respect to meteorology and air pollution and to prepare reasonable COSMO-ART data for the nesting of our high resolution realizations. Also we found tendencies of overestimations of trace gas concentrations in COSMO-ART, likely due to uncertainties in the emission inventories, COSMO-ART reasonably reproduces the SWA meteorological and air pollution characteristics. To support these findings and to meet the concerns of the reviewer, the following 7 figures are attached to this review answer:

- Review-Figure-1: Temporal evolution of the height (m AGL) of the wind speed maximum between 0 and 1500 m AGL for the mean 57 h forecast lead time. (13 June - 30 July 2016) at Savè as observed (black, Doppler Lidar) and modeled with COSMO-ART (blue). The shaded areas denote the standard deviation.

- Review-Figure-2: Wind speed profile (m s-1) between 0 and 2000 m ASL as mean diurnal cycle (13 June - 30 July 2016) at Savè for (a) COSMO-ART and (b) Doppler Lidar observation.

- Review-Figure-3: Vertical profiles (km AGL) of BC (mg m-3) at Savè for (a-c) 5 July 2016, (d-g) 14 July 2016 and (h-i) 15 July 2016. The ALADINA (small unmanned aircraft) observations of total BC are denoted in black, the COSMO-ART results for fresh BC, aged BC (Aitken mode), aged BC (accumulation mode) and total BC are shown in green, blue, brown and red, respectively. The observations were temporally assigned to the 3 hourly model output with a deviation not greater than 1 hour and by subsequently interpolating the model data to the ALADINA altitudes. Within these time steps, ALADINA conduct several ascends and descends. It is assumed that the observations within the time steps are measured instantaneously and the data is sorted according to their altitude, to allow for clearness of the visualization.

- Review-Figure-4: Comparison of Twin Otter measurement flight TO-16 (14 July 2016, 06:44 UTC to 09:50 UTC) results with COSMO-ART. For a comparison the model output of 9 UTC and the measurements 15 minutes around this time step (08:45-09:15 UTC) were selected. (a) Flight altitude (m AGL), (b) flight track, (c) NOx concentration (ppbv) at 750m height and flight track, (d) vertical transect of NOx concentration (ppbv) along the flight track with aircraft observations included, (e) temperature (°C), (f) specific humidity (kg kg-1), (g) CO concentration (ppbv), (h) NO concentration (ppbv), (i) NO2 concentration (ppbv), (j) NOx concentration, (k) O3 concentration (ppbv) and (l) SO2 concentration (ppbv). The panels (e)-(l) present the COSMOART results in blue and the observations in black. The horizontal color lines on top of these panels are denoted to the colors in panel (a) and (b) to illustrate the aircraft location related to the observed trace gas concentrations.

- Review-Figure-5: Mean total AOD averaged from 27 June to 17 July 2016 of (a) COSMO-ART, spatiotemporally collocated with MODIS Terra, (b) MODIS Terra, (c) COSMO-ART, collocated spatiotemporally with MODIS Aqua and (d) MODIS Aqua.

- Review-Figure-6: Number of observations within the time period 27 June - 17 July of (a) MODIS Terra and (b) MODIS Aqua

- Review-Figure-7: AOD (550 nm) at Savè from COSMO-ART (blue), CAMS (green) and AERONET (red) between 13 June - 31 July 2016 for (a) mineral dust, (b) sea salt, (c) anthropogenic aerosol and (d) total aerosol. Consider the different scaling of the ordinates. Data gaps are related to technical issues during the forecast.

Further intercomparison between COSMO-ART and observations obtained within DACCIWA including the supersites and aircraft, other models or remote sensing data is summarized in Section 5 of (https://publikationen.bibliothek.kit.edu/1000077925). However, we have not added the evaluation material since it would distract from the main purpose of the study to disentangle potential effects from aerosol on AI and SCT in a sensitivity study. Nevertheless, we agree that the paper also has to show that it

is generally able to reasonably reproduce the conditions in SWA. To account for your comment, we added an intercomparison of the shortwave, longwave, sensible and latent heat flux with observations at Save supersite in Appendix A and adapted Section 2.2 (Observational data) as follows:

"Within the DACCIWA project, an extensive field campaign took place in June–July 2016 in SWA (Fig. 1b) (Flamant et al., 2018). The time period was selected to capture the onset of the WAM and a period characterized by increased cloudiness. The DACCIWA ground-based measurement campaign encompassed the time period from 13 June to 31 July 2016, including the three supersites Kumasi (Ghana), Savè (Benin) and Ile-Ife (Nigeria) (red dots in Fig. 1b). A complete overview of the DACCIWA ground-based measurement campaign, their supersites, instrumentation and a first insight into the available data is presented in Kalthoff et al. (2018). The DACCIWA airborne measurement campaign captured the time period from 27 June to 17 July 2016 (Flamant et al., 2018). The focus of this study is on Ivory Coast and therefore less observational data from the DACCIWA campaign is available for evaluation. However, a substantial evaluation with respect to meteorology and air pollution is realized with COSMO-ART over SWA with respect to other time periods and by focusing on the eastern part of the research area (not shown). This is presented in Deetz (2018). For this study, observations of the liquid cloud properties from the CDP-100 (Cloud droplet probe, data revision 3) of the British Antarctic Survey (BAS) Twin Otter aircraft on 3 July 2016 are used for a comparison with COSMO-ART. The CDP-100 is a wing mounted canister instrument including a forward-scatter optical system to measure the cloud droplet spectrum between 2-50 μm with a frequency of 1 Hz. Additionally, the comparison of the modeled net downward shortwave and longwave radiation as well as the sensible and latent heat flux with Savè supersite is presented in Figure 17 of Appendix B. COSMO-ART reasonably reproduces the fluxes with lower fluxes with increasing aerosol as expected."

Furthermore, we added an intercomparison between COSMO-ART and the ATR42

SAFIRE aircraft with respect to the aerosol number density. However, this evaluation focuses on the Lome-Save area and not on Ivory Coast (since for this date no observations for Ivory Coast are available). In Section 2.2 (Observational data) we added the following text: "The aerosol aerosol number density is evaluated using observations of the ATR42 SAFIRE (Service des Avions Français 25 Instrumentés pour la Recherche en Environnement) for the 3 July 2016. Additionally, the comparison of the modeled net downward shortwave and longwave radiation as well as the sensible and latent heat flux with Savè supersite is presented in Figure 19 of Appendix B. COSMO-ART reasonably reproduces the fluxes with lower fluxes with increasing aerosol as expected." In Section 4 (Evaluation of modeled cloud and aerosol properties with aircraft observations) we added the following text: "The research aircraft ATR42 SAFIRE also obtained aerosol properties in the Lomé-Savè area on 3 July 2016 (8:32–13:16 UTC). The flight track and altitude is presented in Figure 5, showing similar flight patterns compared to the Twin Otter (Fig. 3). By assuming dry aerosol, Figure 6 shows the comparison between COSMO-ART and the Spectrometer Scanning Mobility Particle Sizer (SMPS) to evaluate the Aerosol Number Density in the size range 0.02–0.5 mu m. Figure 6 reveals that the modeled aerosol number density shows a similar temporal evolution compared to the observations but has a constant bias, overestimating the observed aerosol number density by a factor of about 2 (indicated by the blue dashed line). Therefore, in the subsequent study it has to be considered that the reference case shows already higher aerosol concentrations compared to the current state in SWA as quantified by the aircraft measurements. Overall, the evaluation reveals that COSMO-ART is capable to reproduce the aerosol situation on 3 July 2016 over SWA which is the basis for further sensitivity studies.

The figures related to this passage are attached in this review answer:

Fig.5 -> Review-Figure-8: Flight track of the ATR42 SAFIRE on 3 July 2016 between 08:32 UTC and 13:13 UTC in (a) horizontal and (b) vertical dimension (m AGL). For (a) the topography (m ASL) is added. The flight track in (a) and (b) is separated in hourly

time steps for the subsequent collocation with hourly model data from COSMO-ART, highlighted by the pink (08:32âĂŤ09:30 UTC), blue (09:30–10:30 UTC), gray (10:30–11:30 UTC), red (11:30–12:30 UTC) and black color (12:30–13:13 UTC). Furthermore, the arrows in (a) indicate the flight direction with the takeoff at Lomé, the flight to Savè and the return to Lomé airport. Shortly. Note the meridional compression of the map in (a).

Fig.6 -> Review-Figure-9: Aerosol number density (AND, cm-3) in the size interval 0.02 to 0.5 mu m as measured by the Spectrometer Scanning Mobility Particle Sizer (SMPS) on board the ATR42 (black) and modeled with COSMO-ART (solid blue, reference case). The horizontal dashed blue line shows the COSMO-ART AND divided by 2. The vertical blue dashed lines indicate the COSMO-ART model output hours, which are compared to the observations.

Fig. 19 (Appendix B) -> Review-Figure-10: Comparison between Savè supersite observations (grey) and COSMO-ART reference (black), clean (blue) and polluted (red) of (a) net downward shortwave radiation (W m-2), (b) net downward longwave radiation (W m-2), sensible heat flux (W m-2) and latent heat flux (W m-2). The horizontal lines in (a) denote clouds over Savè in the observations and COSMO-ART.

You mentioned that the study does not explicitly exclude the land sea-breeze but land sea-breeze effects can hardly be disentangled from AI effects because the monsoon flow superimposes the land-sea breeze. The conclusion of the manuscript closes with the suggestion of ideas to assess the aerosol-AI impact via observation. We proposed: "A potential strategy is the analysis of the AI front around noon via remote sensing cloud observations from past to present by assuming a positive trend in the aerosol burden. It is expected that the daytime AI front location has shifted landwards from the past to current conditions but also other phenomena (e.g. decadal SST variations) have the potential to affect the front location." This assessment is suitable for a companion paper but is clearly beyond the scope of this paper.

(1) In the introduction the authors refer twice to "convective-cloud invigoration mechanism," the first time apparently referring to cold clouds and the second time to warm clouds (page 2, line 32). Is this the same mechanism? Please clarify in the text to what degree the mechanism being referred to operates in simulations and under what conditions, versus established in observations and under what conditions.

Saleeby et al. (2014) show that the convective-cloud invigoration mechanism is not restricted to cold clouds. Also in warm cumuliform clouds, the enhanced condensation under polluted conditions can lead to further release of latent heat, intensified upward motion and therefore to more clouds. This is considered by the model. I don't see your point. Could you please explain more in detail what do you expect?

(2) The six simulations vary only aerosol mass and number concentrations, but how this is done is not described. The authors state that the mass and number are scaled by factors of 0.1, 0.25, 0.5, 1, 2 and 4. Since there is "aerosol-chemistry spin up" the only way I can understand this is if the values are scaled only when some process rates are calculated, but which process rates? Please clarify in the text.

Generally, the aerosol amount during the whole simulation period is not changed. Just when it comes to the calculation of the radiative transfer (in case of ADE) and the aerosol activation (AIE) the aerosol mass and number is scaled. We clarified it in the text (Section 2.1): "Note, that the aerosol scaling only comes into consideration when deriving the aerosol optical properties (with respect to ADE) and the aerosol activation (with respect AIE). All aerosol dynamic processes remain unaffected by the scaling."

(3) Please report aerosol properties that correspond to the simulations somehow in Table 1 or similar format. Did the aircraft campaign for this special issue make any aerosol measurements at all that are relevant for comparison? Can the simulated aerosol conditions be compared somehow and somewhere to measurements? I consider it mandatory to indicate in the manuscript in quantitative terms (beyond a multiplicative factor) what is the dynamic range considered in this study in terms of basic

measurable units such as CN, CCN, AOD, PM1, PM2.5 or the like.

Refers to (0). Furthermore we added a plot to quantify the aerosol change that is related to the aerosol scaling: - Review-Figure-11: Temporal evolution of median (a) total aerosol number (cm-3) and (b) total aerosol mass (mu g m-3) in the lowest 2 km AGL over Ivory Coast (7.5–3.0°W) between 2 July 15 UTC to 3 July 21 UTC for the clean (blue dashed), reference (black solid) and polluted case (red solid), based on the aerosol scaling introduced in Table 1.

(4) Owing to the leading role of direct effect, simulated single-scattering albedo should be somehow quantitatively reported from simulated values and compared to measurements or other at a minimum reported simulations somewhere relevant in Africa.

The SSA is calculated in COSMO-ART to derive the aerosol effect on radiation. However, the SSA is not a standard output variable and therefore is not available for a comparison with observations. As far as we know, SSA observations are not available within DACCIWA except of AERONET. AERONET has three relevant stations: KITcube Save, Ilorin and Koforidua. They provide the SSA but only in four discrete wavelength. COSMO-ART uses wavebands (intervals) so a direct comparison is not possible. To focus only on the time period 2-3 July 2016, as done in this study, allows no robust evaluation. The comparison of modeled and observed AOD is compared with AERONET and the CAMS model in Review-Figure-7 for a longer period. It supports our finding that the anthropogenic aerosol is overestimated in COSMO-ART likely due to the uncertainty in the emission inventories.

(5) The authors seem to focus on sensible heat flux without considering the role of soil moisture and latent heat flux (e.g., in the abstract and conceptual diagram). Is latent heat flux irrelevant at this location? Also at locations of previous studies? I have to assume that precipitation within the inner domain is negligible during the monsoon season and the surface starts out very dry, but that is not stated (please clarify in the text).

We agree on that and added the consideration of the latent heat flux in the text. According to that the latent heat flux curve is added in Figure 13 of the manuscript. See Review-Figure-12.

(6) Please clarify in the text how soil moisture is initialized in the simulations, whether results are sensitive to how that is done.

Since we focus on short time periods in the order of days, the COSMO-ART realizations are performed in NWP mode, the soil moisture is initialized via the meteorological boundary conditions of ICON. Therefore there is no long-term spinup of soil moisture as it is done for climate projections e.g. when using the CLM version of COSMO. NLLS is not related to significant amounts of precipitation (sporadical drizzle) and is therefore not altering the soil moisture. We expect that the cool and moist air, advected with AI, dominates the meteorological characteristics as presented in Figure 6. We agree that soil moisture is worth to focus on, when we talk about the onset of convection in the afternoon. However, the sensitivity of soil moisture on the aerosol-AI interactions is beyond the scope of our study. The soil moisture is also important when parameterizing the emission of mineral dust particles. In Deetz et al. (2016) I have shown that the soil moisture has significant impact on the mineral dust emission in Northeastern Germany. But for this SWA case study, the mineral dust contribution (primarily coming from the Sahara) is small and in this arid region the sensitivity towards soil moisture is of less importance than for central Europe.

(7) Please report whether simulations are sensitive to other factors, including inner or outer domain locations or sizes, grid mesh resolution, and boundary layer turbulence or cloud schemes.

As described in the answer to comment (0), we have conducted operational forecasts with COSMO-ART from 8 March to 31 July 2016 with a grid mesh size of 28 km and a large domain capturing wide areas of Africa (25W-40E,20S-35N). It reveals that this coarse setup including parameterized convection shows deficiencies in the

representation of the SWA meteorological conditions. The precipitation forecasts show less discriminance and incoming shortwave radiation and 2 m temperature are underestimated compared to Save observations. Therefore we decided not to use this data as boundary data for the nesting. We performed tests with a higher grid mesh size of 5 km, used explicit and parameterized convection, different turbulence closures available in COSMO and also tested it with and without the two-moment microphysics scheme. It turned out that by using the two-moment microphysics scheme and explicit convection best results are achieved with significant improvement towards the 28 km simulation (see attached Review-Figure-8 to Review-Figure-10, with 28 km grid mesh size (D1, blue) and 5 km (D2, green)) with Save supersite observations (black lines) as a reference.

- Review-Figure-13: Temporal evolution of the surface net downward shortwave radiation (W m-2) for the nine-day spin-up time (25 June - 3 July 2016) at Savè as observed (black, Energy Balance Station) and modeled with COSMO-ART (D1 in blue and D2 in green).

- Review-Figure-14: Temporal evolution of the 2 m temperature (°C) for the nine-day spin-up time (25 June - 3 July 2016) at Savè as observed (black, Energy Balance Station) and modeled with COSMO-ART (D1 in blue and D2 in green).

- Review-Figure-15: Temporal evolution of the 2 m relative humidity (%) for the nine-day spin-up time (25 June - 3 July 2016) at Savè as observed (black, Energy Balance Station) and modeled with COSMO-ART (D1 in blue and D2 in green).

Within this assessment, the turbulence closure had less impact on the results than the treatment of the convection. Therefore we used this 5 km COSMO-ART realization for the nesting simulations with 2,5 km grid mesh size.

(8) page 2, line 19: "react" –> "are" or other fix

We have changed the manuscript accordingly.

(9) page 3, line 1: "dependent" –> "dependence" or other fix

We have changed the manuscript accordingly.

(10) recommend to divide section 5 text up from one long paragraph currently

We agree on that and subdivided Section 5 in five paragraphs.

(11) recommend to guide the reader more graphically in following the transition from figure 2 (schematic diurnal cycle) to later figures (all in UTC), such as by indicating UTC time range on the panels of figure 2

We agree on that and added the approximated UTC time range in the caption of Figure 2. Nevertheless, it has to be noted that this is just a rough estimation. Kalthoff et al. (2018) show that the onset and the evolution of the NLLS can vary considerably from day to day and from one site to an other.

Additional References Deetz, K.: Assessing the Aerosol Impact on Southern West African Clouds and Atmospheric Dynamics, Dissertation, KIT Scientific Publishing, Karlsruhe, 75, 2018.

Deetz, K., Klose, M., Kirchner, I., and Cubasch, U.: Numerical simulation of a dust event in northeastern Germany with a new dust emission scheme in COSMO-ART, Atmos. Environ., 126, 87–97, 2016.

Interactive comment on Atmos. Chem. Phys. Discuss., https://doi.org/10.5194/acp-2018-186, 2018.

Printer-friendly version

Discussion paper

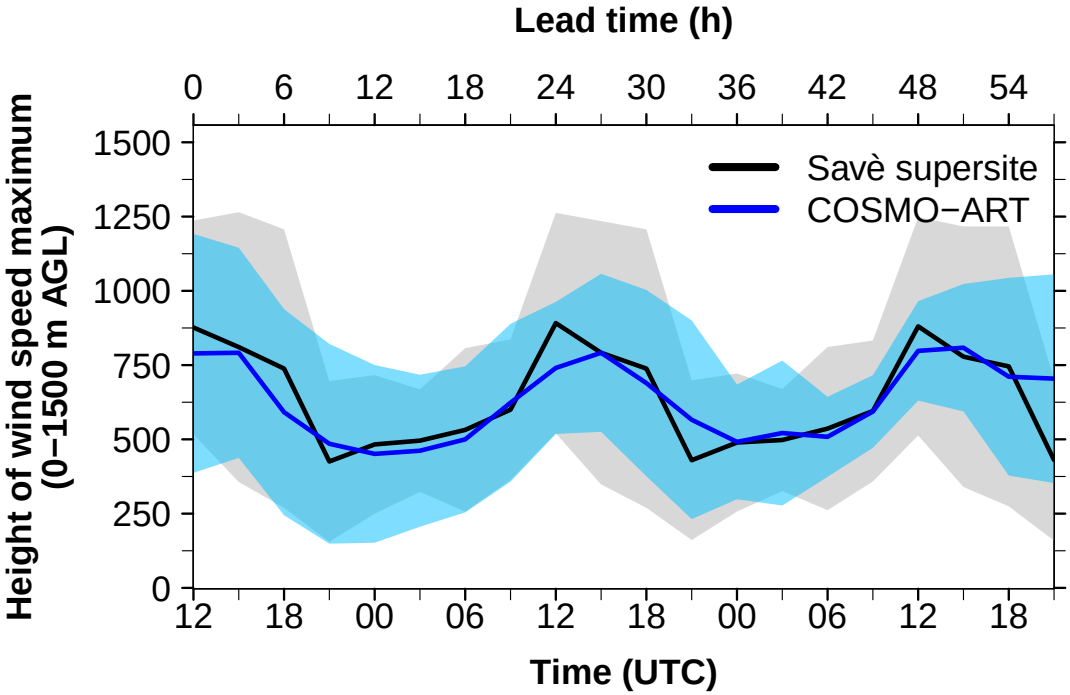

Fig. 1. Review-Figure-1: Temporal evolution of the height (m AGL) of the wind speed maximum between 0 and 1500 m AGL for the mean 57 h forecast lead time. (13 June - 30 July 2016) at Savè.

Printer-friendly version

Discussion paper

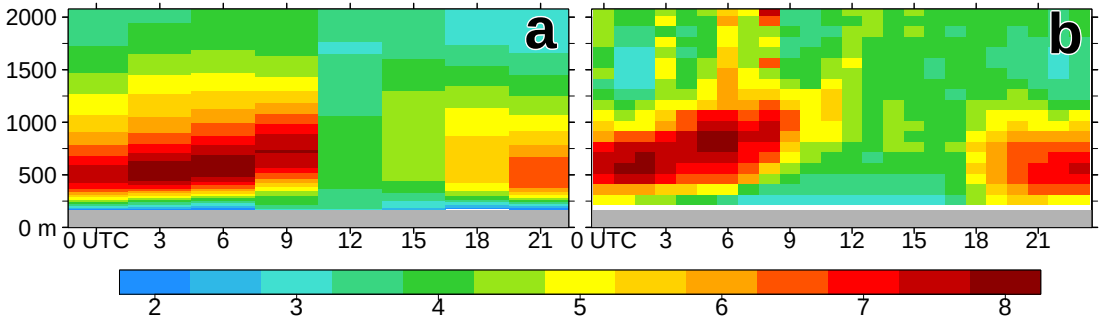

Fig. 2. Review-Figure-2: Wind speed profile (m s-1) between 0 and 2000 m ASL as mean diurnal cycle (13 June - 30 July 2016) at Savè for (a) COSMO-ART and (b) Doppler Lidar observation.

Printer-friendly version

Discussion paper

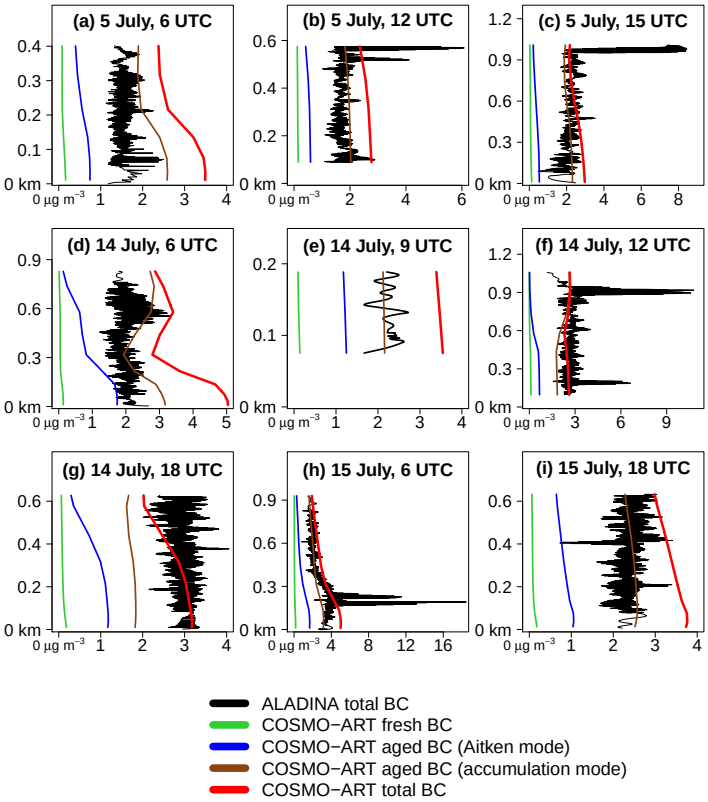

Fig. 3. Review-Figure-3: Vertical profiles (km AGL) of BC (mg m-3) at Savè for (a-c) 5 July 2016, (d-g) 14 July 2016 and (h-i) 15 July 2016.

Printer-friendly version

Discussion paper

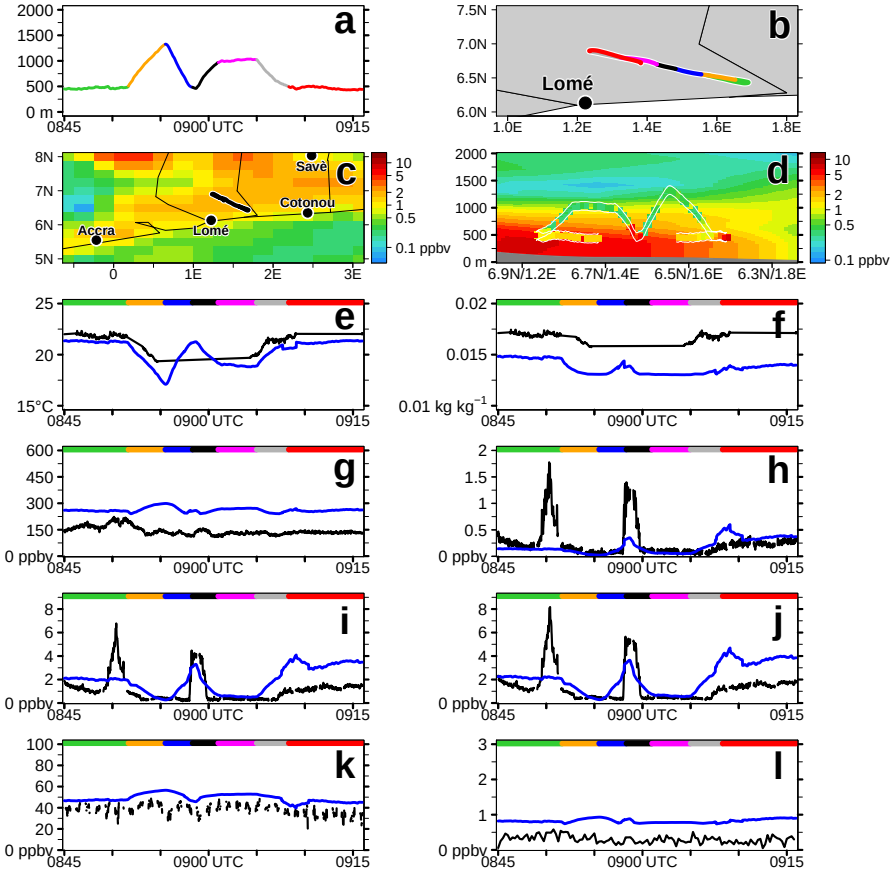

Fig. 4. Review-Figure-4: Comparison of Twin Otter measurement flight TO-16 (14 July 2016, 06:44 UTC to 09:50 UTC) results with COSMO-ART.

Printer-friendly version

Discussion paper

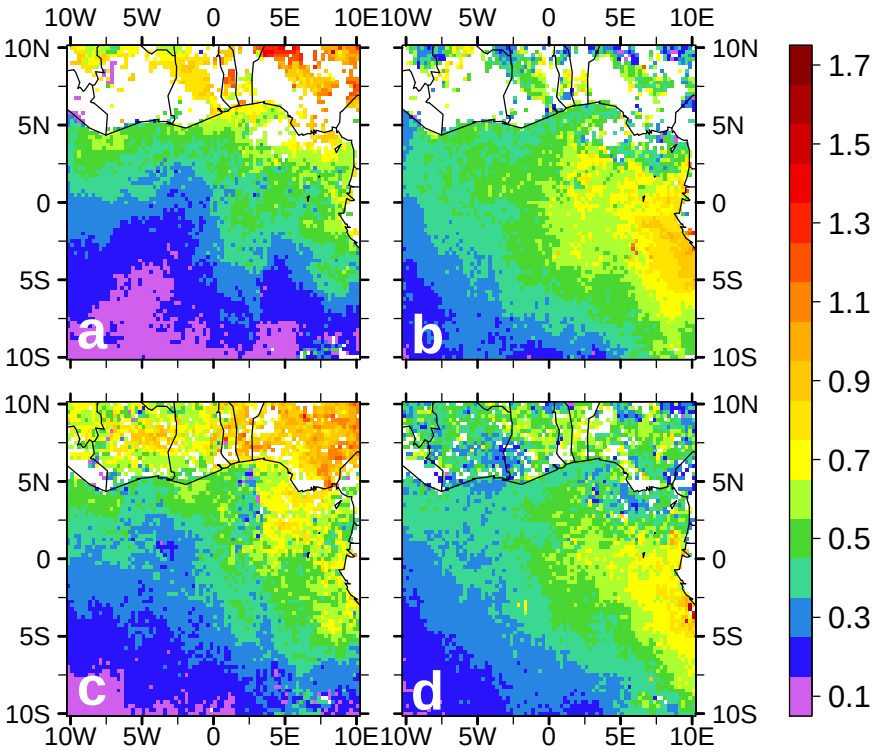

Fig. 5. Review-Figure-5: Mean total AOD averaged from 27 June to 17 July 2016 of (a) COSMO-ART collocated with MODIS Terra, (b) MODIS Terra, (c) COSMO-ART, collocated spatiotemporally with

Printer-friendly version

Discussion paper

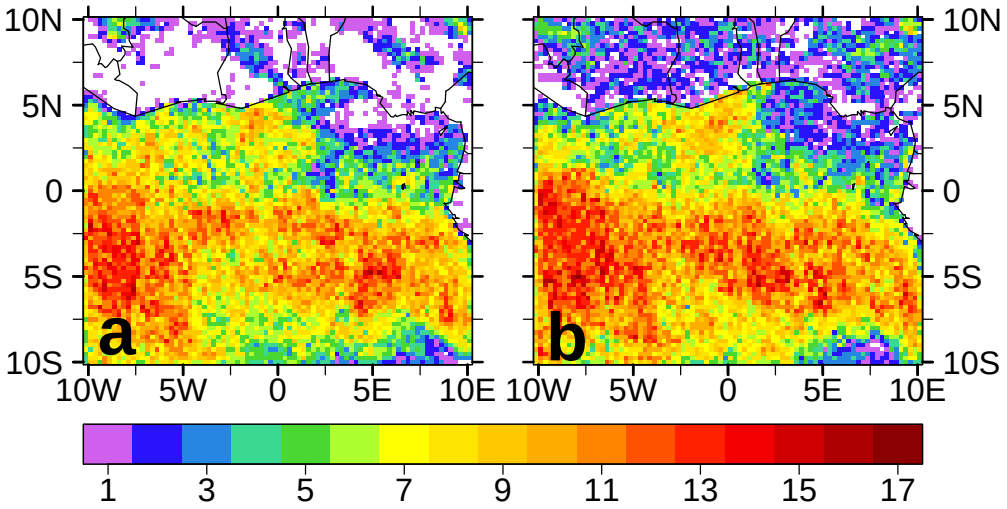

Fig. 6. Review-Figure-6: Number of observations within the time period 27 June - 17 July of (a) MODIS Terra and (b) MODIS Aqua.

Printer-friendly version

Discussion paper

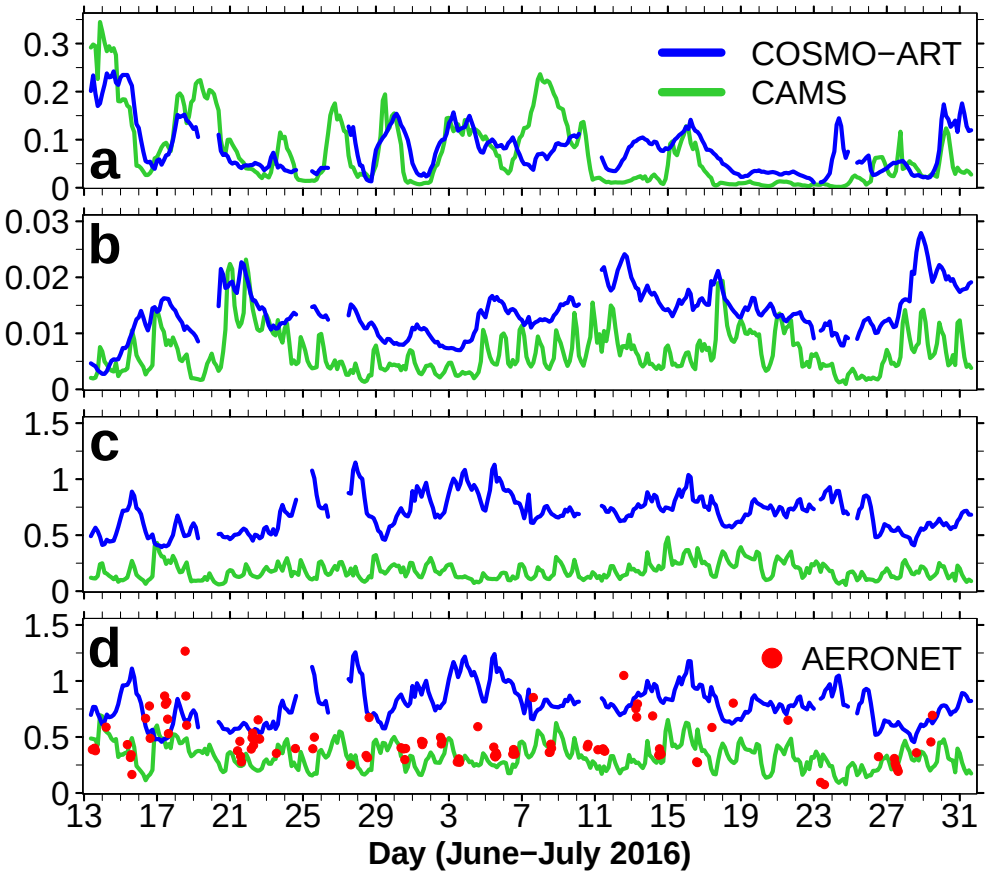

Fig. 7. Review-Figure-7: AOD (550 nm) at Savè from COSMO-ART (blue), CAMS (green) and AERONET (red) between 13 June - 31 July 2016 for (a) mineral dust, (b) sea salt, (c) anthropogenic aerosol and (d) total

Printer-friendly version

Discussion paper

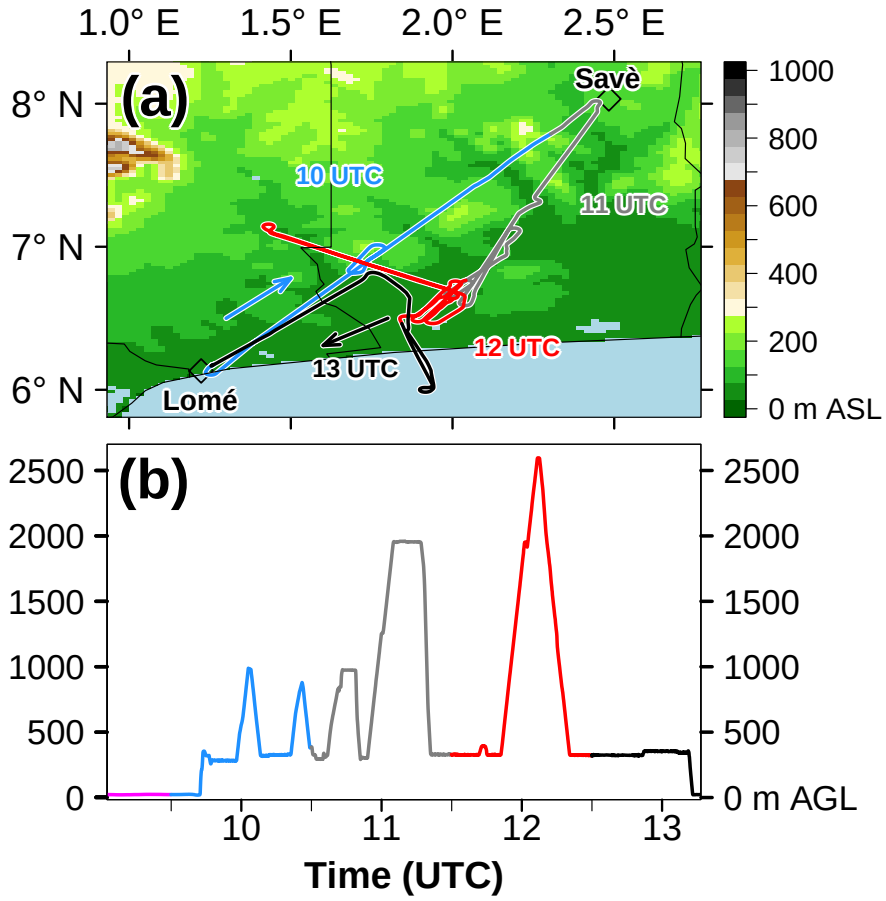

Fig. 8. Review-Figure-8: Flight track of the ATR42 SAFIRE on 3 July 2016 between 08:32 UTC and 13:13 UTC in (a) horizontal and (b) vertical dimension (m AGL). For (a) the topography (m ASL) is added. The flig

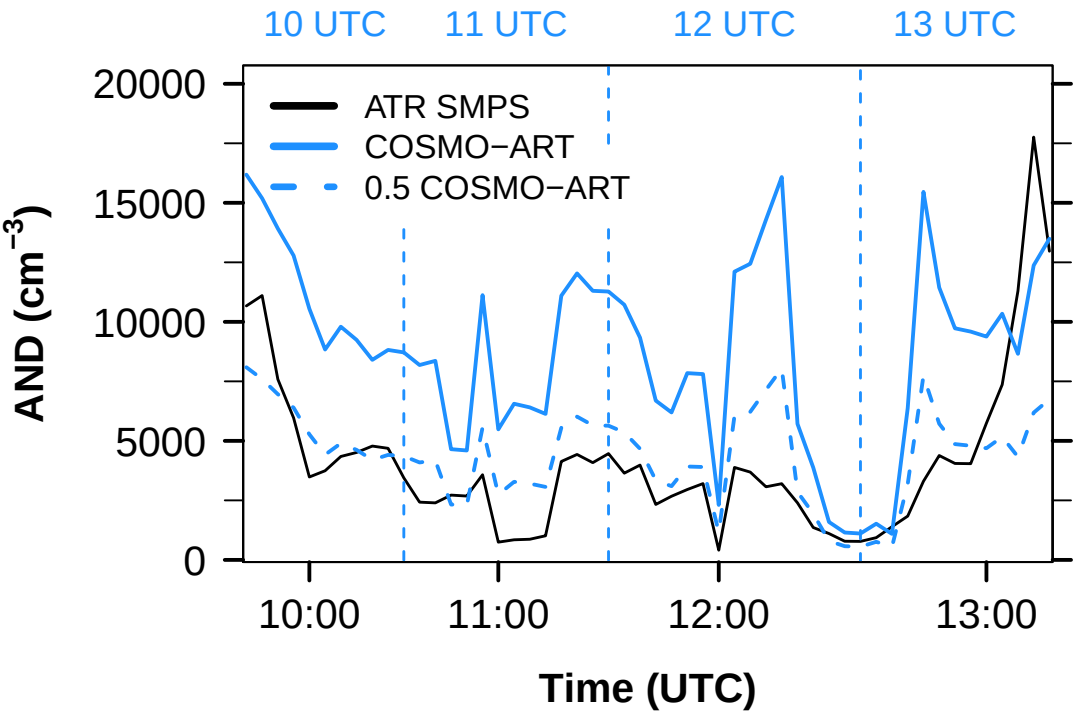

Fig. 9. Review-Figure-9: Aerosol number density (AND, cm-3) in the size interval 0.02 to 0.5 mu m as measured by the Spectrometer Scanning Mobility Particle Sizer (SMPS) on board the ATR42 (black) and modeled

Printer-friendly version

Discussion paper

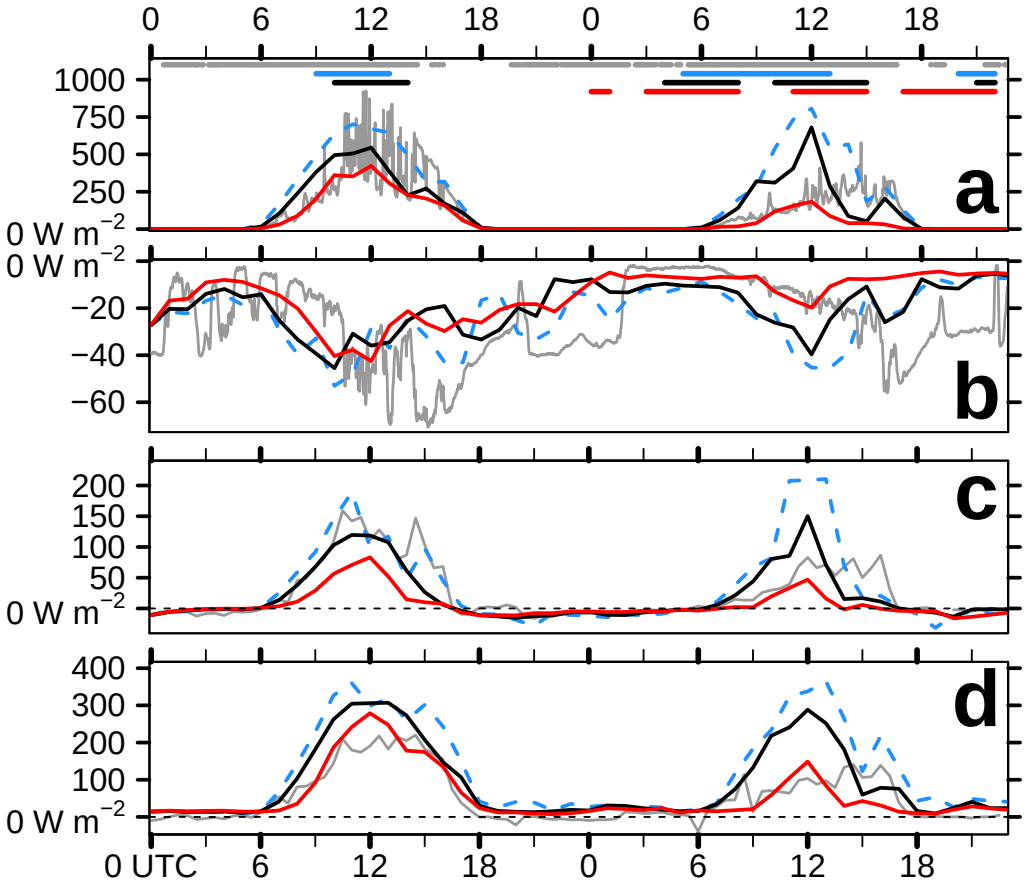

Fig. 10. Review-Figure-10: Comparison between Savè supersite observations (grey) and COSMO-ART reference (black), clean (blue) and polluted (red) of (a) net downward shortwave radiation (W m-2), (b) net downwa

Printer-friendly version

Discussion paper

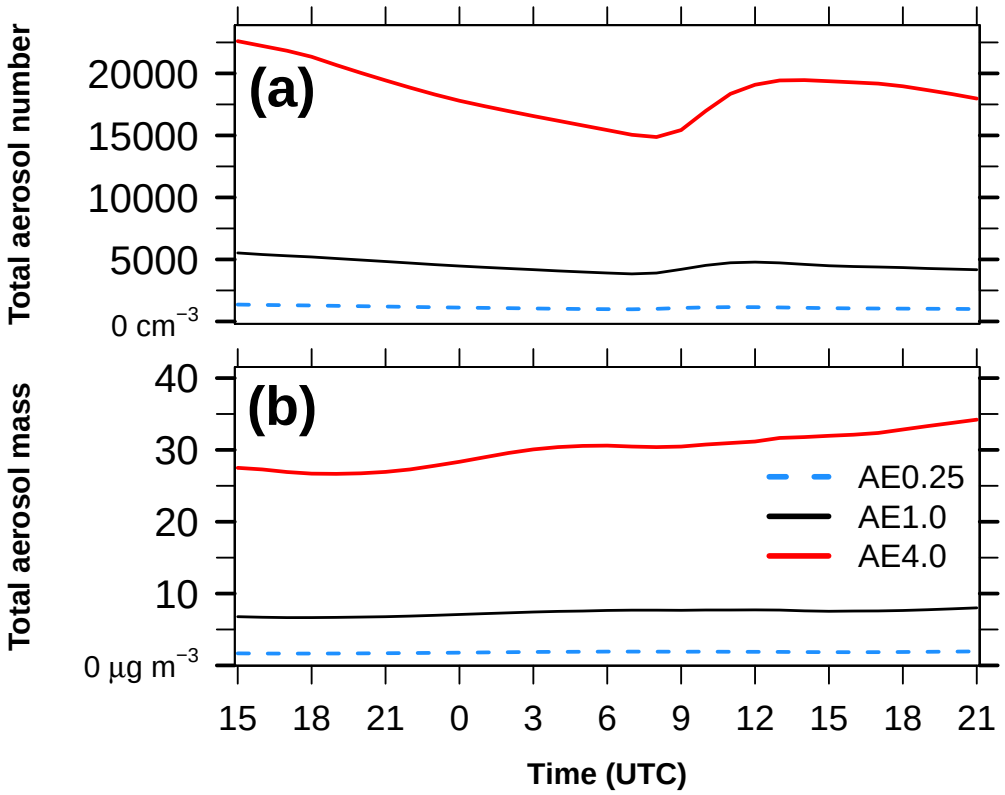

Fig. 11. Review-Figure-11: Temporal evolution of median (a) total aerosol number (cm-3) and (b) total aerosol mass (mu g m-3) in the lowest 2 km AGL over Ivory Coast (7.5–3.0°W) between 2 July 15 UTC to 3 Ju

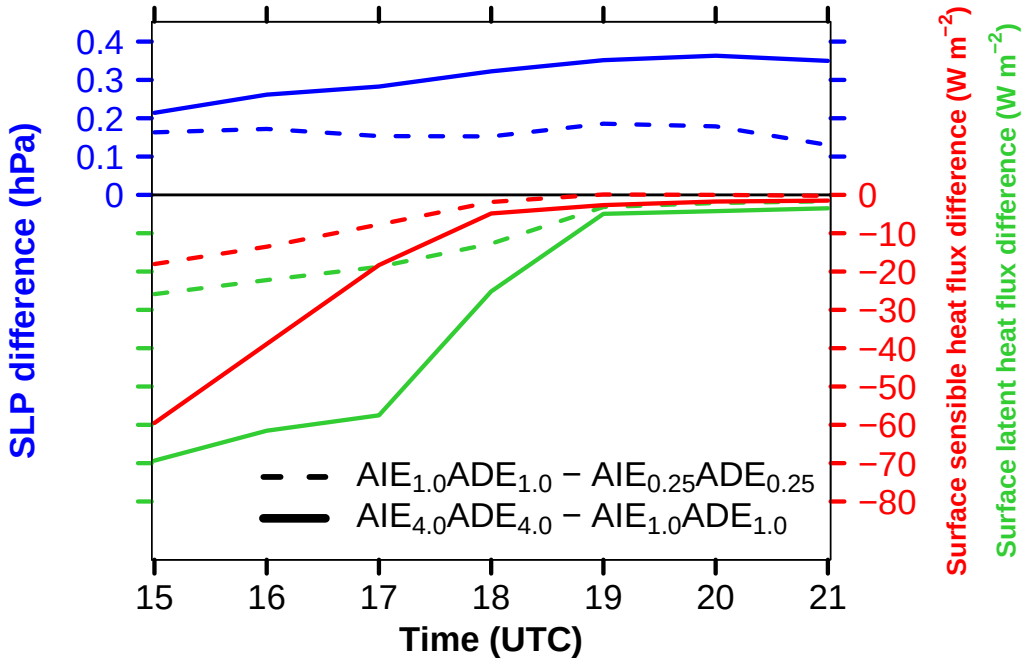

Fig. 12. Review-Figure-12: Temporal evolution of the differences in surface sensible heat flux (red, W m-2), surface latent heat flux (green, W m-2) and surface pressure (blue, hPa).

Printer-friendly version

Discussion paper

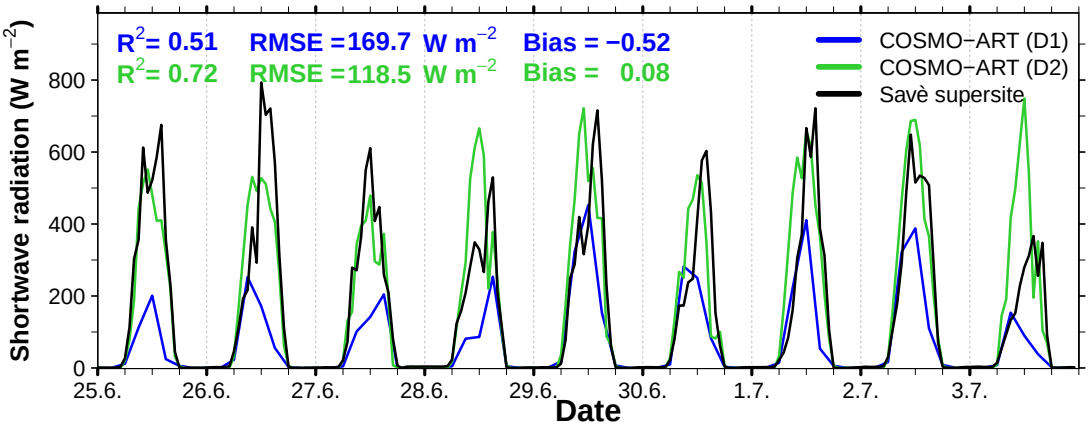

Fig. 13. Review-Figure-13: Temporal evolution of the surface net downward shortwave radiation (W m-2) for the nine-day spin-up time (25 June - 3 July 2016) at Savè as observed (black, Energy Balance Station) a

Printer-friendly version

Discussion paper

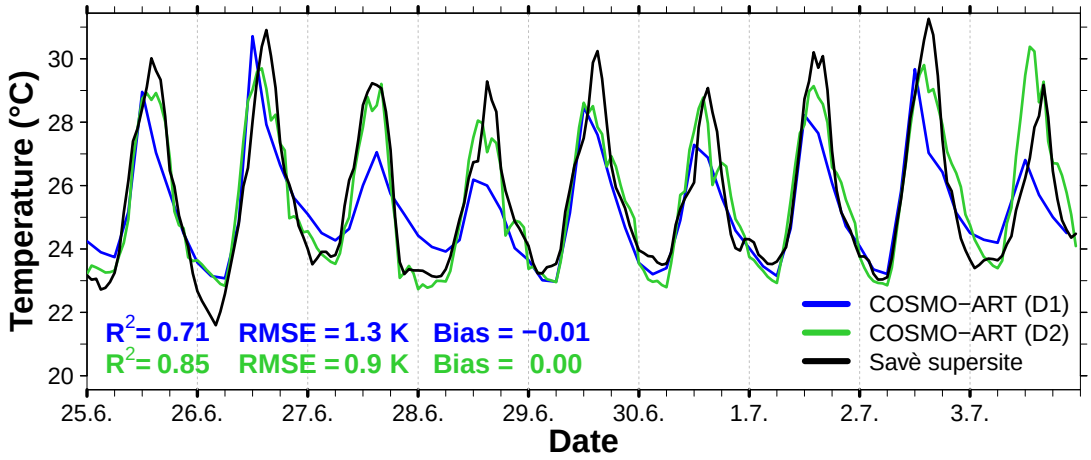

Fig. 14. Review-Figure-14: Temporal evolution of the 2 m temperature (°C) for the nine-day spin-up time (25 June - 3 July 2016) at Savè as observed (black, Energy Balance Station) and modeled with COSMO-ART (

Printer-friendly version

Discussion paper

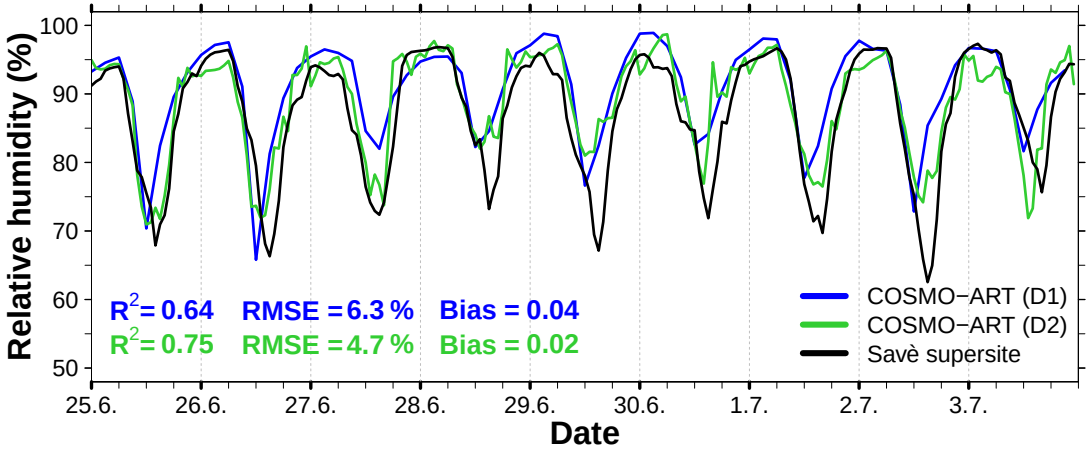

Fig. 15. Review-Figure-15: Temporal evolution of the 2 m relative humidity (%) for the nine-day spin-up time (25 June - 3 July 2016) at Savè as observed (black, Energy Balance Station) and modeled with COSMO-A

Printer-friendly version

Discussion paper

Atmos. Chem. Phys. Discuss.,
https://doi.org/10.5194/acp-2018-186-AC2, 2018

Atmospheric Chemistry and Physics Discussions

Interactive comment on "Cloud and aerosol radiative effects as key players for anthropogenic changes in atmospheric dynamics over southernWest Africa" *by* Konrad Deetz et al.

Konrad Deetz et al.

konrad.deetz@kit.edu

Received and published: 19 June 2018

Answer to Referee #2 Konrad Deetz 19 June 2018

Dear Referee (Atmospheric Chemistry and Physics),

thank you for your report from 16 April 2018. We have accounted for the comments and suggestions in the revised manuscript version. Please find our replies (marked with #) to the individual comments in the following. Before the detailed replies to your comments we want to stress one important overarching point: This study mainly focuses on the sensitivity of atmospheric dynamics and cloud properties to aerosols and not on a

Printer-friendly version

Discussion paper

detailed validation of the model system. Nevertheless, we have done a comprehensive evaluation of the model with the available observations of the DACCIWA measurement campaign. We show corresponding figures in our replies which appear at the end of this document. (The complete figure captions are given within the text because the figure caption space for the uploaded figures is not sufficient.)

Sincerely, Konrad Deetz on behalf of all coauthors

Referee comments:

(0) The authors focus on South West Africa, a region which is in a developing phase with an expected massive population growth and urbanisation. Therefore, an increase in anthropogenic aerosol concentration is expected. The authors assess the implication of aerosols and their possible changes on clouds and atmospheric dynamics. They present a process study with the regional model COSMO-ART. In particular, they discuss the impacts of aerosols on the propagation of the Atlantic Inflow frontal location and the Stratus to Cumulus Transition. In general, the paper is well written and the topic is of general interest. Deetz et al. conducted a detailed analysis of the performed simulations to understand the processes how aerosols influence prominent South West African dynamical features. Their main conclusions are based on three different simulations, the reference, the polluted and the clean case.

(1) I miss the discussion about the realistic representation of the current aerosol distribution in the model. Since an extensive measurement campaign took place during July 2016 it should be possible to evaluate the simulated distribution of aerosols against more measurements (here only a comparison with measures liquid cloud properties are shown).

The DACCIWA observations focus more on the eastern part of SWA and not on central Ivory Coast where we set the focus due to the pronounced evolution of the AI front. The supersites are located in Ghana, Benin and Nigeria. Remote sensing aerosol measurements are impeded by clouds and the supersites does not provide aerosol in-

formation apart from sun photometer observations. The only source of aerosol observations are the research aircrafts. And these information does not suffice to get a clear picture of the current aerosol distribution at least over Ivory Coast. The assessment of the current aerosol distribution is further impeded by the overall uncertainty of the emission datasets. Therefore, we can provide and assess effects of relative changes in the aerosol amount but cannot clearly define the actual state. As mentioned in the text, the period 3-4 July was selected because of extensive NLLS at Save, standing this day out as a golden day for further research. Unfortunately, for 3-4 July no aircraft observations were available for Ivory Coast. This data shortcoming we bypassed by evaluating the model in the eastern part of the domain via aircraft observations in the Lome-Save area (Fig. 3 and 4). To meet your concerns, we added further evaluations of aerosol properties in the Lome-Save area by using observations from the ATR42 SAFIRE aircraft. However, this evaluation focuses on the Lome-Save area and not on Ivory Coast. In Section 2.2 (Observational data) we added the following text: "The aerosol aerosol number density is evaluated using observations of the ATR42 SAFIRE (Service des Avions Français 25 Instrumentés pour la Recherche en Environnement) for the 3 July 2016. Additionally, the comparison of the modeled net downward shortwave and longwave radiation as well as the sensible and latent heat flux with Savè supersite is presented in Figure 19 of Appendix B. COSMO-ART reasonably reproduces the fluxes with lower fluxes with increasing aerosol as expected." In Section 4 (Evaluation of modeled cloud and aerosol properties with aircraft observations) we added the following text: "The research aircraft ATR42 SAFIRE also obtained aerosol properties in the Lomé-Savè area on 3 July 2016 (8:32–13:16 UTC). The flight track and altitude is presented in Figure 5, showing similar flight patterns compared to the Twin Otter (Fig. 3). By assuming dry aerosol, Figure 6 shows the comparison between COSMO-ART and the Spectrometer Scanning Mobility Particle Sizer (SMPS) to evaluate the Aerosol Number Density in the size range 0.02–0.5 mu m. Figure 6 reveals that the modeled aerosol number density shows a similar temporal evolution compared to the observations but has a constant bias, overestimating the observed aerosol number

Printer-friendly version

Discussion paper

density by a factor of about 2 (indicated by the blue dashed line). Therefore, in the subsequent study it has to be considered that the reference case shows already higher aerosol concentrations compared to the current state in SWA as quantified by the aircraft measurements. Overall, the evaluation reveals that COSMO-ART is capable to reproduce the aerosol situation on 3 July 2016 over SWA which is the basis for further sensitivity studies.

The figures related to this passage are attached in this review answer:

Fig.5 -> Review-Figure-1: Flight track of the ATR42 SAFIRE on 3 July 2016 between 08:32 UTC and 13:13 UTC in (a) horizontal and (b) vertical dimension (m AGL). For (a) the topography (m ASL) is added. The flight track in (a) and (b) is separated in hourly time steps for the subsequent collocation with hourly model data from COSMO-ART, highlighted by the pink (08:32âĂŤ09:30 UTC), blue (09:30–10:30 UTC), gray (10:30–11:30 UTC), red (11:30–12:30 UTC) and black color (12:30–13:13 UTC). Furthermore, the arrows in (a) indicate the flight direction with the takeoff at Lomé, the flight to Savè and the return to Lomé airport. Shortly. Note the meridional compression of the map in (a).

Fig.6 -> Review-Figure-2: Aerosol number density (AND, cm-3) in the size interval 0.02 to 0.5 mu m as measured by the Spectrometer Scanning Mobility Particle Sizer (SMPS) on board the ATR42 (black) and modeled with COSMO-ART (solid blue, reference case). The horizontal dashed blue line shows the COSMO-ART AND divided by 2. The vertical blue dashed lines indicate the COSMO-ART model output hours, which are compared to the observations.

Fig. 19 (Appendix B) -> Review-Figure-3: Comparison between Savè supersite observations (grey) and COSMO-ART reference (black), clean (blue) and polluted (red) of (a) net downward shortwave radiation (W m-2), (b) net downward longwave radiation (W m-2), sensible heat flux (W m-2) and latent heat flux (W m-2). The horizontal lines in (a) denote clouds over Savè in the observations and COSMO-ART.

(2) Since the direct aerosol effect depends mainly on the radiative properties of the aerosols it is of interest to show the aerosol composition in the region during the 2nd -3rd of July. And again, it would be helpful if the simulated aerosol radiative properties or the simulated radiative fluxes could be evaluated against observations. To understand the full meaning of polluted and clean case it is necessary to know about the aerosol content and composition in the reference case. Without that knowledge, a fractional increase or decrease is not meaningful. Do the authors change the aerosol concentration of the different types equally? This should be clarified in the revised manuscript.

Refers to (1). We see your point and to consider your remark we have added a comparison of net downward shortwave radiation, net downward longwave radiation, sensible heat flux and latent heat flux with respect to the supersite Save (Appendix B (Fig. 19) -> Review-Figure-3). Yes, all aerosol types are changed equally by the factor. We clarified the following sentence to make this more precise: " All aerosol modes and thus all aerosol types are changed uniformly by the factors."

(3) Another clarification is needed in terms of the general model setup. How are aerosols treated at the outer boundaries? Are they prescribed by output of global model simulations? The meteorological state is initialized every day at 0 UTC. Are the wind and temperature fields pulled back to the ICON forecast every day at 0 UTC? If yes, how is it possible to analyse the impact of the direct and indirect aerosol effect on the dynamics? I also wonder about the choice of the inner model domain (figure 1, indicated by red box). The western as well as the eastern and part of the northern boundary are located in a mountainous region. Could that cause problems due to resolution effects?

As denoted in Section 2.1 and Table 2, the COSMO-ART aerosol-interaction simulations (2.5 km grid mesh size) are realized via a nesting in a COSMO-ART realization with 5 km grid mesh size. For this simulation the aerosol boundary is taken from the global model simulation MOZART (see Tab. 2). Therefore, the aerosol coming from the

boundary into the domain of the 2.5 km domain is a combination of MOZART aerosol and aerosol that is emitted within the 5 km domain. Just for clarification: The aerosol scaling is just done within the aerosol activation and the radiative transfer calculation and not in the entire aerosol dynamics. Therefore it does not matter whether the aerosol is emitted locally in the 2.5 km domain or advected from outside. No, COSMO-ART does not include a two-way nesting. Therefore there is no feedback from the 2.5 km domain to the 5 km domain. This feature will be available in the new model system ICON-ART. Also without two-way nesting, the 2.5 km domain developes its on dynamics. The predominant wind direction is southwest via the monsoon flow. So the wind is coming from the southeast Atlantic. The SST is fixed in the 2,5 km realization as well as in the coarser domain (5 km). The aerosol effect on AI and SCT is therefore only and directly evolving in the 2.5 km realization because the southern AI "boundary condition" (incoming monsoon flow) and the northern AI "boundary condition" (saharan heat low) are unaffected. We are just focusing on the changes in between and this is the 2.5 km domain. The mountains heights in the domain are below 1 km, in most cases below 500 m. With the predominant wind direction southwest we have not faced any problems.

(4) Page 1 line 22: The population is expected to growth.

Please specify. Do you propose to replace the two sentences: "More than half of the global population growth between now and 2050 will occur in Africa. For Nigeria, which has a population of 182 million in 2015 (rank 7), a population increase to 399 million (rank 3) is expected for 2050 (UNO, 2015)." by your sentence? To highlight that especially SWA will be affected by a significant population increase which will be directly linked to a substantial enhancement of air pollution, we would like to include the population projections from UNO (2015).

(5) Page 2 line 19: Please replace “react” with “are”.

We agree on that and have changed the manuscript and the figures accordingly.

(6) Page 10 line 25: Please rewrite that sentence

Please specify. We are interested in the results of LES aerosol-atmosphere interaction simulations in the framework of DACCIWA since the aerosol effects on spatial scales of 100 m might be different to the COSMO-ART results on spatial scales of 2500 m. With this sentence we will express our interest and simultaneously provide an outlook and link to other research that is done in DACCIWA and which is related to our field of research.

(7) Table 1: I recommend to rename the simulations (the names are unnecessary long), ADE and AIE are scaled by the same factor, the simulations could be named as AE0.1, AE0.25... (AE = aerosol effect)

We agree on that and have changed the table as well as figure captions and legends accordingly.

(8) General remark: Maybe it is not necessary to present results of all 6 simulations. It underlines somehow the results but for the discussion it seems not to be important to present them. I recommend that the authors rethink the demand to present the AE0.1, AE0.5, AE2 simulations in the paper.

As you have remarked, the purpose of these additional realizations is to underline the results and to make the conclusions based on the realizations more robust. Just from three realizations it can hardly be concluded about the relationship of aerosol change and atmospheric response, e.g. whether it is linear or nonlinear. Your remark is in contrast to the remarks provided by referee #3, asking for longer simulation periods. These realizations are very expensive but we did these three additional runs and we gained added value from them. Furthermore, we are aware of the problem that showing results of all realizations might confuse the reader. Therefore only two selected figures present all realizations (Fig. 9 and 12). All other figures refer to the key realizations of clean, reference and polluted.

Interactive comment on Atmos. Chem. Phys. Discuss., https://doi.org/10.5194/acp-2018-186, 2018.

Printer-friendly version

Discussion paper

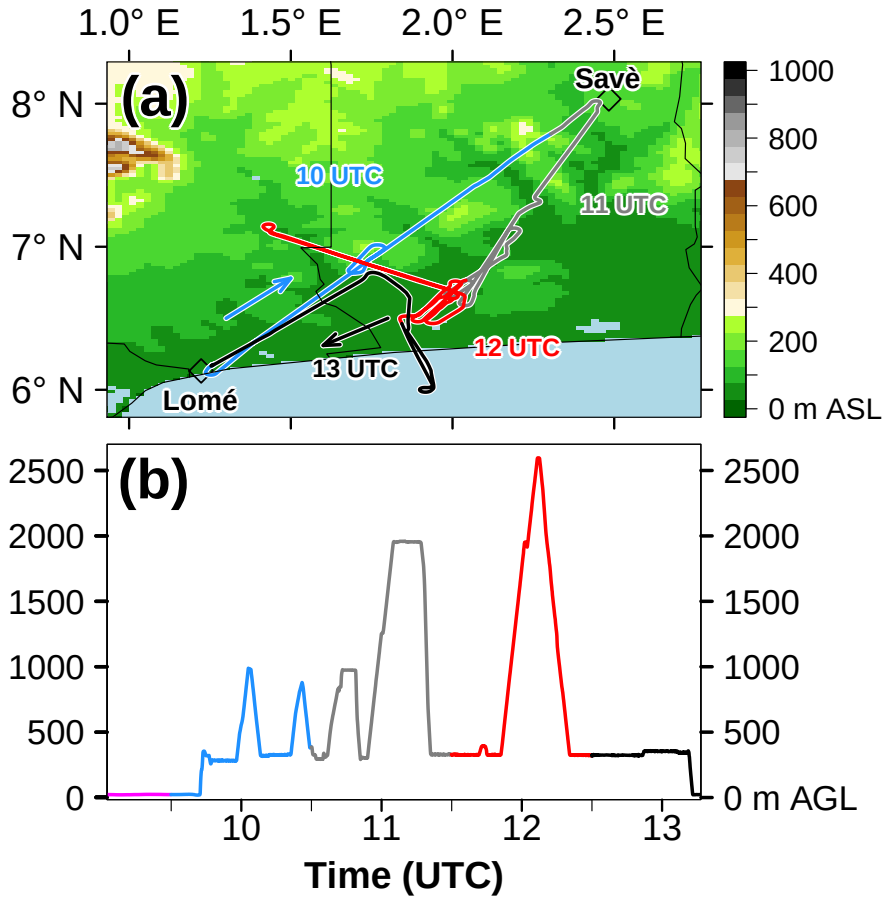

Fig. 1. Review-Figure-1: Flight track of the ATR42 SAFIRE on 3 July 2016 between 08:32 UTC and 13:13 UTC in (a) horizontal and (b) vertical dimension (m AGL). For (a) the topography (m ASL) is added. The flig

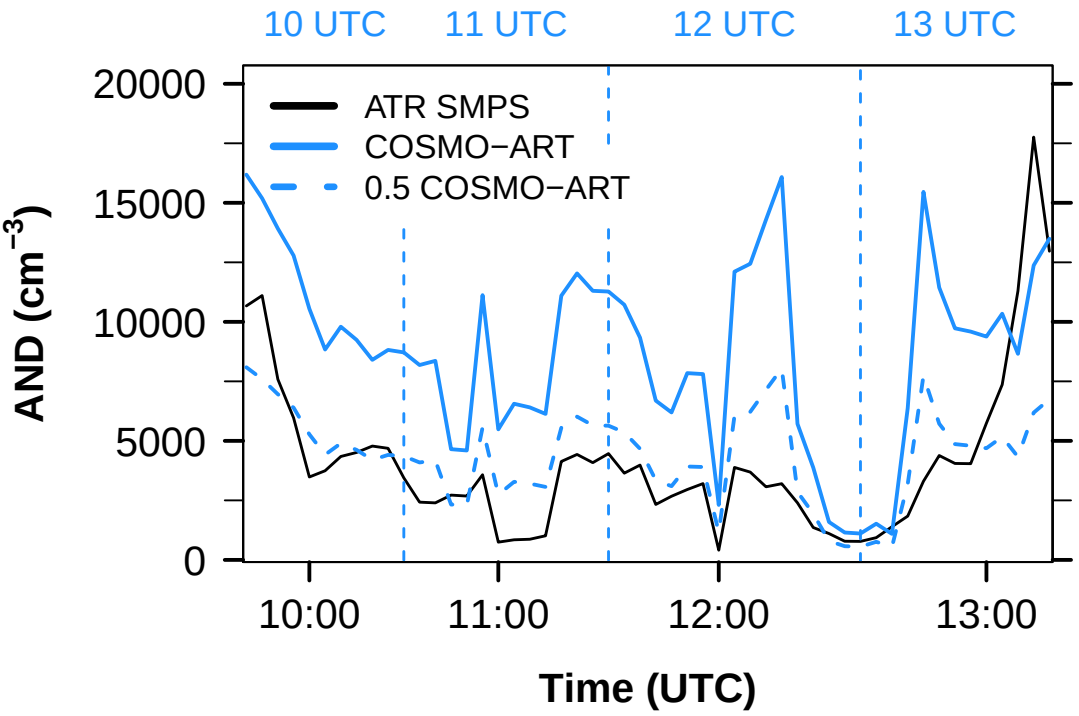

Fig. 2. Review-Figure-2: Aerosol number density (AND, cm-3) in the size interval 0.02 to 0.5 mu m as measured by the Spectrometer Scanning Mobility Particle Sizer (SMPS) on board the ATR42 (black) and modeled

Printer-friendly version

Discussion paper

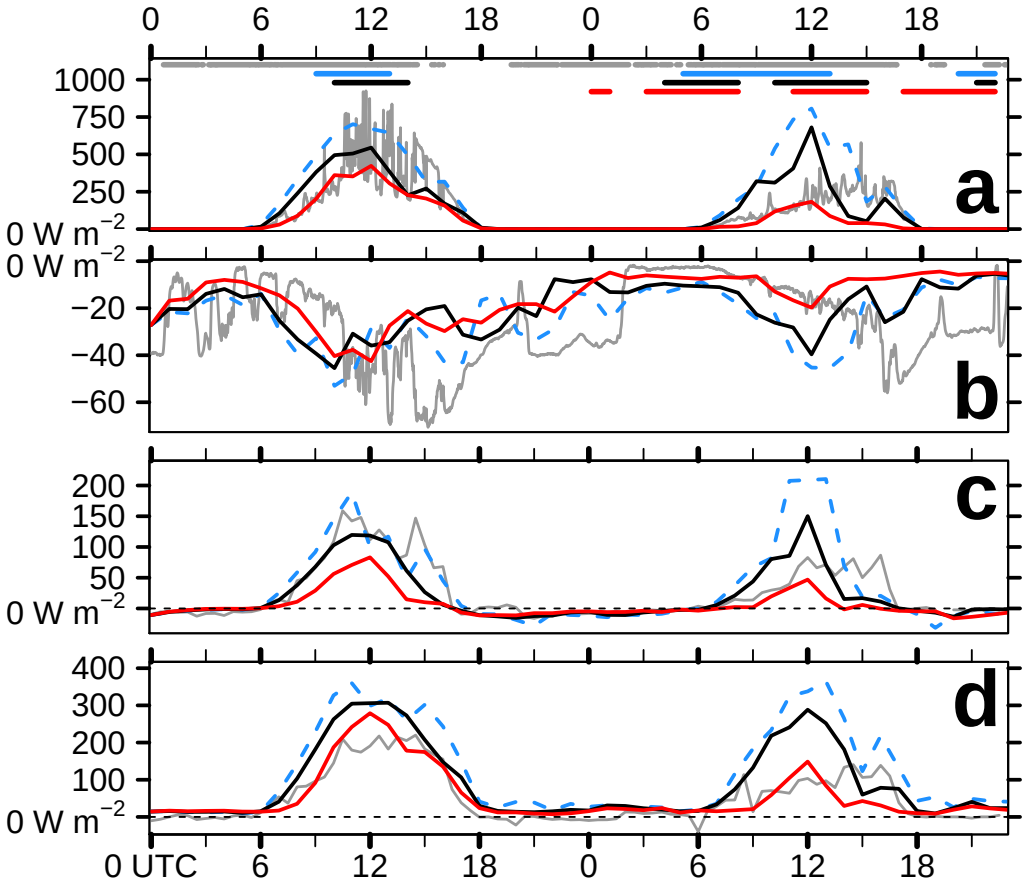

Fig. 3. Review-Figure-3: Comparison between Savè supersite observations (grey) and COSMO-ART reference (black), clean (blue) and polluted (red) of (a) net downward shortwave radiation (W m-2), (b) net downwar

Atmos. Chem. Phys. Discuss.,
https://doi.org/10.5194/acp-2018-186-AC3, 2018

Atmospheric Chemistry and Physics Discussions

Interactive comment on "Cloud and aerosol radiative effects as key players for anthropogenic changes in atmospheric dynamics over southernWest Africa" *by* Konrad Deetz et al.

Konrad Deetz et al.

konrad.deetz@kit.edu

Received and published: 19 June 2018

Answer to Referee #3 Konrad Deetz 19 June 2018

Dear Referee (Atmospheric Chemistry and Physics),

thank you for your report from 17 April 2018. We have accounted for the comments and suggestions in the revised manuscript version. Please find our replies (marked with #) to the individual comments in the following. Before the detailed replies to your comments we want to stress one important overarching point: This study mainly focuses on the sensitivity of atmospheric dynamics and cloud properties to aerosols and not on a

Printer-friendly version

Discussion paper

detailed validation of the model system. Nevertheless, we have done a comprehensive evaluation of the model with the available observations of the DACCIWA measurement campaign. We show corresponding figures in our replies.

Sincerely, Konrad Deetz on behalf of all coauthors

Referee comments:

(0) In this study, the authors ran a regional climate model COSMO-ART at convection-perming resolutions to examine the effects of aerosols on weather and climate based on a 2-day case study. They documented in detail how aerosol affects cloud and atmospheric dynamics over southern West Africa. They further presented detailed analysis of mechanisms that leads to these changes, and provide a conceptual model for this. I think overall the paper is well written, and it is great addition to existing literatures on aerosols effects on climate over Africa. I would recommend it publication after my following comments are addressed:

(1) I understand these are expensive simulations, but I still think it would be really nice if the authors can run model longer, say a month. The current results are interesting, but it is less clear how robust these results are. A longer simulation would definitely be more interesting, and may also produce more robust results.

We see your point. It would be great to have model results for the entire monsoon post-onset phase (22 June to 20 July), but as you said, the realizations are expensive, expensive with respect to computing time and also of handling the very large amounts of data. In terms of resources it is simply not feasible for us to realize this. Therefore, and after due consideration we decided to focus on the 3-4 July 2016, identified by the DACCIWA community as a golden day for further research. As denoted in the manuscript, from our experience during the measurement campaign, there is very small variation in the general meteorological conditions during the monsoon post-onset phase. Therefore we can assume well grounded, that our sample '3-4 July' within the post-onset phase is representative at least qualitatively for the entire post-onset phase

(nearly one month) without simulating the whole period. In our companion paper about the aerosol liquid water content in SWA, submitted on 26 April 2018 to ACP (also DACCIWA special issue) and which is likely soon also in the discussion phase, we added results of the 6-7 July in the Appendix (as a second sample within the monsoon post-onset phase), underlining that the conditions are similar from one day to another.

(2) Their model does have the capability to separately treat AIE and ADE. But in the paper, the authors examined the two effects together. Separating these two may help to answer whether AIE or ADE dominates in this case study.

The decision of using ADE and AIE together as well as using the same factor for both, within one realization, is made after due consideration. Generally, it is possible to have a realization just with AIE (ADE turned off). On the other hand it is not appropriate to have a realization just with ADE since you cannot simply switch off AIE. In any case you have to have aerosol as CCN. If you switch AIE off, you will use the aerosol climatology given in the two-moment scheme of COSMO instead. Simultaneously, in ADE you use the prognostic aerosol of COSMO-ART. This is totally inconsistent and does not allow any conclusions about the single effects of ADE and AIE. The alternative is to use the factors to change the aerosol that is seen by ADE or AIE, as it is done in this study. With this you can reduce e.g. AIE but still (consistently) the same aerosol description (COSMO-ART prognostic) is the basis for AIE and ADE. Now, the question about turning off one of the effects completely changed to the question of using different or the same factors within one realization. We have tested it to gain knowledge by using e.g. ADE0.1-AIE1.0. But again, this is physically inconsistent and cannot be interpreted in terms of realistic conditions in SWA. E.g. in ADE0.1-AIE1.0 the incoming solar radiation would be higher than it would appear in reality (less scattering and absorption), leading very likely to more convective processes (especially sensitive in tropical regions) and therefore implications on AIE that would not occur in the realistic setup ADE1.0-AIE1.0. Using different factors is only appropriate when using the factorialmethod proposed by Montgomery (2015). In my dissertation (Deetz,

2018) I used the factorial method to assess whether the AI frontal shift is caused by AIE or ADE. The findings underline that ADE is dominating the changes, nevertheless we decided not to have this method included in this publication because for robust results an ensemble approach is necessary as realized in Kraut (2015). To have one realization only with AIE (a) and one realization with AIE and ADE together (b) and assessing the effect of ADE by calculating (b) minus (a) is also problematic because this would not only include effects from ADE but also synergistic effects of AIE and ADE. By having the same factor for both effects, every realization is in itself consistent and allows for meaningful, physically-reasonable conclusions. Therefore we decided to use ADE and AIE together and with the same factors.

(3) Title: The paper is about aerosol effects on atmospheric dynamics in a case study. But the title said “cloud and aerosol radiative effects as key players for anthropogenic changes in atmospheric dynamics over southern West Africa”. I think the title is misleading and confusing. FirstïijNËĞ the paper is not about cloud radiative effectsïijN ËĞ though it does talk about aerosol radiative effects through its impact on clouds. But this is different from cloud radiatve effects. Second, the paper only documents aerosol effects on atmospheric dynamics based a case study from model simulations. “anthropogenic changes in atmospheric dynamics” may sound like this is what you observed. As this effect is purely a modeling study, I suggest the authors to clarify this in the title.

We rephrased the title: "Numerical simulations of aerosol radiative effects and their impact on clouds and atmospheric dynamics over southern West Africa"

(4) Section 2.1: model experiments and AIE. It looks like the authors can separately examine the effects of AIE and ADE, but in all model experiments documented here, AIE and ADE are examined together. If the authors examine AIE and ADE separately, this may help to clarify some points the authors made regarding the relative roles of AIE and ADE on SWA. This relates to some of the discussions in Section 6 (e.g., the last paragraph).

Refers to (2).

(5) Section 5: the first paragraph is overly long. Suggest to separate it into several short paragraphs with a focus theme in individual paragraphs.

We agree on that and have changed the manuscript accordingly.

(6) Page 9, line 21: what are these two numbers? The same question is also applied for next three lines (lines 22-24)

As denoted on page 9, line 18-19: "The following values in brackets indicate the median and the 99 th/1th percentile of the surface quantities considering the cloud-free inland area." With this we want to provide quantitative expressions of the observed changes that are consistent between the different meteorological parameters. We decided to present the median and the 99th percentile (in case an increase is observed) or 1th percentile (in case a decrease is observed). This is also consistent for the values in the next three lines.

(7) Page 10, line 4-5: an aerosol increase has large impacts than the aerosol decrease. This is a little bit surprise to me. I would expect when aerosol concentrations further increases, its effects saturate, and its effects decreases (e.g., numerous small particles compete for water vapor so a lower maximum supersaturation is expected). So can you elaborate what might happen here.

Figure 12 (old manuscript version) / Figure 14 (new manuscript version) shows that we have not reached the saturation point. Moreover the strong increase of the CDNC coincides with decrease in the cloud water content, a decrease in the effective radius and a decrease (increase) in light (heavy) precipitation in agreement with the convective invigoration mechanisms of warm clouds as described in Saleeby et al. (2014).

(8) Page 10, lines 12-14: The Twomey effect is also through changes in cloud optical thickness, but not through cloud water. So the second half of this statement is confusing.

We rephrased this sentence: Figure 12 reveals that the aerosol impact on radiation via the Twomey effect is very likely dominating the cloud-radiation interaction, whereas changes in the cloud water, that can also impact the radiative transfer and therefore the cloud formation, are insignificant.

(9) Page 10, lines 28-29: this statement is not clear to me ("it is interesting that ...").

"Nevertheless, it is interesting that the location of the AI front during its stationary phase over Ivory Coast could be used as a proxy for the aerosol burden in that area (under otherwise identical conditions)." The balance between the onshore monsoon flow and the vertical mixture of momentum over land due to turbulence leads to stationarity of the AI front around noon. The higher the aerosol burden, the smaller the vertical mixture of momentum over land and the more the onshore monsoon flow dominates in the denoted balance. Therefore the AI front is shifted inland but is still stationary. With that, the location of the AI front around noon, relative to the coast, is a proxy for the aerosol burden over land (at least in the model under otherwise same conditions).

(10) Page 10, the pressure gradient mechanisms: Here sea surface temperature was not affected by aerosol loading. So this overestimates the effects of aerosols on land-sea temperature differences. Any discussion on this?

Theoretically, we can expect a decrease in SST with increasing aerosol due to less incoming shortwave radiation via scattering and absorption. This SST decrease might lead to a decrease of the near-surface temperature over the ocean. (The near-surface temperature decrease over land due to the aerosol is actually happening in the model.) All in all, this would lead to a stronger land-sea temperature gradient and therefore to a less weak AI inland propagation compared to the results of the polluted case in the manuscript. To study aerosol effects on the SST and its feedbacks on AI, the NWP mode of COSMO is not appropriate. For that, climate studies with the CLM version of COSMO are more meaningful. However, we don't expect significant signals on SST, because on the one hand the surface water is continously moved by the Benguela

current and Southern Equatorial current and on the other hand, the biomass burning aerosol is reaching the Gulf of Guinea not continously but it arriving in plumes as visible e.g. in model realization of COSMO-ART and MACC. Therefore there will be no continuous cooling but a variation of cooled and warmed areas that might counterbalance. Furthermore, a regional (limited-area) model is less appropriate for studying this question, because only the near-surface water within the domain is affected but the incoming water is unaffected. Therefore a global model, consistently having the aersol impact on SST globally considered, would be more appropriate for this questions. We added the following sentence in the conclusions: "Effects on SST are not considered in this study. In case of considering the impact of reduced incoming solar radiation on the SST with increased aerosol, stronger land-sea temperature gradients are expected. Therefore, the estimations of this study with fixed SST denote the upper limit of the magnitude of the effects. However, this model setup in numerical weather prediction mode is less appropriate to study effects on SST. Global models on a longer time scale are more suitable to provide added value on this question."

Additional References Deetz, K.: Assessing the Aerosol Impact on Southern West African Clouds and Atmospheric Dynamics, Dissertation, Wissenschaftliche Berichte des Instituts für Meteorologie und Klimaforschung des Karlsruher Instituts für Technologie, KIT Scientific Publishing, Karlsruhe, 75, 171-172, 2018.

Kraut, I.: Separating the Aerosol Effect in Case of a "Medicane", Wissenschaftliche Berichte des Instituts für Meteorologie und Klimaforschung des Karlsruher Instituts für Technologie, Dissertation, 2015.

Montgomery, D. C.: Design and Analysis of Experiments, 5th ed., John Wiley, New York, 115, 684–686, 2005.

Interactive comment on Atmos. Chem. Phys. Discuss., https://doi.org/10.5194/acp-2018-186, 2018.

List of relevant changes made in the manuscript:

- update references
- apply new recommended abbreviations of the model realizations
- highlight the model evaluation efforts which were realized aside from this study
- add further aircraft observations to evaluate the modeled aerosol number density
- add radiation comparison between measurement and modeling results at Save supersite
- illustrate the aerosol change that comes along with the aerosol scaling realized in this study

~~Cloud and~~ Numerical simulations of aerosol radiative effects ~~as key players for anthropogenic changes in~~ and their impact on clouds and atmospheric dynamics over southern West Africa

Konrad Deetz[1], Heike Vogel[1], Peter Knippertz[1], Bianca Adler[1], Jonathan Taylor[2], Hugh Coe[2], Keith Bower[2], Sophie Haslett[2], Michael Flynn[2], James Dorsey[2], Ian Crawford[2], Christoph Kottmeier[1], and Bernhard Vogel[1]

[1]Institute of Meteorology and Climate Research, Karlsruhe Institute of Technology (KIT), Karlsruhe, Germany
[2]National Centre for Atmospheric Science, and School of Earth and Environmental Sciences, University of Manchester, Manchester, United Kingdom

Correspondence to: Konrad Deetz (konrad.deetz@kit.edu)

Abstract. Southern West Africa (SWA) undergoes rapid and significant socioeconomic changes associated with a massive increase in air pollution. Still, the impact of atmospheric pollutants, in particular that of aerosol particles, on weather and climate in this region is virtually unexplored. In this study, the regional-scale model framework COSMO-ART is applied to SWA for a summer monsoon process study on 2–3 July 2016 to assess the aerosol direct and indirect effect on clouds and the atmospheric dynamics. The modeling study is supported by observational data obtained during the extensive field campaign of the project DACCIWA (*Dynamics-Aerosol-Chemistry-Cloud Interactions in West Africa*) in June–July 2016. As indicated in previous studies, a coastal front is observed that develops during daytime and propagates inland in the evening (Atlantic Inflow). Increasing the aerosol amount in COSMO-ART leads to reduced propagation velocities with frontal displacements of 10-30 km and a weakening of the nocturnal low-level jet. This is related to a subtle balance of processes related to the decrease in near-surface heating: (1) flow deceleration due to reduced land-sea temperature contrast and thus local pressure gradient, (2) reduced turbulence favoring frontal advance inland and (3) delayed stratus-to-cumulus transition of 1-2 h via a later onset of the convective boundary layer. The spatial shift of the Atlantic Inflow and the temporal shift of the stratus-to-cumulus transition are synergized in a new conceptual model. We hypothesize a negative feedback of the stratus-to-cumulus transition on the Atlantic Inflow with increased aerosol. The results exhibit radiation as the key player governing the aerosol affects on SWA atmospheric dynamics via the aerosol direct effect and the Twomey effect, whereas impacts on precipitation are small.

1 Introduction

Atmospheric aerosol particles are highly relevant in terms of weather, climate and human health. They modify the formation of clouds and precipitation, alter the global radiation budget by scattering and absorption and can have adverse effects on the human respiratory system. The globally accelerated industrialization and urbanization are linked with increased emissions of anthropogenic pollutants, in particular in developing and newly industrializing countries.

Southern West Africa (SWA) is densely populated and affected by land use changes and global climate change. More than half

of the global population growth between now and 2050 will occur in Africa. For Nigeria, which has a population of 182 million in 2015 (rank 7), a population increase to 399 million (rank 3) is expected for 2050 (UNO, 2015). Based on these projections, Liousse et al. (2014) show that African anthropogenic emissions will significantly increase from 2005 to 2030, if no emission regulations are implemented. The atmospheric composition over SWA is marked by a superposition of local emissions and emissions from remote areas affecting SWA through long-range transports (in particular biomass burning pollutants, Mari et al., 2008). Emissions of mineral dust, sea salt, biomass burning pollutants, biogenic volatile organic compounds (BVOCs) and anthropogenic emissions from cities and industries with the special case of gas flaring from oil industries play a role. Knippertz et al. (2017) emphasize the complexity of these anthropogenic emissions resulting i.a. from transportation, wood and waste burning or charcoal production. Hopkins et al. (2009) estimate CO, NO_x and volatile organic compound emissions of the SWA megacity Lagos from aircraft measurements to be 1.44, 0.03 and 0.37 Mt yr^{-1}, respectively. Bahino et al. (2017) highlight the relevance of the emissions from domestic fires, with significantly increased NH_3 concentrations as well as traffic and industry.

We know very little about possible impacts on the regional meteorology, partly related to shortcomings in adequate observations. To overcome these shortcomings, the project *Dynamics-Aerosol-Chemistry-Cloud Interactions in West Africa* (DACCIWA, Knippertz et al., 2015) follows a combined observational and modeling effort for SWA. A comprehensive field campaign took place in June–July 2016 including extensive ground-based ~~(?)~~ (Kalthoff et al., 2018) and airborne measurements (Flamant et al., 2018).

With respect to clouds, SWA is characterized by frequent nocturnal low-level stratus (NLLS) and stratocumulus (e.g. Schrage and Fink, 2012; Schuster et al., 2013; van der Linden et al., 2015; Adler et al., 2017) that have a significant influence on the radiation budget (e.g. Hill et al., 2017). How sensitive the cloud radiative properties ~~react~~ are to high aerosol loadings has not been quantified. The modeling study of Lau et al. (2017) focuses on the impacts of aerosol-monsoon interactions on the variability over the northern Indian Himalaya Foothills during the summer of 2008. They highlight that the Aerosol Direct Effect (ADE), i.a. mineral dust transport and radiative heating-induced dynamical feedback processes, have major impacts on the large-scale monsoon circulation. The ADE leads to an increased north-south temperature gradient, a northward displacement of monsoon precipitation and an advanced monsoon onset over the Himalaya Foothills. The mineral dust leads to an increase in atmospheric stability via the aerosol semi-direct effect, whereupon the Aerosol Indirect Effect (AIE) may further enhance ADE by the convective-cloud invigoration mechanism (Rosenfeld et al., 2008). Lau et al. (2017) underline the need to consider aerosol-monsoon interactions even in short-term numerical forecasting of the monsoon circulation and precipitation.

In a modeling study of marine warm-cloud regimes, Saleeby et al. (2014) show that an increase in the amount of cloud condensation nuclei promotes and accelerates the Stratus-to-Cumulus Transition (SCT) due to an increase in evaporation and entrainment at the stratus top and deeper penetrating cumuli within the stratus that lead to a dissolution of the surrounding stratus via entrainment and subsequent subsidence of cold air. Furthermore, the study indicates a domain-wide reduction of clouds with moderate precipitation but a localized precipitation intensification via the convective-cloud invigoration mechanism. The interaction between AIE, the land surface characteristics and tropical sea breeze convection over Cameroon was analyzed by Grant and van den Heever (2014) for boreal summer conditions. The study reveals a weakening of the sea breeze

front with increasing aerosol, due to a reduction in surface shortwave radiation and therefore surface heating, linked with less precipitation. Stevens and Feingold (2009) and Fan et al. (2016) emphasize the need to analyze AIE ~~cloud-regime dependent~~ in dependence of cloud regimes with fine-scale models to explicitly resolve the interacting processes rather than using global models with parameterizations. This is supported by the study of Marsham et al. (2013), which reveals that the West African Monsoon (WAM) representation in the UK Met Office Unified Model shows fundamental differences between realizations with explicit and parameterized moist convection. A comprehensive overview of the current state of research on the AIE is presented in Fan et al. (2016).

This study focuses on the assessment of the aerosol impact on clouds and the atmospheric dynamics over SWA using a two-day process study. The following research questions encompass the focus of this study: What are the dominating aerosol impacts on meteorological characteristics over SWA and which spatial and temporal scales do they exhibit? Do we see changes in radiation and precipitation? To which extent does altered cloud radiative properties play a role?

This study is structured as follows: Section 2 decribes the model system COSMO-ART employed in this study together with the observational data used for evaluation. In Section 3 the *Atlantic Inflow* (AI) and *Stratus-to-Cumulus Transition* (SCT) as prevailing meteorological characteristics in SWA are introduced. The results comprise an evaluation of the modeled cloud properties with aircraft observations (Sect. ??4), the COSMO-ART representation of AI (Sect. 5) and the aerosol impact hereon (Sect. 6). The study concludes with a summary and evaluation of the findings (Sect. 7).

2 Methods and data

2.1 Model framework and setup

For this study, the regional-scale model framework COSMO-ART (Consortium for Small-scale Modeling - Aerosols and Reactive Trace gases, Vogel et al., 2009) is used. COSMO-ART is based on the operational weather forecast model COSMO (Baldauf et al., 2011) of the German Weather Service (DWD). The ART extensions allow for an online treatment of the aerosol dynamics and atmospheric chemistry. The model application of this study is accompanied with significant further developments of the emission parameterizations regarding mineral dust (Rieger et al., 2017) and BVOCs (Weimer et al., 2017). Furthermore, a parameterization for trace gas emissions from gas flaring of the oil industry was developed to reproduce the specific pollution conditions of the research area (Deetz and Vogel, 2017). The model domain comprises Ivory Coast, Ghana, Togo, Benin and the Gulf of Guinea (red rectangles in Fig. 1). The model setup is summarized in Appendix A.

The simulations using the setup denoted in Table 2 are the result of a nesting into a 5 km COSMO-ART simulation (blue rectangle in Fig. 1a) using the ICON operational forecasts (approximately 13 km grid mesh size) as meteorological boundary conditions. These cover the time period 25 June to 3 July to allow for an aerosol-chemistry spin up. The meteorological state is initialized every day at 0 UTC.

To assess the sensitivity of the ADE and AIE on the meteorological conditions, two factors F_{ADE} and F_{AIE} were introduced in COSMO-ART, which allow to scale the total aerosol mass and number densities, respectively, by simultaneously preserving the underlying aerosol distribution. All aerosol modes are changed uniformly by the factors~~but the scaling is limited to the~~

derivation of . Note, that the aerosol scaling only comes into consideration when deriving the aerosol optical properties in case of ADE(with respect to ADE) and the aerosol activation in case of AIE(with respect AIE). All aerosol dynamic processes remain unaffected by the scaling. Within a simulation the constraint F_{ADE}=F_{AIE} is used to allow for physically consistent results. Table 1 summarizes the realizations used in this study. F_{ADE}=F_{AIE}=1.0 is used as the reference case whereas the factor variations 0.1, 0.25, 0.5, 2.0 and 4.0 are applied to assess the aerosol sensitivity. The terms *clean*, *reference* and *polluted* should be seen in a relative sense as a part of this experimental setup. They do not imply general evaluation of the SWA aerosol conditions. The period 2–3 July was selected due to the intense and persistent NLLS at Savè supersite during that time (?) (Kalthoff et al., 2018) . Furthermore, 3 July is the center of the monsoon *Post-onset phase* and it is expected that the undisturbed monsoon condition favor and support the process studies. Since the meteorological conditions show less variation from day to day, it is assumed that, even with a focus on a very short time period, insight can be achieved that can be generalized at least qualitatively to the length of the *Post-onset phase* (22 June – 20 July).

2.2 Observational data

Within the DACCIWA project, an extensive field campaign took place in June–July 2016 in SWA (Fig. 1b) (Flamant et al., 2018). The time period was selected to capture the onset of the WAM and a period characterized by increased cloudiness. The DACCIWA ground-based measurement campaign encompassed the time period from 13 June to 31 July 2016, including the three supersites Kumasi (Ghana), Savè (Benin) and Ile-Ife (Nigeria) (red dots in Fig. 1b). A complete overview of the DACCIWA ground-based measurement campaign, their supersites, instrumentation and a first insight into the available data is presented in ? Kalthoff et al. (2018) . The DACCIWA airborne measurement campaign captured the time period from 27 June to 17 July 2016 (Flamant et al., 2018). The focus of this study is on Ivory Coast and therefore less observational data from the DACCIWA campaign is available for evaluation. However, a substantial evaluation with respect to meteorology and air pollution is realized with COSMO-ART over SWA with respect to other time periods and by focusing on the eastern part of the research area which is not presented in this study but can be found in Deetz (2018) . For this study, observations of the liquid cloud properties from the CDP-100 (Cloud droplet probe, data revision 3) of the British Antarctic Survey (BAS) Twin Otter aircraft on 3 July 2016 are used for a comparison with COSMO-ART. The CDP-100 is a wing mounted canister instrument including a forward-scatter optical system to measure the cloud droplet spectrum between 2-50 μm with a frequency of 1 Hz. The aerosol aerosol number density is evaluated using observations of the ATR42 SAFIRE (Service des Avions Français Instrumentés pour la Recherche en Environnement) for the 3 July 2016. Additionally, the comparison of the modeled net downward shortwave and longwave radiation as well as the sensible and latent heat flux with Savè supersite observations (Kohler et al., 2016) is presented in Figure 19 of Appendix B. COSMO-ART reasonably reproduces the fluxes with lower fluxes with increasing aerosol as expected.

3 SWA meteorological characteristics

Knippertz et al. (2017) separated the DACCIWA measurement campaign period into phases of similar meteorological conditions by using the precipitation difference between the coastal zone and the Soudanian-Sahelian zone. The monsoon *Onset phase* is identified as the period 16–26 June. The monsoon *Post-onset phase*, characterized by undisturbed monsoon conditions, is identified between 22 June and 20 July. Especially in the *Post-onset phase*, SWA is frequently covered by NLLS ~~(Knippertz et al., 2017; ?)~~ (Knippertz et al., 2017; Kalthoff et al., 2018) . The formation mechanisms of NLLS are not entirely clear. Figure 2 is a schematic to emphasize the general meteorological patterns relevant for the subsequent process study. In the nighttime a frequent occurrence of a nocturnal low-level jet (NLLJ, black arrows in Fig. 2a) can be observed with a jet maximum at 300 m above ground level (AGL) of around 6 m s^{-1} ~~(?)~~ (Kalthoff et al., 2018) . The NLLS is formed at the height of the jet maximum via shear-driven vertical mixing of moisture and maintained via cloud-top radiative cooling and cold advection (Schuster et al., 2013). Also topographic lifting (Schuster et al., 2013; Adler et al., 2017) as well as vertical cold air advection in gravity waves and cloud formation upstream of existing clouds contribute to the NLLS formation (Adler et al., 2017). After sunrise a gradual SCT takes place ~~(e.g. ?)~~ (e.g. Kalthoff et al., 2018) . This is accompanied by a lifting of the cloud base (Fig. 2b). The increase of the liquid water path shortly after sunrise is related to the growth of the convective boundary layer. Further analysis of this topic will be conducted within the framework of DACCIWA using observational data gathered during the ground-based field campaign. In the morning hours the maximum spatial coverage of NLLS can be observed (Fig. 2b). In the subsequent hours the NLLS deck breaks up to cumuliform clouds (Fig. 2c). Adler et al. (2017) identify a regular occurrence of a stationary coast-parallel front over SWA about 30 km inland that propagates northwards during undisturbed monsoon conditions after about 16 UTC. Similar characteristics were described in Grams et al. (2010) for Mauritania. Grams et al. (2010) indicate that the stationarity results from a balance between horizontal advection with the monsoon flow over the ocean and inland turbulence in the boundary layer that mixes the momentum vertically (Fig. 2d). With the reduction in turbulence in the afternoon the front begins propagating inland. The studies of Grams et al. (2010) and Adler et al. (2017), both based on modeling studies using the COSMO model, highlight the need to distinguish this feature from the land-sea breeze and the sea breeze front, since the dominating monsoon flow suppresses the formation of a land wind during night. In the following, we use the term *Atlantic Inflow* (AI) as proposed by Grams et al. (2010), which is connected with an AI front and an AI airmass located behind the front. The potential feedbacks between the aerosol on the one hand and the NLLS and the AI front on the other hand have not been quantified for SWA.

4 Evaluation of modeled cloud and aerosol properties with aircraft observations

To evaluate the modeled cloud properties, observations of the research aircraft *British Antarctic Survey (BAS) Twin Otter* on 3 July 2016 between 10:47 UTC and 14:06 UTC (flight number TO-02) are used, capturing the Lomé-Savè area. The following figures show the flight path and altitude (Fig. 3) as well as the observed and modeled cloud droplet number concentration (CDNC, Fig. 4a,b) and effective radii (Fig. 4c,d). The aircraft position between 10:45–11:30 UTC, 11:30–12:30 UTC, 12:30–13:30 UTC and 13:30–14:06 UTC is shown in blue, grey, red and black, respectively, for the flight track (Fig. 3a) and the

altitude (Fig. 3b). For a more robust statistical comparison of the observed and modeled cloud location, the comparison with COSMO-ART is not realized along the flight track but by using the cubes that are spanned horizontally by the rectangles around the flight track sections for 11-14 UTC (according to the hourly output of COSMO-ART) and vertically by the lowest 2.3 km AGL in accordance to the Twin Otter maximum flight altitude during this flight. The observed and modeled CDNC and effective radii are compared via boxplots (Fig. 4) for the flight track sections at 2 July between 11 UTC and 14 UTC. The boxplot colors follow the definition in Figure 3. For 11 UTC, the observations are omitted since the Twin Otter did not penetrate clouds during that time. The modeled CDNC (Fig. 4b) are generally higher than the observed ones (Fig. 4b) but both stay below a median of 400 cm^{-3}. The model shows a general trend of increasing median CDNC with time. This is expected during the SCT, since cumulus clouds tend to have a higher CDNC than stratus. Miles et al. (2000) provided a data base of observed cloud properties of low-level stratiform clouds. For example for the Madeira Islands they identified CDNC around 50 cm^{-3} for nocturnal stratiform clouds and around 300 cm^{-3} for cumulus and stratocumulus. The smaller CDNC at 14 UTC is likely related to a reduced number of observations in clouds due to the approach of the Twin Otter at Lomé. In addition to the uncertainty in the modeled aerosol number and number of activated particles also the limited number of cloud penetrations of the Twin Otter can contribute to the deviations. The Twin Otter did not fly continuously in clouds but performed descents and ascents (see Fig. 3b). The modeled increase in CDNC with time in Figure 4b is related to a slight decrease in the effective radii in Figure 4d. Generally, the observed and modeled median effective radii are around 6 μm and thus in good agreement.

The research aircraft ATR42 SAFIRE also obtained aerosol properties in the Lomé-Savè area on 3 July 2016 (8:32–13:16 UTC). The flight track and altitude is presented in Figure 5, showing similar flight patterns compared to the Twin Otter (Fig. 3). By assuming dry aerosol, Figure 6 shows the comparison between COSMO-ART and the Spectrometer Scanning Mobility Particle Sizer (SMPS) to evaluate the Aerosol Number Density in the size range 0.02–0.5 μm.

Figure 6 reveals that the modeled aerosol number density shows a similar temporal evolution compared to the observations but has a constant bias, overestimating the observed aerosol number density by a factor of about 2 (indicated by the blue dashed line). Therefore, in the subsequent study it has to be considered that the reference case shows already higher aerosol concentrations compared to the current state in SWA as quantified by the aircraft measurements. Overall, the evaluation reveals that COSMO-ART is capable to reproduce the aerosol situation on 3 July 2016 over SWA which is the basis for further sensitivity studies.

5 Model representation of the Atlantic Inflow (AI)

All the realizations in Table 1 exhibit the AI phenomenon. Following Grams et al. (2010), the AI front position can be estimated by the location at which a specific isentrope of virtual potential temperature $\theta_{v,s}$ crosses a specific height h_s. For Mauritania Grams et al. (2010) used $\theta_{v,s}$=310 K at the surface pressure level. For this study, reasonable results are achieved by using the potential temperature θ_s=302 K and the height h_s=250 m AGL. These values are selected empirically and are related to the COSMO-ART results of this study. They do not claim general applicability. However, in contrast to the definition in Grams et al. (2010), here it seems more appropriate to use a level elevated from the ground to identify the front, since the frontal

gradients are most prominent at the height of the NLLJ axis (about 250 m AGL), whereas the frontal passage is hard to detect in surface observations (N. Kalthoff, personal communication).

Figure 7 shows the location of the AI front between 15 and 22 UTC for 2 July 2016 (Fig. 7a) and 3 July 2016 (Fig. 7b) in the reference case. Although the focus is on 2 July, 3 July is added to underline that the AI is a robust feature occurring frequently over SWA, which is also indicated by the results of Adler et al. (2017). The θ_s method for the AI front location is only an estimation, since the potential temperature is also altered by surface conditions and diabatic effects. We focus on the front location of the time period 15–22 UTC that coincides well with the wind speed patterns as presented subsequently. With the increasing nighttime cooling over land after 22 UTC, the temperature gradient between the AI post-frontal and pre-frontal airmass diminishes, impeding the localization of the front. Figure 7 shows an inland propagation of the AI front with time (coded by the line colors). Generally the front is parallel to the coast. This is most obvious for the domain west of 2°W. In contrast, the Lake Volta area and also the area east of the Atakora Mountains show higher variability in the frontal location. Lake Volta is a flat area with fixed surface temperatures in the model and reduced roughness, likely affecting the frontal propagation. For the following analysis, the focus is set to Ivory Coast (7.5–3.0°W).

The distance between the hourly frontal locations reveals that in the evening (approximately 15–18 UTC) the propagation velocity is slow at the beginning but then increases. At 15 UTC the front is located about 100 km inland. Before 15 UTC the AI front is not detectable, since the inland area is subject to warming, which shifts θ_s in coastal direction. However, between 11 UTC and 15 UTC already a horizontal wind speed gradient develops in an area between the coastline and 100 km inland with enhanced (reduced) values over the Gulf of Guinea (over land). Meridional vertical transects of wind speed and potential temperature for this time period are provided in Appendix C. Interestingly, these transects also emphasize the reduced monsoon flow further inland with the development of the AI front (compare 6–7 °N between Fig. 20a and Fig. 20b-e), which is also shown schematically in Fig. 2d. The estimated frontal propagation velocity for the reference case on 2 July stagnates around 7 m s^{-1} after 19 UTC. This is on the same order of magnitude as the findings of Grams et al. (2010) of 10 ± 1 m s^{-1} for Mauritania.

To gain further insight in the general structure of the AI, Figure 8 shows the meridional vertical transects along 5.75°W (central Ivory Coast) for the reference case. Figure 8a shows the horizontal wind speed as shading and the isentropes of 301, 302 and 303 K as solid black contours. As described above, the AI front (vertical dashed line) is identified by using the 302 K isentrope (bold solid line). Several general characteristics can be concluded from Figure 8a: (1) The AI front marks the location of strongest horizontal gradients in wind speed and potential temperature. (2) The post-frontal wind speeds are significantly higher than the pre-frontal wind speeds. The post-frontal area reveals a band of high wind speeds below approximately 900 m ASL with a maximum at around 300 m AGL. This is typical of the NLLJ with the jet axis highlighted by the horizontal dashed line. The entire post-frontal area is affected by this low-level wind band or "blanket" when considering the entire SWA domain. (3) The pre-frontal wind speed is vertically more homogeneous than in the post-frontal area indicating that the AI front is also a border between a predominant well-mixed boundary layer pre-frontally and ongoing stabilization post-frontally. (4) The post-frontal airmass is characterized by cooler temperatures than the pre-frontal area. Therefore the AI frontal passage is related to an increase in wind speed and a decrease in temperature. (5) In agreement to the findings of Grams et al. (2010)

the flow patterns are structurally similar to that of a density current where fast moving cold air and surface friction lead to the formation of an overhanging nose and a head that can extend to higher altitudes than the tail (Simpson, 1969; Sun et al., 2002). Vertical extensions of the head of about 1 km are found for atmospheric density currents (Simpson, 1969), which agrees with the flow in Figure 8a. Sun et al. (2002) emphasize that the wind surge behind the nose, that propagates close to the ground, leads to strong turbulent mixing. This can also be observed in this process study when focusing on the vertical transect of TKE (Fig. 8b). Generally, the post-frontal area shows higher TKE values than pre-frontally. Especially in the area behind the nose TKE is enhanced. Strongest turbulence is not within the jet axis (horizontal dashed line) but below (near the surface) and above due to shear. The location of the 302 K isentrope, which is used for the AI front detection, corresponds well with the layer of increased TKE at the upper border of the AI. It is expected that the near-surface turbulence favors the vertical mixing of moisture as indicated e.g. by Schuster et al. (2013).

The study of Adler et al. (2017) reveals that the AI frequently occurs under undisturbed monsoon conditions over SWA, reaching Savè around 21 UTC. This agrees well with the latitudinal AI front evolution in this study (not shown).

6 Aerosol impacts and mechanisms

6.1 First insight in the aerosol impact on AI

After describing the general AI properties in Section 5, this section presents first insight into the aerosol influence on AI. To give an impression of the aerosol change related to the clean, reference and polluted case, Figure 21 in Appendix D shows the mean total aerosol number and mass over Ivory coast in the lowest 2 km AGL as diurnal cycle from 2 July 15 UTC to 3 July 21 UTC. Figure 9 shows the horizontal wind speed difference at 250 m AGL (h_s) on 2 July 22 UTC between the clean and the reference case together with the corresponding AI front locations. The wind speed difference exhibits a filament structure in zonal direction that covers nearly the entire SWA domain. Furthermore, it propagates inland with time (not shown). Especially over Ivory Coast a coherent pattern can be observed with a spatial shift between the two AI fronts with that of the clean case (black dashed line in Fig. 9) ahead of the reference case front (black solid line in Fig. 9). This anomaly pattern results from the fact that the post-frontal wind speeds are generally higher than the pre-frontal wind speed, as shown in Fig. 8a. To assess the aerosol impact on the vertical structure of the AI, Figure 10 shows the meridional vertical transect of wind speed and potential temperature for the clean (Fig. 10a) and polluted case (Fig. 10b) in the same way as presented for the reference case in Figure 8a. When comparing the results between the clean and polluted cases, and by considering the reference case (Fig. 8a) as intermediate, aerosol-specific characteristics can be identified in addition to the general AI characteristics presented in Section 5. Whereas the temperature characteristics over the ocean are similar for the realizations, the inland temperature decreases with increasing aerosol amount. This is especially visible in the pre-frontal area (Fig. 10). In the polluted case the advective cooling is more effective, since the daytime inland near-surface air is a priori cooler due to a lower sensible heat flux from aerosol extinction. The reduced ocean-land temperature gradient in the polluted case leads to reduced temperature contrasts at the AI front (compare the 302 K isentrope for the clean case (bold line in Fig. 10a) and the polluted case (bold line in Fig. 10b)). With the change in the ocean-land temperature gradient, the AI frontal position and the NLLJ strength and vertical extension

is altered. The higher the aerosol amount, the more the AI front is lagging behind and the weaker the NLLJ. In the polluted case the vertical extension of the inland NLLJ and its wind speed in the jet axis is reduced by about 150 m and 2–3 m s^{-1}, respectively. The AI frontal difference averaged over Ivory Coast at 21 UTC is 10 km between the clean and reference case and 20 km between the clean and the polluted case. With the decrease in temperature with increasing aerosol amount, the pre-frontal wind speed generally increases (contrarily to the post-frontal area). This leads, with respect to the polluted case (Fig. 10b), to some areas of increased wind speed in the pre-frontal area, at a height that is typical of the NLLJ. Generally, the polluted case is characterized by a blurring of the pre- and post-frontal temperature and wind speed differences.

The temporal evolution of the median coastal distance of the AI front over Ivory Coast is presented in Figure 11 for the six realizations. The polluted case (solid red) denotes a special case in Figure 11. The other realizations with scaling factors between 0.1 and 2.0 show a systematic behavior. As expected, the front propagates inland with time. The higher the aerosol amount (dashed blue to solid green) the slower the inland propagation. This leads to a median spatial difference of about 27 km between factor 0.1 (dashed blue) and 2.0 (solid green) at 22 UTC. Furthermore, Figure 11 reveals two regimes, one before and one after 17 UTC. For the latter the frontal propagation diverges according to the aerosol amount as described above. Before 17 UTC an opposite behavior can be observed leading to the circumstances that with less aerosol the AI front is closer to the coastline. Therefore the starting point for the inland propagation at 15 UTC is not equal for all realizations but a reversed order can be observed compared to the situation at 22 UTC. The underlying mechanisms for the occurrence of these two regimes that switch around 17 UTC is assessed in the subsequent section. With a further increase in the aerosol amount, as realized in the polluted case (solid red line in Fig. 11), the ocean-land temperature gradient is reduced as shown in Figure 10b. The AI front evolution is therefore less pronounced than for the other realizations. In the eastern part of Ivory Coast the location of θ_s persists inland and does not form a coherent front near the coast. Averaging the frontal location over Ivory Coast therefore leads to a temporal evolution, which does not follow the behavior of the other realizations. By reducing the benchmark of θ_s from 302 K to 301 K, also the polluted case follows the trend of a weaker frontal propagation with increasing aerosol (grey line in Fig. 11). In this polluted case, with its cooler lower layers, the 301 K isentrope better represents the frontal location, as also visible in Figure 10b.

6.2 Aerosol-AI impact mechanism

After diagnosing the characteristics of AI and the AI changes with changing aerosol amounts in Section 5 and 6.1, respectively, the question of the underlying feedback mechanism arises. The stationarity of the AI front near the coast in the early afternoon is related to the balance between the onshore directed monsoon flow over the ocean and the turbulence over land (e.g. Grams et al., 2010). Therefore the change in the turbulence can alter the balance and lead to differences in the AI front propagation (turbulence mechanism). With increased aerosol amounts, a near-surface cooling (relative to the realizations with less aerosol) is expected during daytime (as observed in Fig. 10b), either due to the ADE via scattering and absorption on aerosol particles or due to to AIE via an increased albedo with reduced cloud droplet effective radii (Twomey effect). A reduced surface heating with increased aerosol amounts might lead to an increase in surface pressure. By considering the fact that the Sea-Surface Temperature (SST) is fixed in COSMO-ART and that the surface temperature over the ocean will therefore not be subject to

substantial changes, a reduction in the land-sea pressure gradient can be expected, which could affect the AI front propagation (pressure gradient mechanism). In order to further elaborate this, Figure 12 shows the spatial distribution of total cloud water (Fig. 12a) and precipitation (Fig. 12b) for the reference case on 2 July, 15 UTC. The red line denotes the AI front. Clouds and precipitation occur primarily in the AI post-frontal area over Ivory Coast due to convergence and vertical lifting, upstream of mountain areas due to topographic lifting (especially at the Mampong Range and the Atakora Mountains) and via localized convection (primarily in the AI pre-frontal area over Ivory Coast). To shed light on potential effects from the turbulence mechanism and the pressure gradient mechanism, Figure 13 shows the differences in surface net downward radiation (Fig. 13a), 2-m temperature (Fig. 13b) and sea level pressure (Fig. 13c) between the reference and the clean case. In addition, Figures 13b,d,f present the same variables but for the areas that are cloud free in both realizations to exclude effects from displaced clouds and to highlight the ADE in a cloud-free environment.

The differences in surface meteorological quantities presented in Figure 13 reveal a clear signal. The following values in brackets indicate the median and the $99^{th}/1^{th}$ percentile of the surface quantities considering the cloud-free inland area. With increasing aerosol, more downward shortwave radiation is scattered and absorbed, leading to an average decrease in surface net downward shortwave radiation (-37 W m^{-2}, -185 W m^{-2}; Fig. 13b). The decrease in incoming shortwave radiation leads to a decrease in 2-m temperature (-0.5 K,-2.5 K; Fig. 13d). The temperature decrease furthermore leads to a domain-wide inland surface pressure increase (+0.16 hPa, +0.45 hPa; Fig. 13f). Omitting the negative pressure anomaly over lake Volta due to the fixed SST, slightly higher domain-wide pressure anomalies are found (+0.17 hPa, +0.45 hPa; Fig. 13f).

To prove the hypothesis that the surface pressure difference is caused by the temperature difference, the surface pressure over Ivory Coast at 15 UTC (over land and in cloud-free areas) is estimated from the pressure and temperature at 850 hPa using the barometric equation. This approach yields a spatially averaged value of +0.12 hPa that broadly agrees with the modeled value of +0.17 hPa (compare Fig. 13f). It can be concluded that the pressure changes are dominated by changes in low-level temperature. In the cloudy areas around the SWA mountains a higher pressure difference can be observed (Fig. 13e), indicating that also cloud-radiative effects are contributing. To assess whether the reduction of incoming shortwave radiation due to clouds is related to a change in the cloud water content and therefore the optical thickness of the clouds or due to the Twomey effect with a change in cloud droplet number concentration (CDNC) and effective radius, Figure 14 exhibit the Empirical Cumulative Distribution Function (ECDF) with respect to the COSMO-ART realizations of the CDNC (Fig. 14a), cloud droplet effective radius (Fig. 14b), cloud water (Fig. 14c) and precipitation (Fig. 14d). This figure corresponds to the cloud and precipitation patterns presented in Figure 12 for 2 July, 15 UTC. A strong susceptibility of the CDNC and effective radii towards a change in the aerosol amount can be observed (Fig. 14). The factor variation from 0.1 to 4.0 leads to an increase in the median CDNC by one order of magnitude from 100 to 1000 cm^{-3} (Fig. 14a) and a reduction in the median effective radius from 9 to about 3.5 μm. When considering the green and red curves in Figure 14, which are related to an aerosol change symetrically around the reference case (black), the effect on the CDNC and effective radius is nonlinear (e.g. Bréon et al., 2002). An aerosol increase (solid green and red lines) has significantly stronger impacts than the aerosol decrease (dashed green and red lines).

In contrast to these remarkable changes, the effect on cloud water and precipitation (Fig. 14c,d, respectively) is insignificant. Except of the polluted case (solid red lines) all realizations show similar ECDFs, indicating that the aerosol increase neither

leads to a cloud water increase due to precipitation suppression or due to enhanced water vapor condensation on the aerosol particles nor a cloud water decrease via enhanced evaporation. The polluted case shows a tendency of precipitation decrease (increase) for the weak (strong) precipitating areas, related to an increase (a decrease) in cloud water. This effect of greater local rainfall amounts is in agreement with the findings of Saleeby et al. (2014) likely via the convective-cloud invigoration mechanism. However, the deviations from the other realizations are small. Figure 14 reveals that the aerosol impact on radiation via the Twomey effect is very likely dominating the cloud-radiation interaction, whereas the cloud optical thickness impact (via a change in the amount of cloud water) is of minor importance. The weak precipitation response to the changing aerosol amount underlines the finding that the radiation and its variation is the key player in the observed changes over SWA due to the ADE in and outside of clouds and the Twomey effect. There is ongoing work within DACCIWA with respect to Large Eddy Simulations (LES) of aerosol-atmosphere interactions. It will be of interest to see whether the COSMO-ART results are consistent with the outcomes of these studies on smaller scales.

The turbulence and pressure gradient mechanisms are counteracting. With respect to the turbulence mechanism, a reduced heating weakens the turbulence in the PBL. Therefore the AI balance between the monsoon flow and the inland turbulence is shifted to the monsoon flow, favoring an inland propagation. Regarding the pressure gradient, a reduced heating decreases the land-sea pressure gradient, shifting the AI balance in the opposite direction and suppressing the inland propagation. When going back to the temporal evolution of the coastal distance of the AI front in Figure 11, both mechanisms are evident and cause the two observed regimes before and after 17 UTC. The first regime includes the stationary phase of the AI front near the coast. With the decrease in incoming solar radiation with increasing aerosol the turbulence decreases and therefore the stationary front location shifts inland. Unfortunately, the AI front detection via the θ_s method fails for the time period earlier than 15 UTC. Therefore the total difference in the stationary AI front location with changing aerosol cannot be assessed. Nevertheless, it is interesting that the location of the AI front during its stationary phase over Ivory Coast could be used as a proxy for the aerosol burden in that area (under otherwise identical conditions).

For the time period after 17 UTC, when turbulence has decreased sufficiently, the pressure gradient mechanism dominates, because the AI front in the clean case - although lagging behind at 15 UTC, is 11 km ahead of the reference case at 22 UTC (Fig. 11).

Figure 15 summarizes the counteracting components turbulence and pressure difference that govern the inland propagation of the AI front by comparing the temporal evolution of the differences between the reference and clean case (dashed lines) and the polluted and reference case differences (solid lines) in surface sensible heat flux (red, positive downward), surface latent heat flux (green, positive downward) and surface pressure (blue), spatially averaged for the AI pre-frontal area over Ivory Coast. The temporal evolution clearly shows that the sensible ~~heat flux~~ and latent heat fluxes differences (and the absolute values itself) decrease strongly with time in contrast to the pressure differences. After sunset (e.g. 18:24 UTC at Kumasi) the sensible ~~heat flux~~ and latent heat fluxes is negligible but the pressure differences continue. In fact, the altered land-sea pressure gradient is maintained till the AI front and the subsequent cool airmass have passed the area and compensates the differences (not shown). It is expected that the high moisture in the monsoon layer prevents it to cool significantly and to reduce the differences that developed during daytime. The factor increase of 4 from 1.0 to 4.0 reduces (increases) the sensible heat flux (sea level

pressure) more than the increase from 0.25 to 1.0, in agreement with the findings of the sensitivity of CDNC and effective radius in Figure 14.

The monsoon flow over SWA is driven by the temperature gradient between the cool SSTs over the eastern equatorial Atlantic Ocean that are fixed in the model and the Saharan Heat Low that is not part of the modeling domain. With this location of the modeling domain, changes in the aerosol amount can serve as an amplifier for the monsoon flow that is able to increase or decrease the temperature gradients and thereby the AI front characteristics. In agreement, Grant and van den Heever (2014) show that the sea breeze front over Cameroon weakens with enhanced aerosol number concentration. Longwave cooling is not significantly reduced, likely due to the water vapor saturation in the monsoon layer (not shown). In contrast, the coherent differences in 2-m temperature and pressure, which were observed at 15 UTC (Fig. 13), also persist during nighttime. The daytime heating of the land, stronger in the clean case and weaker in the polluted case, persists during night and exceeds potential effects from longwave cooling. The differences between the realizations are finally equalized by the passage of the AI front and post-frontal airmass.

6.3 Aerosol-SCT impact mechanism

In addition to the aerosol impact on AI, also impacts on the SCT can be observed. Figure 16 shows the vertical transect of modeled cloud water between Lomé and Savè (Fig. 1b) regarding the clean case (left) and the reference case (right) for 2 July 10 UTC (top) and 11 UTC (bottom). The red shaded area below the cloud layer denotes the development of the convective boundary layer (CBL) identified by $d\theta/dz<0$. The black (red) solid line shows the top of this unstable layer regarding the reference (polluted) case to allow for comparison between the three realizations. After sunrise the CBL starts to evolve. Via the same mechanism as described in Section 6.2, less shortwave radiation reaches the ground with increased amounts of aerosol and therefore also the surface sensible and latent heat fluxes decrease. This leads to a decelerated daytime CBL development and with that to a reduction of the cloud base height (Fig. 16, left). To underline that this effect is visible not only in the Lomé-Savè transect but for the entire SWA region, Figure 17 shows the temporal evolution of the spatial average of total cloud cover (Fig. 17a), total cloud water (Fig. 17b) and the cloud base height (Fig. 17c) over SWA, for the clean (blue dashed), reference (black solid) and polluted case (red solid). Between 21 UTC and the time of sunrise (5:30 UTC) the cloud cover increases (Fig. 17a) due to clouds that are advected onshore or develop inland. This is linked with a reduction in the mean cloud base (Fig. 17c). Between 1 UTC and 7 UTC the clean case shows lower cloud base values than the reference and polluted cases. A detailed analysis reveals that this deviation is not related to NLLS but to mid-level clouds over the Lake Volta Basin and in the northwestern part of the domain (not shown). After sunrise it is assumed that the NLLS intensifies via vertical mixing of moisture in the developing convective PBL. With respect to the spatial average in Figure 17c this leads to a reduction in mean cloud base height. The maximum cloud cover (Fig. 17a) is related to the minimum cloud base (Fig. 17c), underlining the dominance of NLLS. After reaching the cloud cover maximum, the SCT continues, which is related to a lifting of the cloud base and a decrease in cloud cover. For this SCT a clear temporal shift of about one hour can be observed between the clean and the reference case and two hours between the clean and the polluted case. The realizations with increased aerosol amounts react slower to the insolation after sunrise, reach the NLLS maximum coverage later and start later with the SCT as observed

for the Lomé-Savè transect in Figure 16. After 15 UTC this finally leads to a cloud cover that is increased compared to the clean case (Fig. 17a) implying an additional reduction in surface shortwave radiation that can be used for further cooling the surface and decelerating the AI front. The cloud water (Fig. 17b) shows a similar temporal shift with increasing aerosol amounts as for the cloud cover and cloud base. The weakening of the SCT with a higher aerosol burden leads to reduced amounts of cloud water after 13 UTC (Fig. 17b) likely due to reduced convective activity. However, during nighttime, the polluted case uniformly shows higher cloud water values than the clean and reference cases.

Figure 22 in Appendix E shows the cloud analysis by restricting to the clouds below 1500 m AGL to assess the sensitivity of the spatial averaging towards the considered vertical column. The cloud cover (Fig. 22a) shows a similar temporal evolution as presented in Figure 17a. The cloud water and cloud base temporal evolution in the lowest 1500 m AGL (Fig. 22b,c) show less variations between the realizations compared to Figures 17b,c. However, the temporal shift in the onset of the SCT is obvious in both figures. As expected, the initiation of the cloud base increase via the SCT occurs earlier when considering only the clouds below 1500 m AGL in the averaging (compare Fig. 22c with Fig. 17c).

The aerosol feedback process study simulations presented in Section 6.2 and Section 6.3 revealed several mechanisms relevant for SWA, affecting the location and propagation of the AI front and the temporal evolution of the SCT. In the following section a proposal for a conceptual model will be presented.

6.4 Conceptual model of aerosol-atmosphere interactions in SWA

This section aims to synthesize the findings that have been obtained with this aerosol feedback process study. We showed that AI affects the entire SWA domain through the course of the day via cold air advection, the NLLJ that can be found in the AI post-frontal area and convergence-induced convection and precipitation. Two distinct meteorological responses to changes in the amount of aerosol via ADE and the Twomey effect were identified: *1. A spatial shift of the Atlantic Inflow (AI)* and *2. a temporal shift of the Stratus-to-Cumulus Transition (SCT).*

Figure 18 shows a conceptual scheme that combines both responses. The bigger loop is related to the first response (AI) and the smaller loop to the second (SCT). Following the AI loop in Figure 18, the increase in the amount of aerosol (number and mass) by a factor of 4 (0.25 to 1.0) is the initial perturbation of the system. The subsequent numbers in parenthesis are related to the median value over Ivory Coast (cloud-free inland areas) on 2 July 15 UTC to provide guiding values for the denoted changes.

Via ADE the aerosol increase leads to a decrease in surface net downward shortwave radiation (-37 W m^{-2}) and surface temperature (-0.5 K). Previous studies showed that till the early afternoon, the AI front is stationary near the coast due to the balance between the monsoon flow from the sea and the sensible heat flux (turbulence) over land. With the afternoon decrease in sensible heat flux, the AI front propagates inland. This study showed that the decreased surface heating leads to a positive pressure anomaly over land (+0.16 hPa) and with that to a reduced land-sea pressure gradient. The latter is more persistent than the sensible heat flux that vanishes around sunset (compare Fig. 15). The reduced pressure gradient leads to a reduced AI frontal velocity and therefore to a southward shift in the case of increased aerosol (11 km on 2 July 22 UTC). The post-frontal area is characterized by stronger wind speeds in the lowest 1000 m AGL with the maximum around 250 m AGL that is

characteristic of the NLLJ. Therefore an AI frontal shift leads to a shift in the NLLJ inland propagation. Since the AI frontal propagation is linked to convergence-induced convection and convective precipitation, also a meridional shift of the AI-related precipitation is observed. These effects are primarily related to the afternoon but the AI frontal and NLLJ shift also leads to a shift in the inland propagation of coastal NLLS with a similar spatial magnitude as observed for the AI front (not shown).

The AI loop denoted in Figure 18 includes a further mechanism, related to the counteracting effects of the monsoon flow over the ocean and the sensible heat flux over land in the stationary phase of the AI front. With increasing aerosol the inland sensible heat flux decreases, which relocates the front farther from the coast. Therefore with increased aerosol the AI frontal inland propagation starts farther from the coast but is slower than in the low aerosol case due to the reduced land-sea pressure gradient as soon as the turbulence has declined after sunset.

The SCT loop is coupled to the AI loop via the decrease in surface shortwave radiation and temperature. This study pointed out that the deficit in surface heating due to ADE and cloud brightening via the Twomey effect lead to a decrease in sensible heat flux and therefore to a delayed development of the CBL. The lower CBL height leads to a lower cloud base and therefore to a later SCT and breakup of the closed cloud layer to scattered cumuli (compare Fig. 17a). Both loops are initialized after sunrise with the input in shortwave radiation. The SCT loop implies a positive cloud cover anomaly after 15 UTC with increasing aerosol. Sunset is around 18:30 UTC. Although the AI front already starts penetrating inland around 14-15 UTC, approximately a 3.5-hour period is available for an additional surface cooling from the later cloud-layer breakup. This is a pathway for a further deficit in surface shortwave radiation and surface heating that could further weaken the AI loop as emphasized by the red arrow in opposite direction in Figure 18. However, the latter coupling between the two loops is only hypothesized. A future study needs to assess the significance of the contribution in inland surface pressure increase that comes from the deficit in shortwave heating via the later cloud-layer breakup.

The mechanisms described in Figure 18 raise the question about the possibility to generalize these results. The AI feature is very likely a regular phenomenon under undisturbed monsoon conditions as confirmed by previous studies that focus on longer time periods. Within this process study the AI frontal shift was obvious for both days in the evening. However, the results presented above are related to Ivory Coast that shows a more coherent AI frontal pattern than the eastern part of the domain, likely related to topographic features. This conceptual picture reveals radiation as a key player governing the feedbacks, either via ADE or via a change in cloud albedo (Twomey effect). The AIE assessment within the process study reveals the known mechanisms, in particular the increase (decrease) of the CDNC (effective radius) with an increase in the aerosol number concentration. However, the AI-related clouds and precipitation reveal, aside from a meridional shift, no statistically significant difference. Although, the possibility for substantial effects from AIE cannot be excluded, a conceptual view as presented for the radiative effects has to be left for subsequent studies.

7 Conclusions

This study focused on southern West Africa (SWA) to assess the implications of aerosols on clouds and atmospheric dynamics using a process study with the regional model COSMO-ART on 2–3 July 2016, a time period in the well-established West

African Monsoon (WAM) without impacts of Mesoscale Convective Systems. The results revealed an elongated front over SWA that develops during daytime between the monsoon flow over the ocean and the turbulence over land being stationary near the coast around noon and propagating inland in the evening. This phenomenon has been identified for several African coastal regions and was conceptually separated from the classical land-sea breeze. Based on Grams et al. (2010) we used the term *Atlantic Inflow* (AI). The AI post-frontal area is characterized by a distinct decrease in temperature and increase in wind speed and relative humidity, emphasizing that the nocturnal low-level jet (NLLJ) in SWA is a widespread phenomenon related to AI.

Changing the aerosol number and mass in COSMO-ART, the aerosol direct effect (ADE) and indirect effect (AIE) was quantified, indicating a considerable sensitivity of the AI frontal location towards changes in the aerosol amount. With increasing aerosol the AI front shows reduced propagation velocities over Ivory Coast leading to frontal displacements of 10-30 km. Grant and van den Heever (2014) modeled a similar behavior for the sea breeze over Cameroon. Longwave cooling influences the AI pre-frontal area but even after sunset the positive temperature anomaly from daytime solar heating persists and dominates. Effects on SST are not considered in this study. In case of considering the impact of reduced incoming solar radiation on the SST with increased aerosol, stronger land-sea temperature gradients are expected. Therefore, the estimations of this study with fixed SST denote the upper limit of the magnitude of the effects. However, this model setup in numerical weather prediction mode is less appropriate to study effects on SST. Global models on a longer time scale are more suitable to provide added value on this question.

In addition to the effect on AI, the decrease in near-surface heating leads to a delayed Stratus-to-Cumulus Transition (SCT) via a later onset of the convective boundary layer. We synergized this subtle aerosol-atmosphere feedback in a new conceptual model combining the AI and SCT loops (Fig. 18). Furthermore, we hypothesize that the additional radiation deficit due to the later SCT leads to a further weakening of AI.

The results exhibit the radiation as the key player governing the aerosol affects on SWA atmospheric dynamics during boreal summer, via ADE and the Twomey effect. In contrast, effects on precipitation are small. Saleeby et al. (2014) identified AIE as relevant for the SCT over tropical oceans with an accelerated transition with increasing aerosol. This study identified ADE and the Twomey effect as predominant for the SCT over tropical land areas with a decelerated transition with increasing aerosol. The importance of ADE on monsoon-related processes has also been shown by Lau et al. (2017) for the Indian monsoon. For Northern India, they reveal that the ADE dominates large-scale aerosol-monsoon interactions. A detailed literature study suggests that in the current aerosol research, ADE and the cloud-radiation interactions are underrepresented. Especially with respect to monsoon regimes, a special focus should be set on ADE. Whether the AI frontal displacement is detectable in long-term observations is left for subsequent studies. A potential strategy is the analysis of the AI front around noon via remote sensing cloud observations from past to present by assuming a positive trend in the aerosol burden. It is expected that the daytime AI front location has shifted landwards from the past to current conditions but also other phenomena (e.g. decadal SST variations) have the potential to affect the front location.

Data availability. The underlying research data are available upon request from the corresponding author.

Competing interests. The authors declare that they have no conflict of interest.

Special issue statement. This article is part of the special issue *Results of the project "Dynamics–aerosol–chemistry–cloud interactions in West Africa" (DACCIWA)*

Appendix A: COSMO-ART model configuration

Tab. 2

Appendix B: Intercomparison with Savè supersite

Fig. 19

Appendix C: Early AI evolution on 2 July 2016

Fig. 20

Appendix D: Change in aerosol number and mass due to scaling

Fig. 21

Appendix E: Temporal evolution of clouds below 1500 m AGL

Fig. 22

Acknowledgements. The research leading to these results has received funding from the European Union 7th Framework Programme (FP7/2007-2013) under Grant Agreement no. 603502 (EU project DACCIWA: Dynamics-aerosol-chemistry-cloud interactions in West Africa). ~~We thank~~ Thanks to the German Weather Service (DWD) for providing access to the ICON forecast data and to the Steinbuch Centre for Computing (SCC) for providing the computational resources for the model realizations. We also thank Joel Brito and Régis Dupuy for their efforts in providing the SMPS measurement data. The data analysis of our study was done by using the software R (2013) .

References

Adler, B., Kalthoff, N., and Gantner, L.: Nocturnal low-level clouds over southern West Africa analysed using high-resolution simulations, Atmos. Chem. Phys., 17, 899–910, 2017.

Athanasopoulou, E., Vogel, H., Vogel, B., Tsimpidi, A. P., Pandis, S. N., Knote, C., and Fountoukis, C.: Modeling the meteorological and chemical effects of secondary organic aerosols during an EUCAARI campaign, Atmos. Chem. Phys., 13, 625–645, 2013.

Bahino, J., Yoboué, V., Galy-Lacaux, C., Adon, M., Akpo, A., Keita, S., Liousse, C., Gardrat, E., Chiron, C., Ossohou, M., Gnamien, S., and Djossou, J.: Spatial distribution of gaseous pollutants (NO_2, SO_2, NH_3, HNO_3 and O_3) in Abidjan, Côte d'Ivoire, Atmos. Chem. Phys., submitted, 2017.

Baldauf, M., Seifert, A., Förstner, J., Majewski, D., and Raschendorfer, M.: Operational Convective-Scale Numerical Weather Prediction with the COSMO model: Description and Sensitivities, Mon. Wea. Rev., pp. 3887–3905, 2011.

Bangert, M.: Interaction of Aerosol, Clouds, and Radiation on the Regional Scale, Institut für Meteorologie und Klimaforschung, Karlsruher Institut für Technologie, Dissertation, 2012.

Bréon, F.-M., Tanré, D., and Generoso, S.: Aerosol Effect on Cloud Droplet Size Monitored from Satellite, Science, 295, 834–838, 2002.

CAMS: Copernicus Atmosphere Monitoring Service (http://apps.ecmwf.int/ datasets/data/cams-gfas/, last access: 30 July 2017), 2017.

CCSM: https://svn-ccsm-inputdata.cgd.ucar.edu/trunk/inputdata/lnd/clm2/raw data/pftlanduse.3minx3 min.simyr2000.c110913/ (last access: 10 June 2017), 2015.

Deetz, K.: Assessing the Aerosol Impact on Southern West African Clouds and Atmospheric Dynamics, Wissenschaftliche Berichte des Instituts für Meteorologie und Klimaforschung des Karlsruher Instituts für Technologie, KIT Scientific Publishing, Karlsruhe, Dissertation, 75, 99–144, 2018.

Deetz, K. and Vogel, B.: Development of a new gas-flaring emission dataset for southern West Africa, Geosci. Model Dev., 10, 1607–1620, 2017.

EDGAR: Emission Database for Global Atmospheric Research, http://edgar.jrc.ec.europa.eu/htap_v2/index.php?SECURE=123 (last access: 10 June 2017), 2010.

Fan, J., Wang, Y., Rosenfeld, D., and Liu, X.: Review of Aerosol-Cloud Interactions: Mechanisms, Significance, and Challenges, J. Atmos. Sci., 73, 4221–4250, 2016.

Flamant, C., Knippertz, P., Fink, A. H., Akpo, A., Brooks, B., Chiu, C., Coe, H., Danuor, S., Evans, M., Jegede, O., Kalthoff, N., Konaré, A., Liousse, C., Lohou, F., Mari, C., Schlager, H., Schwarzenboeck, A., Adler, B., Amekudzi, L., Aeyee, J., Ayoola, M., Bessardon, G., Bower, K., Burnet, F., Catoire, V., Colomb, A., Fossu-Amankwah, K., Lee, J., Lothon, M., Manaran, M., Marsham, J., Meynadier, R., Ngamini, J.-B., Rosenberg, P., Sauer, D., Schneider, J., Smith, V., Stratmann, G., Voigt, C., and Yoboue, V.: The Dynamics-Aerosol-Chemistry-Cloud Interactions in West Africa field campaigns: Overview and research highlights, Bull. Amer. Meteor. Soc., 2018.

Fountoukis, C. and Nenes, A.: Continued development of a cloud droplet formation parameterization for global climate models, J. Geophys. Res., 110, 2005.

Fountoukis, C. and Nenes, A.: ISORROPIA II: a computationally efficient thermodynamic equilibrium model for K^+ -Ca^{2+} -Mg^{2+} -NH_4^+ -SO_4^{2-} -NO_3^- -CL^--H_2O aerosol, Atmos. Chem. Phys., 7, 4639–4659, 2007.

GlobCover: GlobCover Land Cover Map - European Space Agency GlobCover Project (http://www.gelib.com/globcover-2009.htm, last access: 10 June 2017), 2009.

Grams, C. M., Jones, S. C., Marsham, J. H., Parker, D. J., Haywood, J. M., and Heuveline, V.: The Atlantic Inflow to the Saharan heat low: Observations and Modelling, Quart. J. Roy. Meteor. Soc., 136, 125–140, 2010.

Grant, L. D. and van den Heever, S. C.: Aerosol-cloud-land surface interactions within tropical sea breeze convection, J. Geophys. Res., 119, 8340–8361, 2014.

Hill, P. G., Allan, R. P., and Chiu, J. C.: Quantifying the contribution of different cloud types to the radiation budget, Atmos. Chem. Phys., under review, 2017.

Hopkins, J. R., Evans, M. J., Lee, J. D., Lewis, A. C., Marsham, J. H., McQuaid, J. B., Parker, D. J., Steward, D. J., Reeves, C. E., and Purvis, R. M.: Direct estimates of emissions from the megacity of Lagos, Atmos. Chem. Phys., 9, 8471–8477, 2009.

HWSD: HWSD (FAO/IIASA/ISRIC/ISSCAS/JRC), 2012: Harmonized World Soil Database (version 1.2), FAO, Rome, Italy and IIASA, Laxenburg, Austria, 2012.

Kalthoff, N., Louhou, F., Brooks, B., Jegede, O., Adler, B., Babić, K., Dione, C., Ajao, A., Amekudzi, L. K., Aryee, J. N. A., Ayoola, M., Bessardon, G., Danuor, S. K., Handwerker, J., Kohler, M., Lothon, M., Pedruzo-Bagazgoitia, X., Smith, V., Sunmonu, L., Wieser, A., Fink, A. H., and Knippertz, P.: An overview of the diurnal cycle of the atmospheric boundary layer during the West African monsoon season: results from the 2016 observational campaign, Atmos. Chem. Phys., 18, 2913–2928, 2018.

Knippertz, P., Coe, H., Chiu, J. C., Evans, M. J., Fink, A. H., Kalthoff, N., Liousse, C., Mari, C., Allan, R. P., Brooks, B., Danour, S., Flamant, C., Jegede, O. O., Fabienne, L., and Marsham, J. H.: The DACCIWA Project, Bull. Amer. Meteor. Soc., pp. 1451–1460, 2015.

Knippertz, P., Fink, A. H., Deroubaix, A., Morris, E., Tocquer, F., Evans, M. J., Flamant, C., Gaetani, M., Lavaysse, C., Mari, C., Marsham, J. H., Meynadier, R., Affo-Dogo, A., Bahaga, T., Brosse, F., Deetz, K., Guebsi, R., Latifou, I., Maranan, M., Rosenberg, P. D., and Schlüter, A.: A meteorological and chemical overview of the DACCIWA field campaign in West Africa in June-July 2016, Atmos. Chem. Phys., pp. 10 893–10 918, 2017.

Kohler, M., Kalthoff, N., Seringer, J., and Kraut, S.: DACCIWA field campaign, Savè super-site, Surface measurements; SEDOO OMP,https://doi.org/10.6096/DACCIWA.1690 (last access: 8 December 2017), 2016.

Lana, A., Bell, T. G., Simó, R., Vallina, S. M., Ballabrera-Poy, J., Kettle, A. J., Dachs, J., Bopp, L., Saltzman, E. S., Stefels., J., Johnson, J. E., and Liss, P. S.: An updated climatology of surface dimethylsulfide concentrations and emission fluxes in the global ocean, Global Biogeochem. Cycles, 25, G1004, 2011.

Lau, W. K. M., Kim, K.-M., Shi, J.-J., Matsui, T., Chin, M., Tan, Q., Peters-Lidard, C., and Tao, W. K.: Impacts of aerosol-monsoon interaction on rainfall and circulation over Northern India and the Himalaya Foothills, Climate Dynamics, 49, 1945–1960, 2017.

Liousse, C., Assamoi, E., Criqui, P., Granier, C., and Rosset, R.: Explosive growth in African combustion emissions from 2005 to 2030, Environ. Res. Lett., 9, 1–10, 2014.

Lundgren, K., Vogel, B., Vogel, H., and Kottmeier, C.: Direct radiative effects of sea salt for the Mediterranean region under conditions of low to moderate wind speeds, J. Geophys. Res., 118, 1906–1923, 2013.

Mari, C. H., Cailley, G., Corre, L., Saunois, M., Attié, J. L., Thouret, V., and Stohl, A.: Tracing biomass burning plumes from the Southern Hemisphere during the AMMA 2006 wet season experiment, Atmos. Chem. Phys., 8, 3951–3961, 2008.

Marsham, J. H., Dixon, N. S., Garcia-Carreras, L., Lister, G. M. S., Parker, D. J., Knippertz, P., and Birch, C. E.: The role of moist convection in the West African monsoon system: Insights from continental-scale convection-permitting simulations, Geophys. Res. Lett., 40, 1843–1849, 2013.

Miles, N. L., Verlinde, J., and Clothiaux, E. E.: Cloud Droplet Size Distributions in Low-Level Stratiform Clouds, J. Atmos. Sci., 57, 295–311, 2000.

MOZART: MOZART-4/GEOS-5 forecasts, National Center for Atmospheric Research (NCAR), University Corporation for Atmospheric Research, Atmospheric Chemistry Observations & Modeling (https://www.acom.ucar.edu/acresp/AMADEUS/mz4_output/chemfcst/, last access: 30 July 2017), 2017.

Philipps, V. T. J., DeMott, P. J., and Andronache, C.: An Empirical Parameterization of Heterogeneous Ice Nucleation for Multiple Chemical Species of Aerosol, J. Atmos. Sci., 65, 2757–2783, 2008.

R: R Core Team, R: A Language and Environment for Statistical Computing, R Foundation for Statistical Computing, Vienna, Austria, (http://www.R-project.org/, last access: 9 August 2017), 2013.

Rieger, D., Steiner, A., Bachmann, V., Gasch, P., Förstner, J., Deetz, K., Vogel, B., and Vogel, H.: Impact of a Saharan dust outbreak on the photovoltaic power generation in Germany, Atmos. Chem. Phys., 17, 13 391–13 415, 2017.

Riemer, N., Vogel, H., Vogel, B., and Fiedler, F.: Modeling aerosols of the mesoscale-y: Treatment of soot aerosols and its radiative effects, J. Geophys. Res., 108, 2003.

Rosenfeld, D., Lohmann, U., Raga, G. B., O'Dowd, C., Kulmala, M., Fuzzi, S., Reissell, A., and Andreae, M. O.: Flood or Drought: How Do Aerosols Affect Precipitation?, Science, 321, 1309–1313, 2008.

Saleeby, S. M., Herbener, S. R., and van den Heever, S. C.: Impacts of Cloud Droplet-Nucleating Aerosols on Shallow Tropical Convection, J. Atmos. Sci., 72, 1369–1385, 2014.

Schrage, J. M. and Fink, A. H.: Nocturnal Continental Low-Level Stratus over Tropical West Africa: Observations and Possible Mechanisms Controlling Its Onset, Mon. Wea. Rev., 140, 1794–1809, 2012.

Schuster, R., Fink, A. H., and Knippertz, P.: Formation and Maintenance of Nocturnal Low-Level Stratus over the Southern West African Monsoon Region during AMMA 2006, J. Atmos. Sci., 70, 2337–2355, 2013.

Seifert, A. and Beheng, K. D.: A two-moment cloud microphysics parameterization for mixed-phase clouds. Part 1: Model description, Meteor. Atmos. Phys., 92, 45–66, 2006.

Simpson, J. E.: A comparison between laboratory and atmospheric density currents, Quart. J. Roy. Meteor. Soc., 95, 758–765, 1969.

Stevens, B. and Feingold, G.: Untangling aerosol effects on clouds and precipitation in a buffered system, Nature Reviews, 461, 607–613, 2009.

Sun, J., Burns, S. P., Lenschow, D. H., Banta, R., Newsom, R., Coulter, R., Frasier, S., Ince, T., Nappo, C., Cuxart, J., Blumen, W., and Hu, X.-Z.: Intermittent turbulence associated with a density current passage in the stable boundary layer, Bound.-Layer Meteor., 105, 199–219, 2002.

UNO: World Population Prospects 2015 – Data Booklet (ST/ESA/ SER.A/377)., United Nations, Department of Economic and Social Affairs, 2015.

van der Linden, R., Fink, A. H., and Redl, R.: Satellite-based climatology of low-level continental clouds in southern West Africa during the summer monsoon season, J. Geophys. Res., 120, 1186–1201, 2015.

Vogel, B., Vogel, H., Bangert, M., Lundgren, K., Rinke, R., and Stanelle, T.: The comprehensive model system COSMO-ART - Radiative impact of aerosol on the state of the atmosphere on the regional scale, Atmos. Chem. Phys., 9, 8661–8680, 2009.

Walter, C., Freitas, S. R., Kottmeier, C., Kraut, I., Rieger, D., Vogel, H., and Vogel, B.: The importance of plume rise on the concentrations and atmospheric impacts of biomass burning aerosol, Atmos. Chem. Phys., 16, 9201–9219, 2016.

Weimer, M., Schröter, J., Eckstein, J., Deetz, K., Neumaier, M., Fischbeck, G., Hu, L., Millet, D. B., Rieger, D., Vogel, H., Vogel, B., Reddmann, T., Kirner, O., Ruhnke, R., and Braesicke, P.: An emission module for ICON-ART 2.0: implementation and simulations of acetone, Geosci. Model Dev., 10, 2471–2494, 2017.

Table 1. Overview of the COSMO-ART realizations capturing the variation in the aerosol amount with respect to the Aerosol Direct Effect (ADE) and Aerosol Indirect Effect (AIE). The realization abbreviations include the prefix AE (Aerosol Effect) and the corresponding factor.

Abbreviation	**Description of Simulation**
~~AIE$_{0.1}$ADE$_{0.1}$~~ AE0.1	$F_{AIE} = 0.1$ and $F_{ADE} = 0.1$
~~AIE$_{0.25}$ADE$_{0.25}$~~ AE0.25	$F_{AIE} = 0.25$ and $F_{ADE} = 0.25$ (clean case)
~~AIE$_{0.5}$ADE$_{0.5}$~~ AE0.5	$F_{AIE} = 0.5$ and $F_{ADE} = 0.5$
~~AIE$_{1.0}$ADE$_{1.0}$~~ AE1.0	$F_{AIE} = 1.0$ and $F_{ADE} = 1.0$ (reference case)
~~AIE$_{2.0}$ADE$_{2.0}$~~ AE2.0	$F_{AIE} = 2.0$ and $F_{ADE} = 2.0$
~~AIE$_{4.0}$ADE$_{4.0}$~~ AE4.0	$F_{AIE} = 4.0$ and $F_{ADE} = 4.0$ (polluted case)

Table 2. COSMO-ART model configuration used for this study.

Characteristics	**Description**
Model version	COSMO5.1-ART3.1
Time period	2–3 July 2016
Simulation domain	9.0°W–4.4°E, 3.0°N–10.8°N
Grid mesh size	2.5 km (0.0223°)
Vertical levels	80 up to 30 km (28 in the lowest 1.5 km ASL)
Meteorological boundary and initial data	COSMO-ART (5 km grid mesh size using ICON operational forecasts from DWD)
Pollutant boundary and initial data	COSMO-ART (5 km grid mesh size using MOZART, 2017) GlobCover (2009) land use data CCSM (2015) plant functional types
Cloud microphysics	Two-moment microphysics scheme (Seifert and Beheng, 2006)
Pollutant emissions	Mineral dust (online): Rieger et al. (2017) using HWSD (2012) Sea salt (online): Lundgren et al. (2013) DMS (online): using Lana et al. (2011) BVOCs (online): Weimer et al. (2017) Biomass burning (prescribed/online): Walter et al. (2016) using GFAS (CAMS, 2017) Anthropogenic (prescribed): EDGAR (2010) Gas flaring (prescribed): Deetz and Vogel (2017)
Aerosol dynamics	MADEsoot (Riemer et al., 2003; Vogel et al., 2009) Secondary inorganic aerosol: ISORROPIA II (Fountoukis and Nenes, 2007) Secondary organic aerosol: VBS (Athanasopoulou et al., 2013)
Chemical mechanisms	Gas phase chemistry: RADMKA (Vogel et al., 2009)
Aerosol direct effect (ADE)	Vogel et al. (2009)
Aerosol indirect effect (AIE)	Warm phase: Bangert (2012) and Fountoukis and Nenes (2005) Cold phase: Philipps et al. (2008)

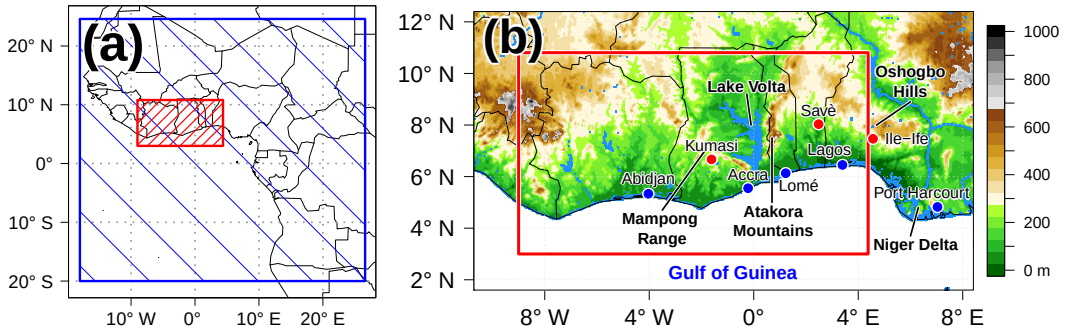

Figure 1. (a) Modeling domain SWA (red rectangle, 2.5 km grid mesh size) together with its coarse domain (blue, 5 km grid mesh size). (b) Map of the research area SWA. The color shading denotes the topography (m above sea level, ASL). Topographic features are named in bold, coastal cities are shown as blue dots and the three DACCIWA supersites as red dots. The modeling domain SWA is again denoted with red rectangle.

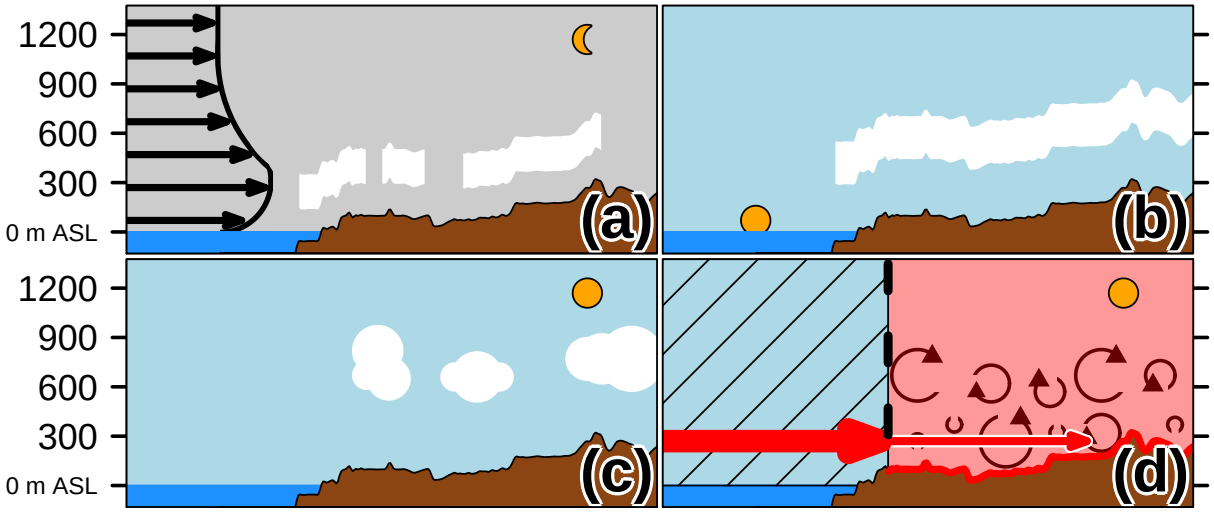

Figure 2. Schematic view on SWA atmospheric dynamics via a meridional-vertical transect (m ASL) through the Gulf of Guinea (blue shading) and adjacent land (brown shading). (a) During nighttime the NLLJ leads to a wind maximum at about 300 m AGL as emphasized by the black arrows. Over land, NLLS forms at the level of the NLLJ axis. The NLLS establishment occurs around 22 UTC over Kumasi and 1 UTC over Savé (Kalthoff et al., 2018) . (b) The maximum spatial coverage of NLLS is reached in the morning hours around 9 to 10 UTC. After sunrise (5:30 UTC) a lifting of the cloud base height can be observed. (c) During late morning or early afternoon the NLLS deck breaks up to cumuliform clouds (around 11 UTC over Kumasi and 12 UTC over Savé, Kalthoff et al., 2018) . (d) During daytime (5:30-18:00 UTC) the momentum of the onshore monsoon flow (bold red arrow) is mixed vertically over land due to atmospheric turbulence from solar heating (eddies). The balance between the monsoon flow and the turbulence leads to a frontal structure inland from the coast (black dashed line).

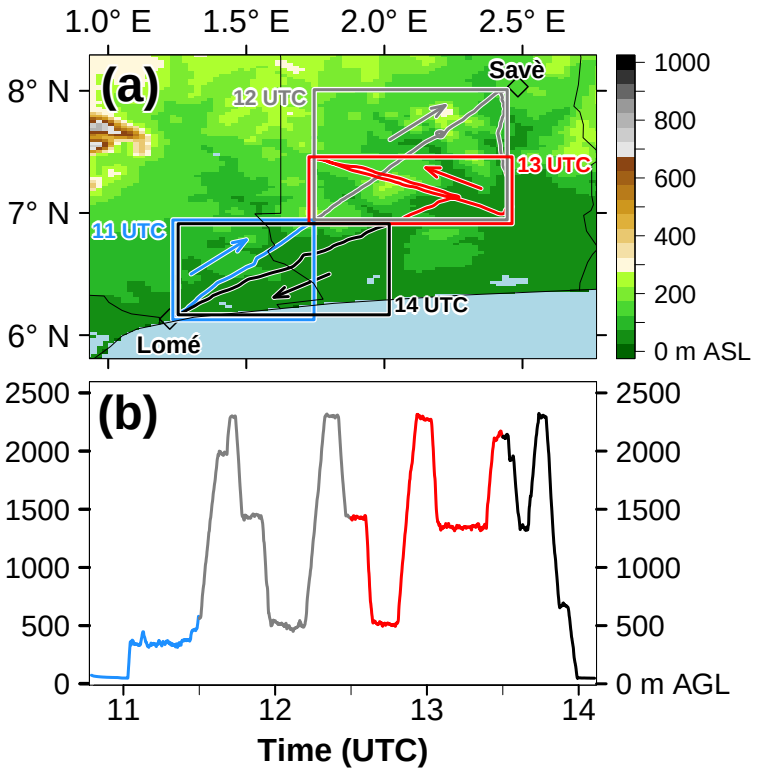

Figure 3. Flight track of the Twin Otter aircraft on 3 July 2016 between 10:47 UTC and 14:06 UTC (flight number TO-02) in (a) horizontal and (b) vertical dimension (m AGL). For (a) the topography (m ASL) is added. The flight track in (a) and (b) is separated in hourly time steps for the subsequent collocation with hourly model data from COSMO-ART, highlighted by the blue (10:47–11:30 UTC), gray (11:30–12:30 UTC), red (12:30–13:30 UTC) and black color (13:30–14:06 UTC). The rectangles, spanned by the horizontal extension of the hourly flight sections, are used for the selection of model data. Furthermore, the arrows in (a) indicate the flight direction with the takeoff at Lomé, the flight to Savè and the return to Lomé airport. Shortly after 12 UTC (with a flight altitude of 0.5 km AGL) the Twin Otter reached Savè. Note the meridional compression of the map in (a).

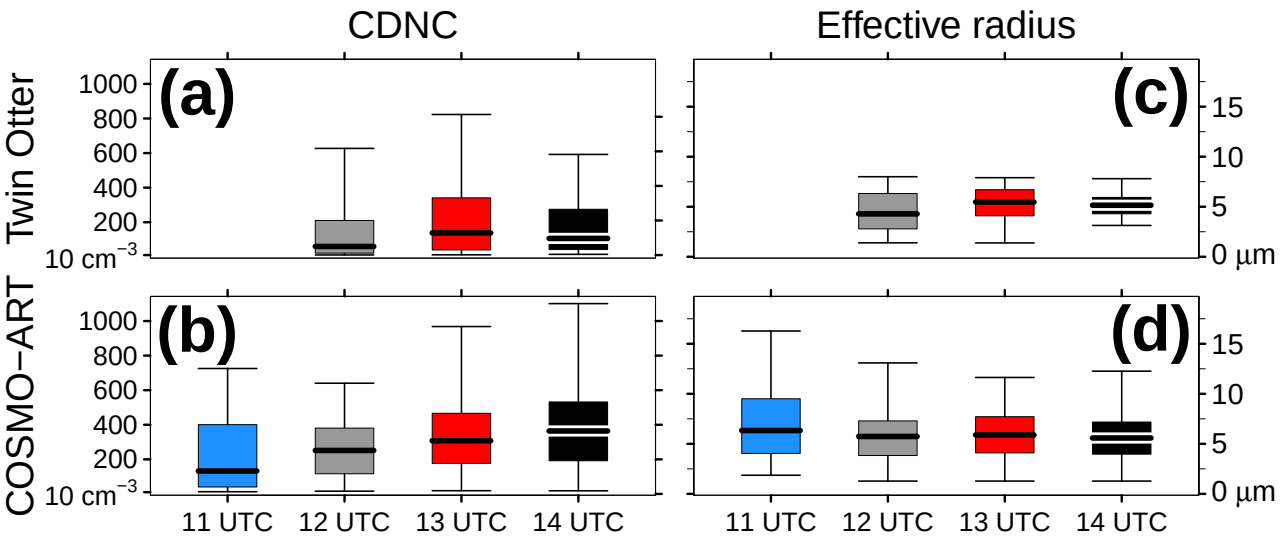

Figure 4. Boxplots of (left) the CDNC (cm^{-3}) and (right) the cloud droplet effective radius (μm) according to the flight track denoted in Figure 3a for (top) Twin Otter observations and (bottom) COSMO-ART reference case. The flight track is separated in hourly time steps from 11 UTC to 14 UTC as highlighted by the colors (compare Fig. 3). Regarding (a,c) the observations according to the flight track section with 1 s temporal resolution of the CDP device are used. Regarding (b,d) the simulation results of the cube that is spanned horizontally by the rectangles in Figure 3a and vertically about 2.3 km (in agreement with the Twin Otter maximum flight altitude) are considered. The whiskers capture the data from the 0.025 to the 0.975 quantile (95% of the data). Data outside this range are not shown. CDNC below 10 cm^{-3} were omitted, leading to an observational data basis of 34, 443, 403 and 115 observations at 11, 12, 13 and 14 UTC, respectively. Due to the low observational data coverage 11 UTC is omitted.

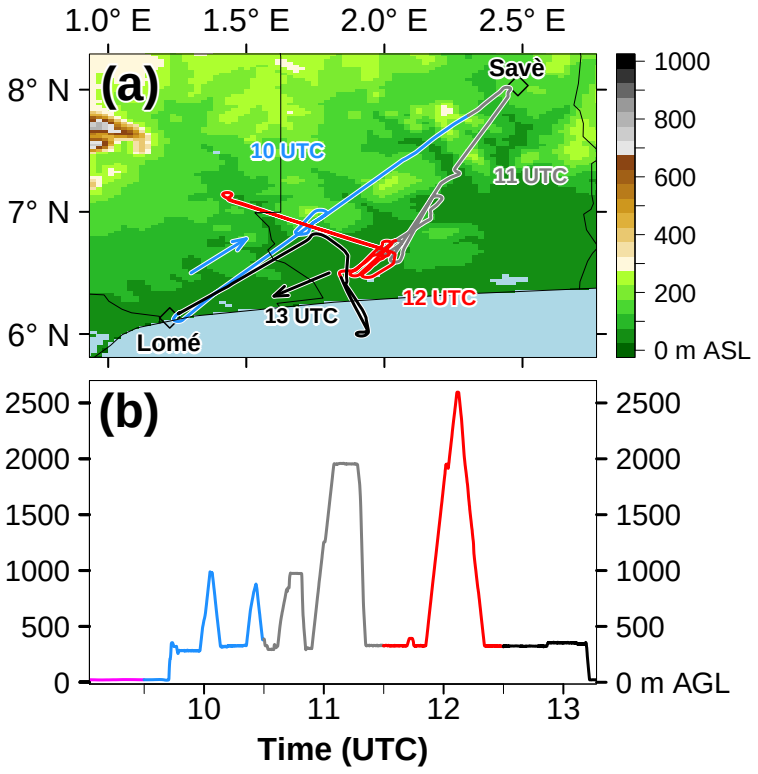

Figure 5. Flight track of the ATR42 SAFIRE on 3 July 2016 between 08:32 UTC and 13:13 UTC in (a) horizontal and (b) vertical dimension (m AGL). For (a) the topography (m ASL) is added. The flight track in (a) and (b) is separated in hourly time steps for the subsequent collocation with hourly model data from COSMO-ART, highlighted by the pink (08:32—09:30 UTC), blue (09:30–10:30 UTC), gray (10:30–11:30 UTC), red (11:30–12:30 UTC) and black color (12:30–13:13 UTC). Furthermore, the arrows in (a) indicate the flight direction with the takeoff at Lomé, the flight to Savè and the return to Lomé airport. Shortly. Note the meridional compression of the map in (a).

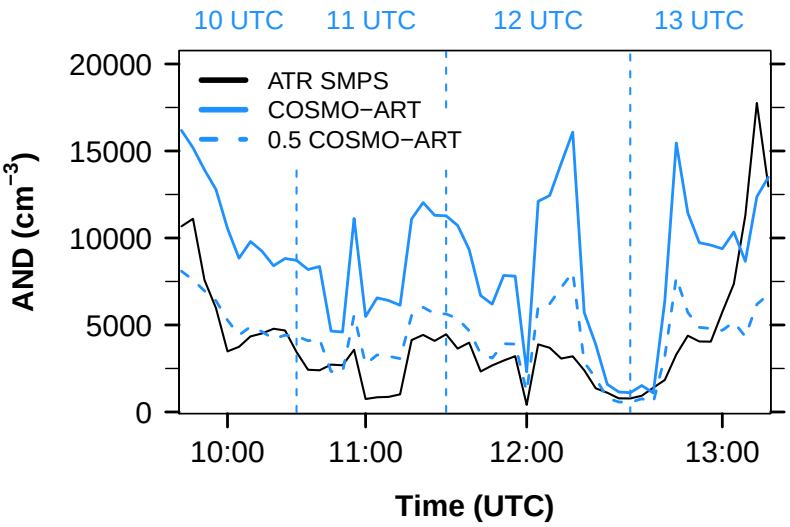

Figure 6. Aerosol number density (AND, cm^{-3}) in the size interval 0.02 to 0.5 μm as measured by the Spectrometer Scanning Mobility Particle Sizer (SMPS) on board the ATR42 (black) and modeled with COSMO-ART (solid blue, reference case). The horizontal dashed blue line shows the COSMO-ART AND divided by 2. The vertical blue dashed lines indicate the COSMO-ART model output hours, which are compared to observations.

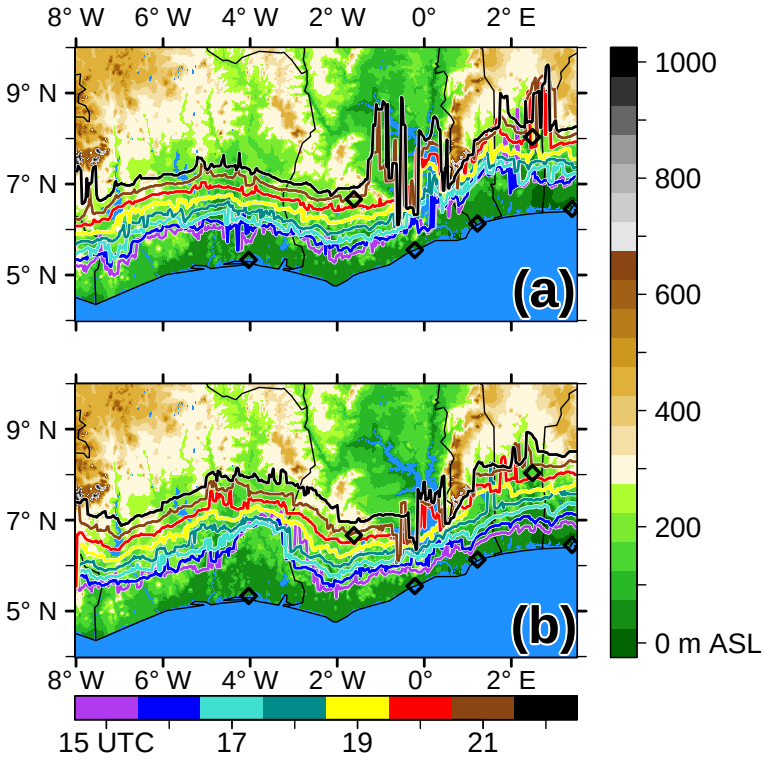

Figure 7. Localization of the AI front on (a) 2 July 2016 and (b) 3 July 2016 between 15 and 22 UTC for the reference case. The front is detected by the arrival of the isentropic surface θ_s=302 K at h_s=250 m AGL. The color of the front denotes the time (UTC, bottom legend). The underlying shading shows the topography of SWA (m ASL, legend on the right). The black diamonds denote the cities shown in Figure 1.

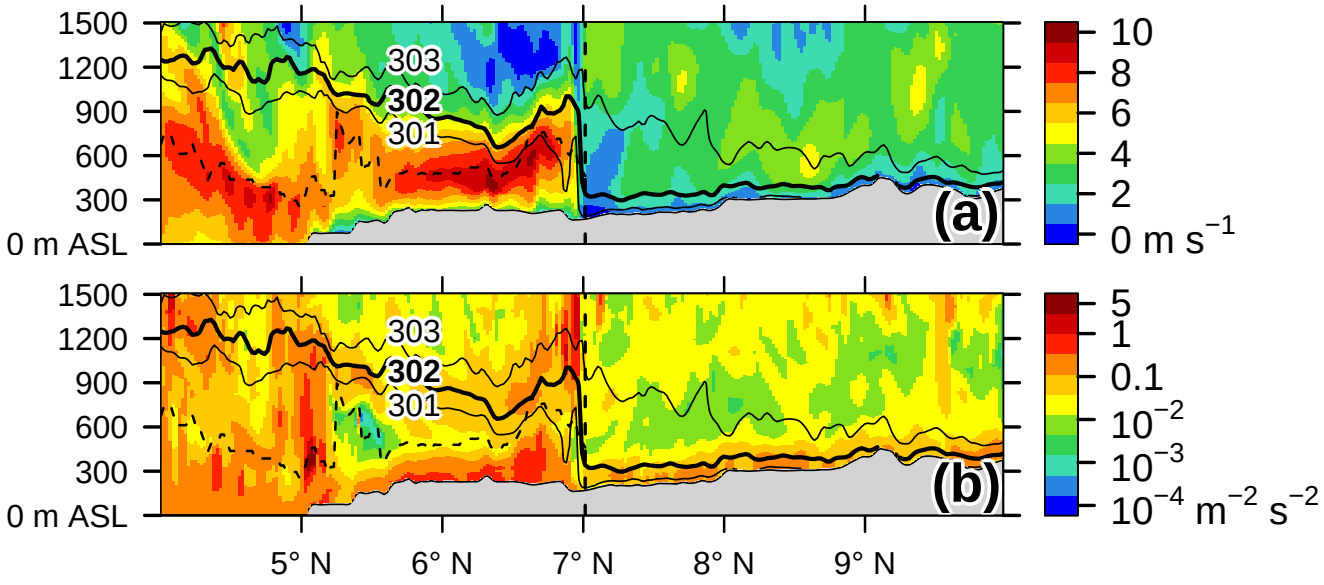

Figure 8. Meridional vertical transects (m ASL) of (a) wind speed (shading, m s^{-1}) and (b) Turbulent Kinetic Energy (TKE, m^{-2} s^{-2} in logarithmic scale) along 5.75°W (central Ivory Coast) for 2 July 21 UTC with respect to the reference case. The solid black contours show the potential temperature for 301, 302 and 303 K while the bold isentrope (302 K) is used for the identification of the AI front (vertical dashed line). The horizontal dashed line shows the NLLJ wind speed maximum (jet axis) in the AI post-frontal area. The gray shading indicates the topography.

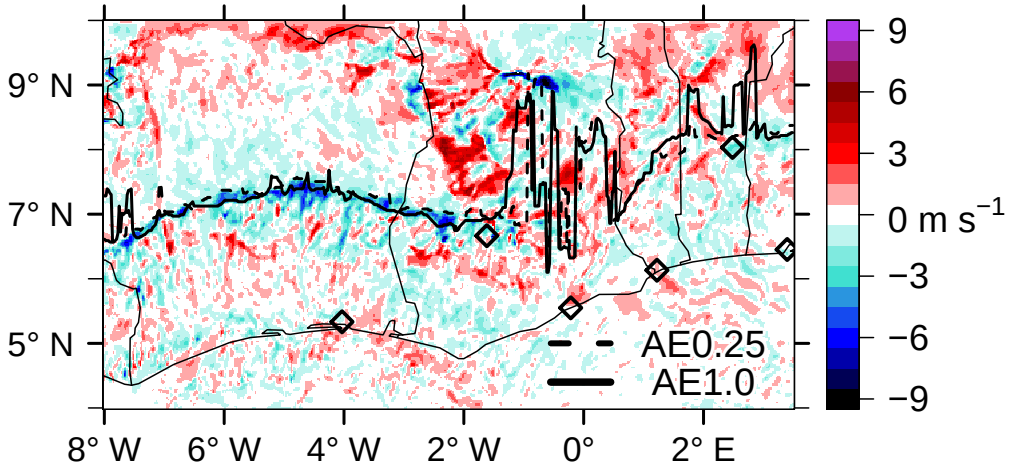

Figure 9. Wind speed difference at 250 m AGL on 2 July 22 UTC (m s^{-1}) between the reference and the clean case. The black dashed (solid) line shows the AI front for the clean (reference) case.

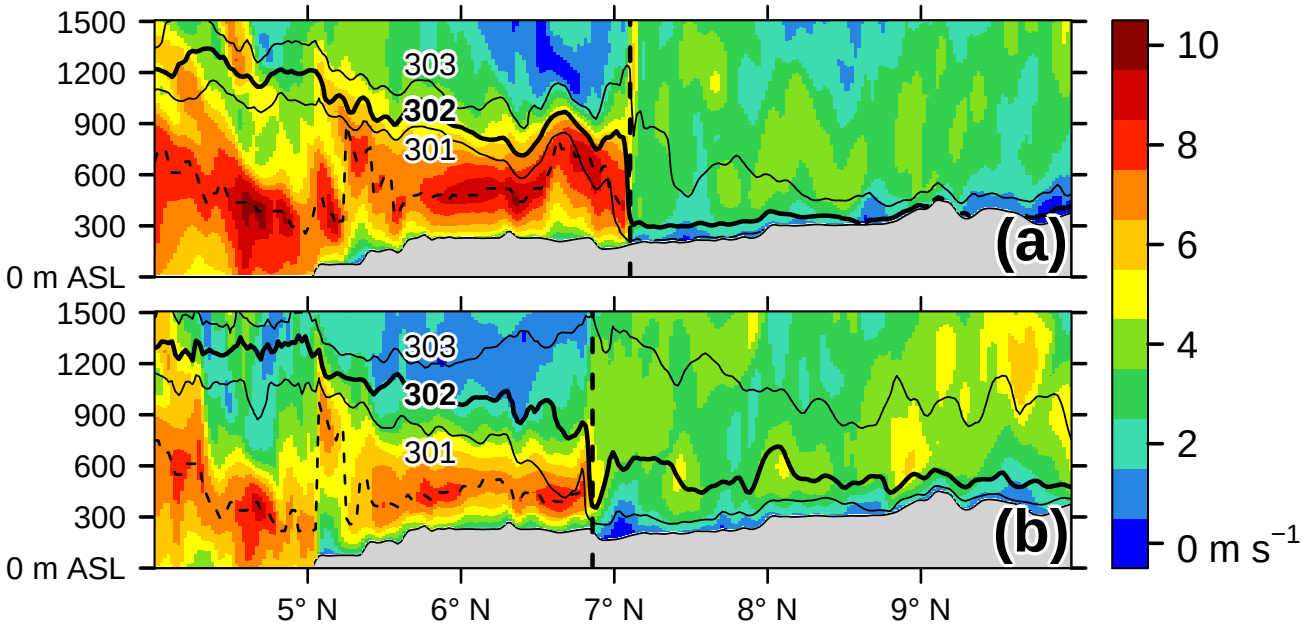

Figure 10. Same as Figure 8a but for (a) clean and (b) polluted case.

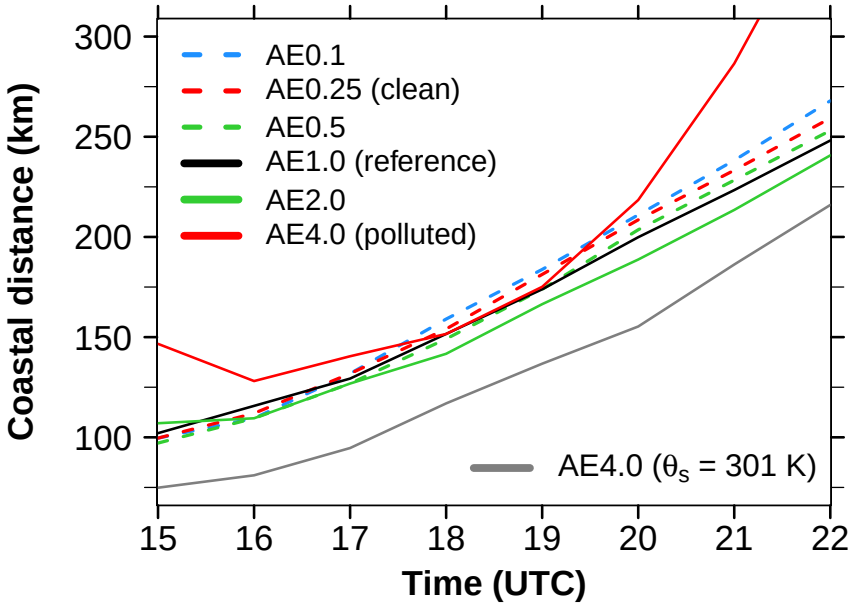

Figure 11. Temporal evolution of the inland propagation of the AI front via the distance from the coast (km) on 2 July 2016 between 15–22 UTC, spatially averaged over Ivory Coast (7.5–3.0°W) for the six experiments of Table 1. Dashed lines denote realizations with aerosol amounts below that of the reference case (black solid). The grey line shows the frontal propagation of the polluted case by using θ_s=301 K instead of 302 K for the front detection.

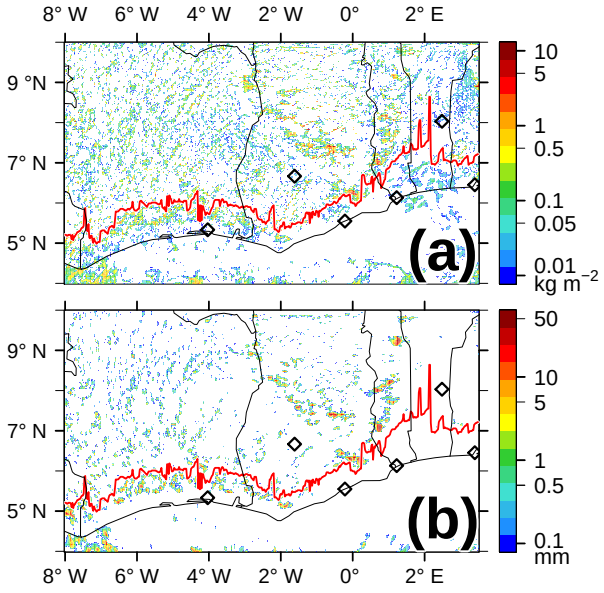

Figure 12. (a) Total cloud water (kg m^{-2}) and (b) precipitation (mm) on 2 July 15 UTC for the reference case. The red line denotes the AI front.

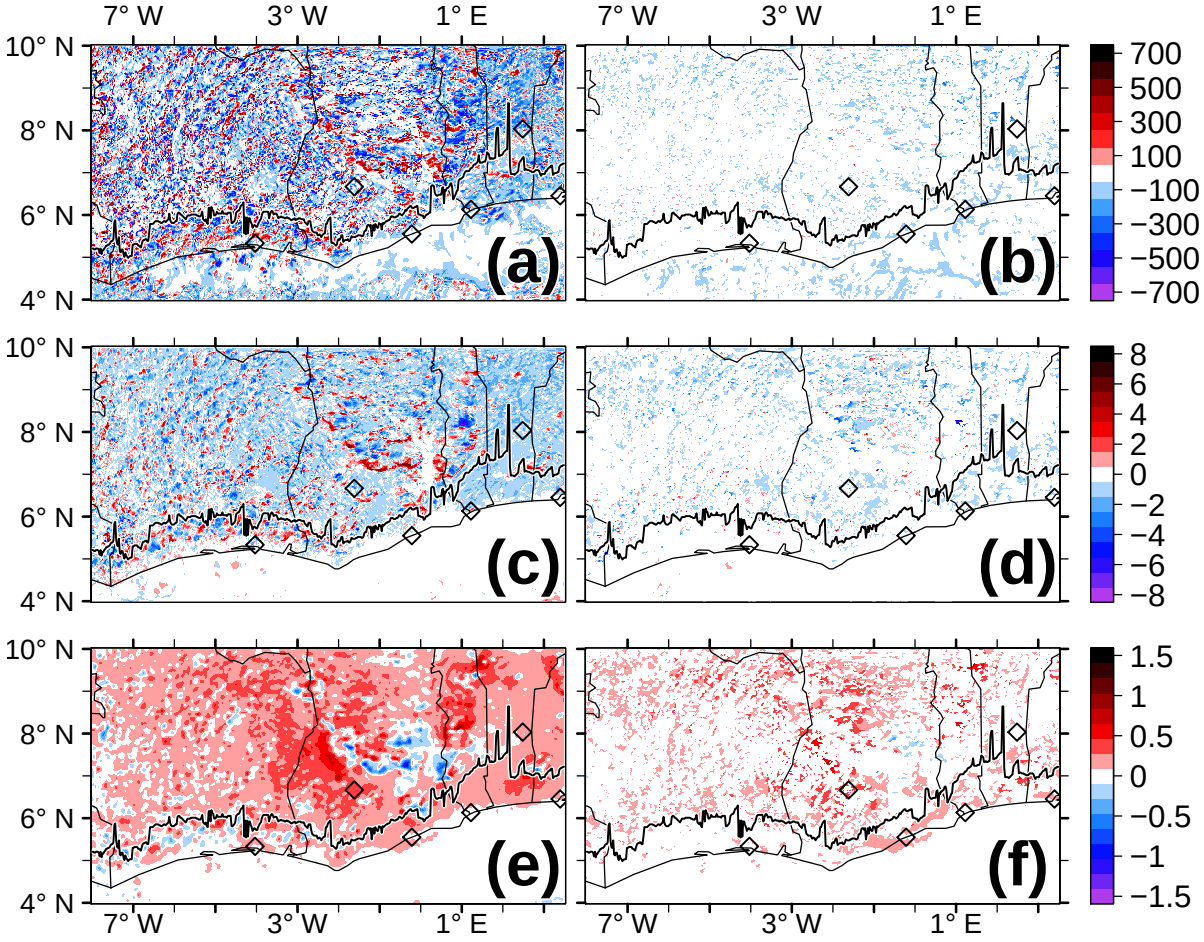

Figure 13. Surface meteorological quantities over SWA on 2 July 15 UTC as differences between the reference and the clean case (~~$AIE_{1.0}$~~ ~~$ADE_{1.0}$~~ AE1.0 - ~~$AIE_{0.25}$~~ ~~$ADE_{0.25}$~~ AE0.25), (left) including cloudy and cloud-free areas and (right) over areas that are simultaneously cloud free in the clean and reference case. (a-b) Surface net downward shortwave radiation difference (W m^{-2}), (c-d) 2-m temperature difference (K) and (e-f) sea level pressure difference (hPa). The black solid lines denote the location of the reference case AI front.

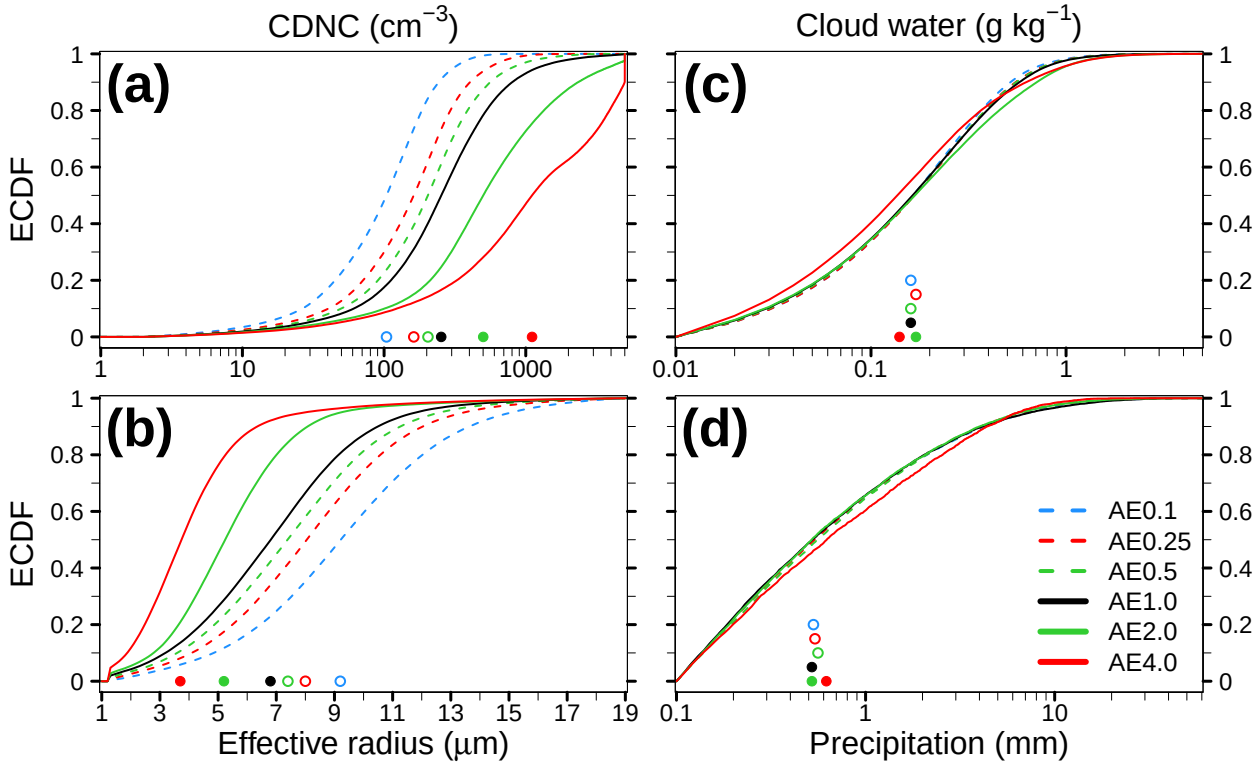

Figure 14. Empirical Cumulative Distribution Function (ECDF) of (a) CDNC (cm^{-3}), (b) cloud droplet effective radius (μm), (c) cloud water (g kg^{-1}) and (d) precipitation (mm) for the six experiments of Table 1 considering the full vertical column over the inland area of SWA on 2 July, 15 UTC. The circles and dots highlight the median values. Dashed lines and circles relate to realizations with less aerosol than the reference case and solid lines and dots refer to simulations with aerosol amounts greater/equal the reference case.

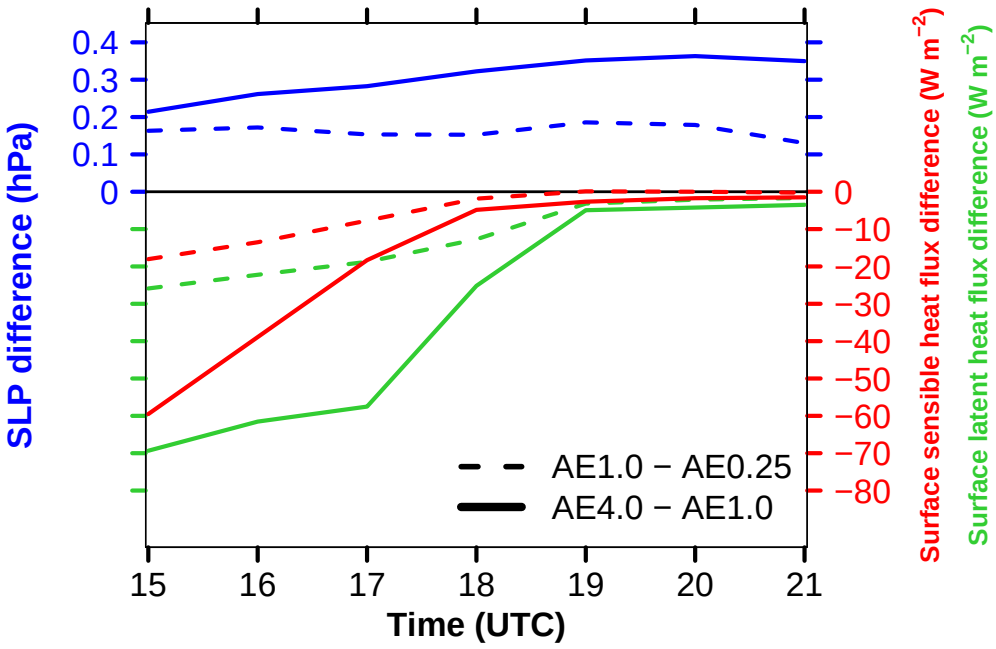

Figure 15. Temporal evolution of the differences in surface sensible heat flux (red, W m^{-2}), surface latent heat flux (green, W m^{-2}) and surface pressure (blue, hPa) between the reference and the clean case (dashed line) and between the polluted and the reference case (solid line) for the time period 2 July 15-21 UTC spatially averaged for the AI pre-frontal area over Ivory Coast as defined by the θ_s method. The sensible heat flux is defined positive downward.

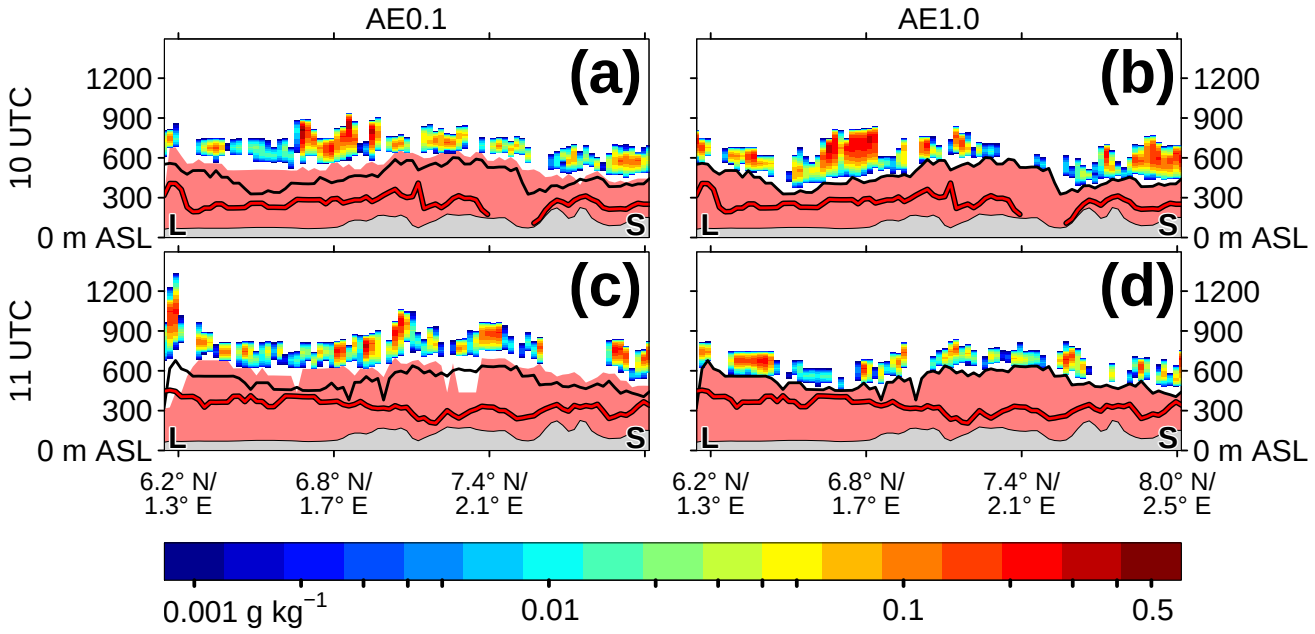

Figure 16. Cloud water (g kg^{-1}, shading) along the Lomé (L) - Savè (S) vertical transect (m ASL) for the temporal evolution on 3 July (top) 10 UTC and (bottom) 11 UTC, considering (left) the clean case and (right) the reference case. The red shading reflects instability (dθ/dz<0) to highlight the evolution of the CBL. The black solid (red solid) line denotes the height of the CBL in the reference case (polluted case), simultaneously added to the panels on the left and right hand side.

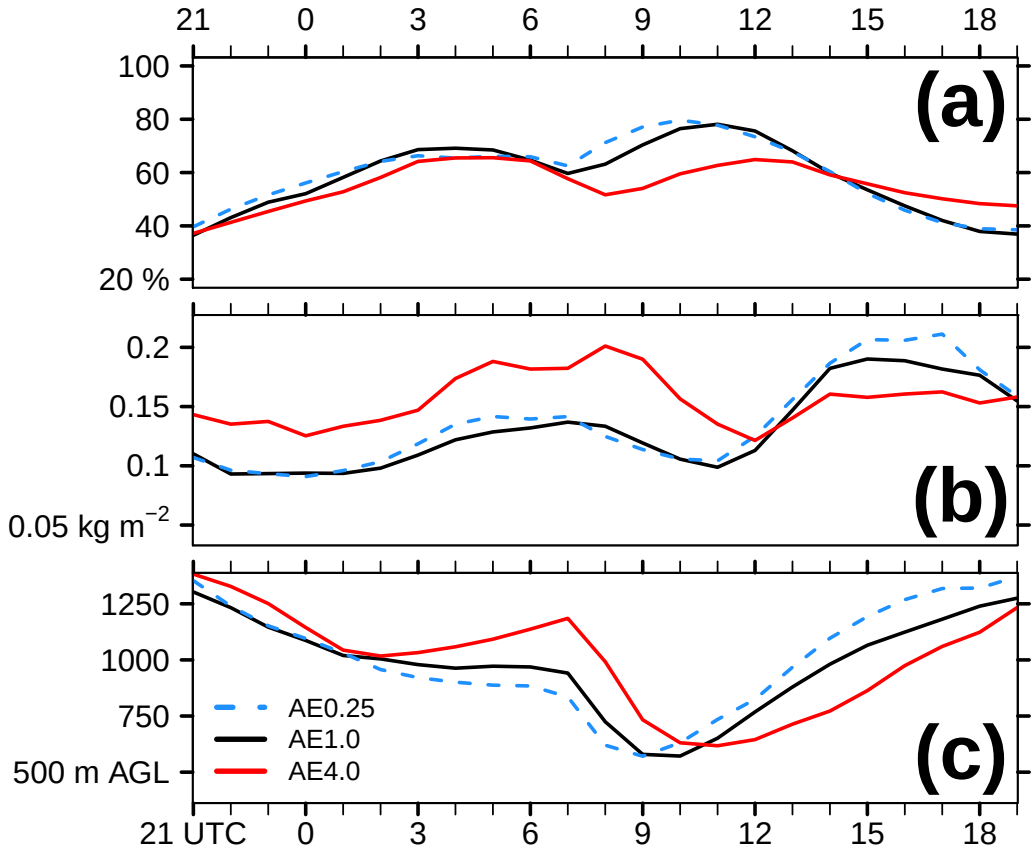

Figure 17. Spatial average (8°W–3.5°E, 5–10°N) of (a) total cloud cover (%), (b) total cloud water (kg m^{-2}) and (c) cloud base height (m AGL) for the temporal evolution between 2 July 21 UTC and 3 July 19 UTC. The cloud cover is detected by non-zero values of total cloud water. A value of 60 % denotes that 60 % of the domain is covered by clouds. For the spatial average of total cloud water, values below 10 g m^{-2} were omitted. The cloud base height is detected via the lowest height AGL with a non-zero cloud water value. The blue dashed, black solid and red solid lines denote the clean, reference and polluted case, respectively.

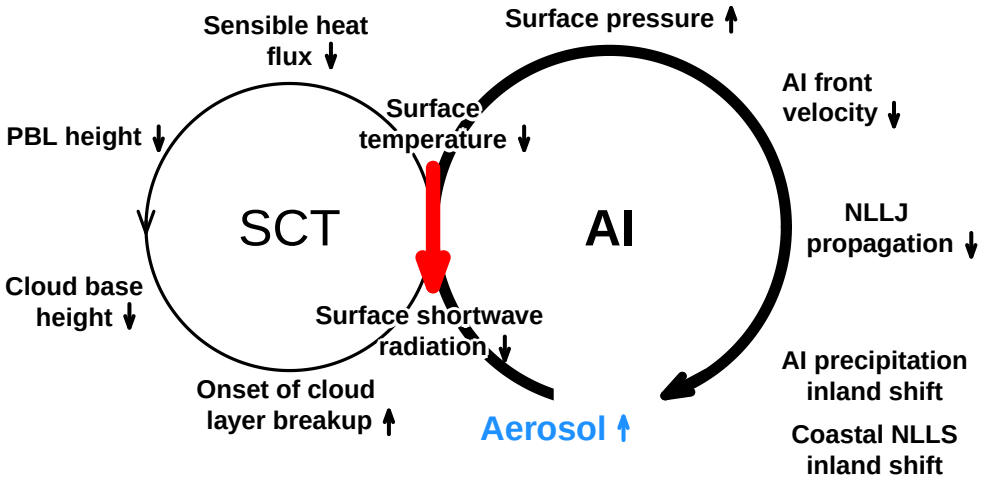

Figure 18. Scheme of the aerosol-related atmospheric feedbacks summarizing the findings of the process study simulations on 2–3 July 2016. The main loop is labeled AI (Atlantic Inflow) and the additional loop SCT (Stratus-to-Cumulus Transition). The small arrows in upward and downward direction denote whether a quantity reacts with a decrease (downward) or increase (upward) to the increase of aerosol mass and number (blue) as the initial perturbation. The red arrow shows the linkage between AI and SCT via the decrease in shortwave radiation and surface temperature and a potential pathway for a negative feedback of SCT on AI.

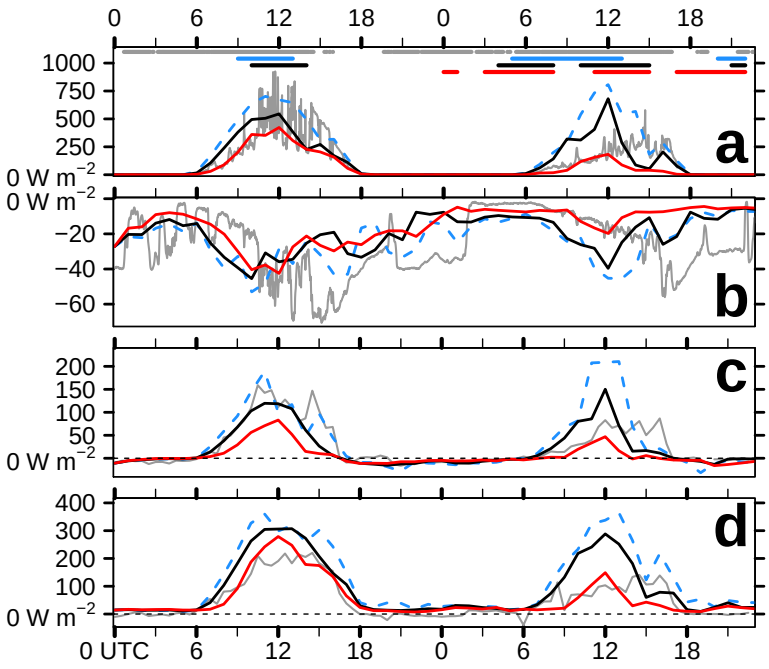

Figure 19. Comparison between Savè supersite observations (Kohler et al., 2016, grey) and COSMO-ART reference (black), clean (blue) and polluted (red) of (a) net downward shortwave radiation (W m^{-2}), (b) net downward longwave radiation (W m^{-2}), sensible heat flux (W m^{-2}) and latent heat flux (W m^{-2}). The horizontal lines in (a) denote clouds over Savè in the observations and COSMO-ART.

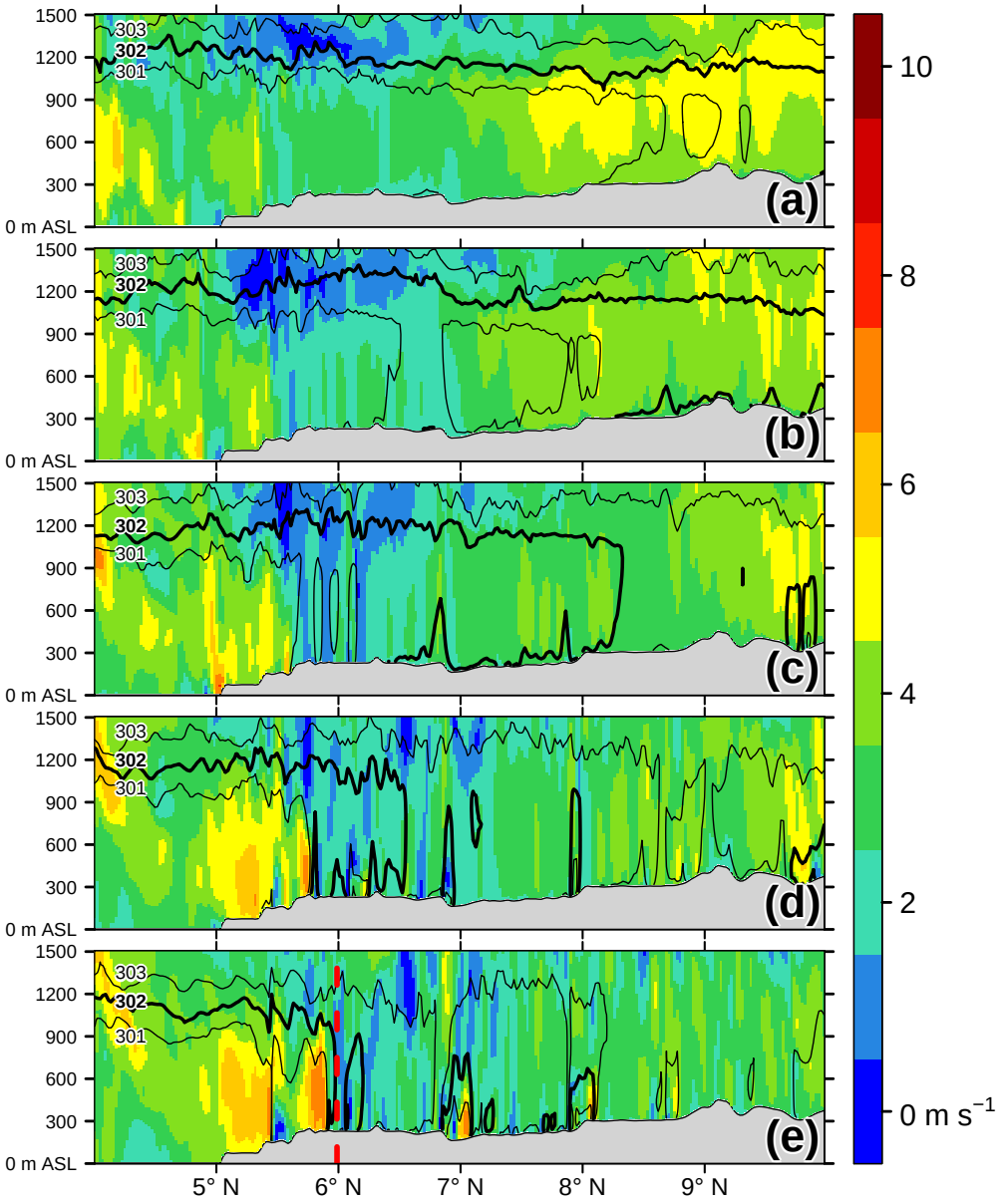

Figure 20. Meridional vertical transects (m ASL) of wind speed (shading, m s^{-1}) along 5.75°W (central Ivory Coast) for 2 July (a) 11 UTC, (b) 12 UTC, (c) 13 UTC, (d) 14 UTC and (e) 15 UTC for the reference case. The solid black contours show the potential temperature for 301, 302 and 303 K, while the bold isentrope (302 K) is used for the identification of the AI front (vertical red dashed line in (e)). The gray shading indicates the topography.

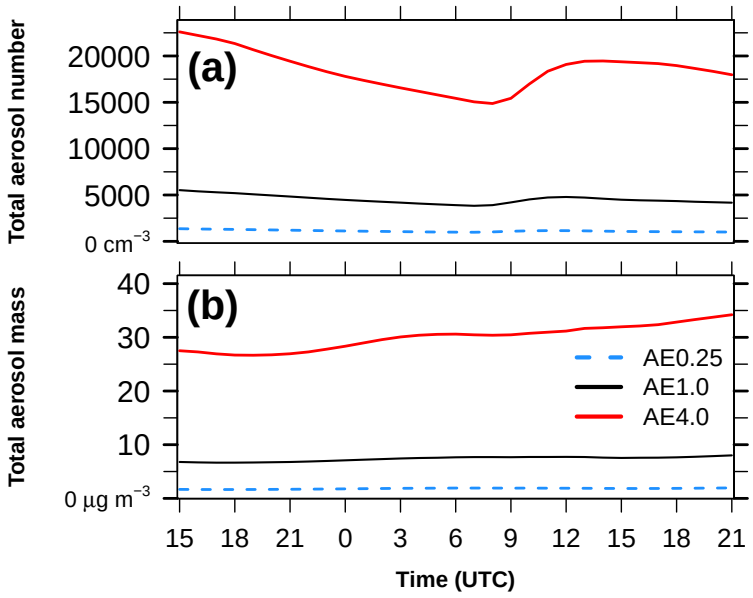

Figure 21. Temporal evolution of median (a) total aerosol number (cm^{-3}) and (b) total aerosol mass (μg m^{-3}) in the lowest 2 km AGL over Ivory Coast (7.5–3.0°W) between 2 July 15 UTC to 3 July 21 UTC for the clean (blue dashed), reference (black solid) and polluted case (red solid), based on the aerosol scaling introduced in Table 1.

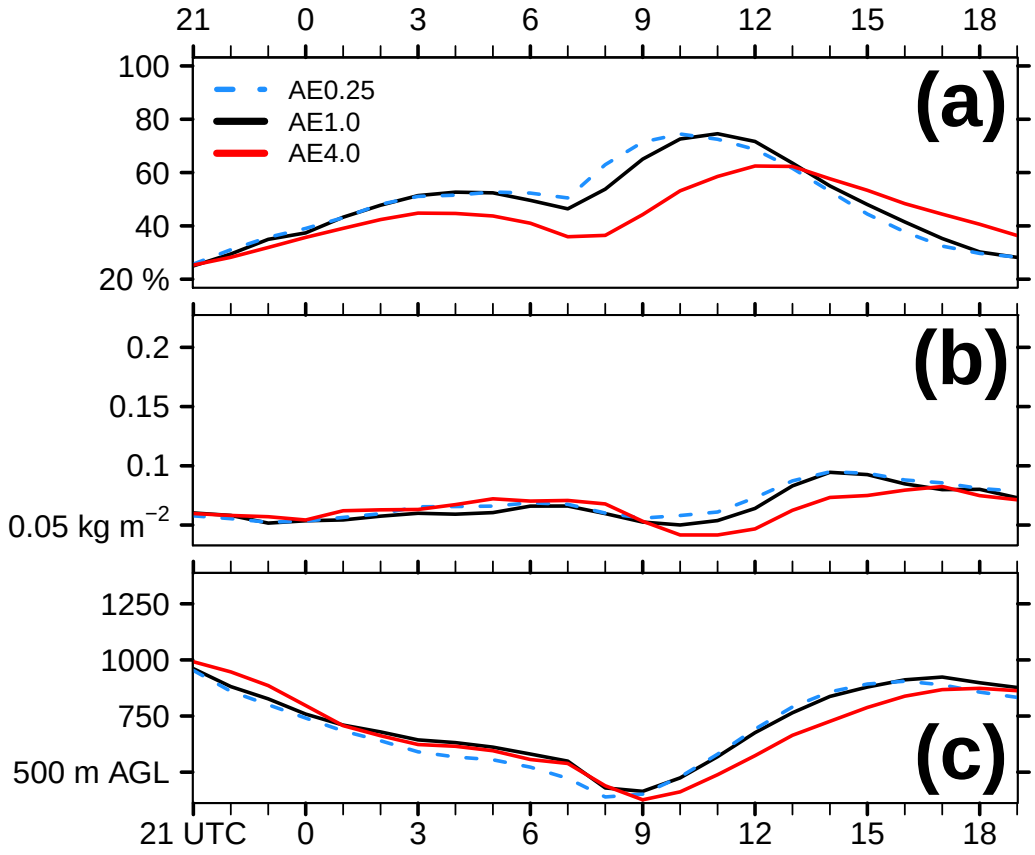

Figure 22. Spatial average (8°W–3.5°E, 5–10°N) of (a) cloud cover (%), (b) cloud water (kg m^{-2}) and (c) cloud base height (m AGL) for the temporal evolution between 2 July 21 UTC and 3 July 19 UTC with respect to clouds below 1500 m AGL. The cloud cover is detected by non-zero values of cloud water. A value of 60 % denotes that 60 % of the domain is covered by clouds. For the spatial average of cloud water, values below 10 g m^{-2} are omitted. The cloud base height is detected via the lowest height AGL with a non-zero cloud water value. The blue dashed, black solid and red solid lines denote the clean, reference and polluted case, respectively.